NASA CR-159752
Vought Technical Report 2-30320/0R-52360

LOW SPEED TEST OF THE AFT INLET DESIGNED FOR A TANDEM FAN V/STOL NACELLE

(NASA-CR-159752) LOW SPEED TEST OF THE AFT INLET DESIGNED FOR A TANDEM FAN V/STOL NACELLE (Vought Corp., Dallas, Tex.) 79 p
HC A05/MF A01 CSCL 21E

N80-18042

Unclas
G3/07 47321

W. W. RHOADES
A. H. YBARRA

Contract NAS3-21468
February 1980

VOUGHT CORPORATION

NASA

NASA CR-159752
VOUGHT REPORT 2-30320/0R-52360

LOW SPEED TEST OF THE AFT INLET DESIGNED FOR A TANDEM FAN V/STOL NACELLE

BY: W. W. RHOADES

A. H. YBARRA

FEBRUARY 1980

PREPARED UNDER CONTRACT NO. NAS3-21468

BY VOUGHT CORPORATION
DALLAS, TEXAS

FOR

LEWIS RESEARCH CENTER
NATIONAL AERONAUTICS AND SPACE ADMINISTRATION

1. Report No.	2. Government Accession No.	3. Recipient's Catalog No.
NASA CR-159752		

4. Title and Subtitle	5. Report Date
Low Speed Test of the Aft Inlet Designed for a Tandem Fan V/STOL Nacelle	February 1980
	6. Performing Organization Code 80378
7. Author(s)	8. Performing Organization Report No.
W. W. Rhoades and A. H. Ybarra	TR-2-30320/0R-52360
	10. Work Unit No.
9. Performing Organization Name and Address	11. Contract or Grant No.
Vought Corporation P. O. Box 225907 Dallas, Texas 75265	NAS3-21468
	13. Type of Report and Period Covered
12. Sponsoring Agency Name and Address	Contractor Report
National Aeronautical and Space Administration - Washington D.C., 20546	14. Sponsoring Agency Code

15. Supplementary Notes

Project Manager, Robert C. Williams, Low Speed Aerodynamics Branch, NASA Lewis Research Center, Cleveland, Ohio

16. Abstract

An approximately .25 scale model of a Tandem Fan nacelle designed for a Type A V/STOL aircraft configuration was tested in the NASA Lewis Research Center 10-by-10 foot wind tunnel. A 12-inch, tip driven, turbofan simulator was used to provide the suction source for the aft fan inlet. The front fan inlet was faired over for this test entry. Model variables consisted of a long aft inlet cowl, a short aft inlet cowl, a shaft simulator, blow-in door passages and diffuser vortex generators. Inlet pressure recovery, distortion, inlet angle of attack separation limits were evaluated at tunnel velocities from 0 to 240 knots, angles of attack from -10 to 40 degrees and inlet flow rates representative of throat Mach numbers of 0.1 to 0.6.

High inlet performance and stable operation was verified at all design forward-speed and angle of attack conditions. The short aft inlet configuration provided exceptionally high pressure recovery except at the highest combination of angle of attack and forward speed. The flow quality at the fan face was somewhat degraded by the addition of blow-in door passages to the long aft inlet configuration due to the pressure disturbances generated by the flow entering the diffuser through the auxiliary air passages. Addition of the vortex generator patterns to the long aft inlet model produced a slight improvement in pressure recovery at the fan face while the shaft simulator had no appreciable effect on either fan face pressure recovery or distortion levels.

17. Key Words (Suggested by Author(s))	18. Distribution Statement
V/STOL Inlet Tandem Fan Turbofan Simulator Angle of Attack	

19. Security Classif. (of this report)	20. Security Classif. (of this page)	21. No. of Pages	22. Price*
Unclassified	Unclassified	82	

* For sale by the National Technical Information Service, Springfield, Virginia 22161

TABLE OF CONTENTS

LIST OF FIGURES

LIST OF FIGURES (Continued)

LIST OF FIGURES (continued)

LIST OF TABLES

1.0 SUMMARY

An approximately .25 scale model of a Tandem Fan nacelle designed for a Type A (Subsonic Cruise)V/STOL aircraft configuration was tested in the NASA Lewis Research Center 10-by-10 foot (3.048-by-3.048 meter) wind tunnel. A 12-inch (.3048 meter), tip driven, turbofan simulator was used to provide the suction source for the aft fan inlet. The front fan inlet was faired over for this test entry. Model variables consisted of a long aft inlet cowl, a short aft inlet cowl, a shaft simulator, blow-in door passages and diffuser vortex generators. Inlet pressure recovery, distortion, and inlet angle of attack separation limits were evaluated at tunnel velocities from 0 to 240 knots (123.5 m/s), angles of attack from -10 to 40 degrees and inlet flow rates corresponding to throat Mach numbers of 0.1 to 0.6.

High inlet performance and stable operation was verified at all design forward speed and angle of attack conditions. The short aft inlet configuration provided high pressure recovery except at the highest combination of angle of attack and forward speed. The flow quality at the fan face was somewhat degraded by the addition of blow-in door passages to the long aft inlet configuration due to the pressure disturbances generated by the flow entering the diffuser through the auxiliary air passages. Addition of the vortex generator patterns to the long aft inlet model produced a slight improvement in pressure recovery at the fan face while the shaft simulator had no appreciable effect on either fan face pressure recovery or distortion levels.

2.0 INTRODUCTION

V/STOL aircraft require propulsion system inlets which can operate over a wide range of flight speeds, mass flow and angles of attack and yaw. In addition, these configurations require nozzles which can provide high thrust coefficients and efficient turning over a wide range of deflection angles. Requirements placed on the inlets and nozzles can be especially severe due to the operating environment on board various types of combat ships. Thus considerable research and configuration development is required to design inlets and nozzles for such an application.

The V/STOL aircraft being developed by the Vought Corporation for Navy Type A (Subsonic Cruise) applications employs a tandem fan propulsion system arranged in two nacelles, integrated structurally with the fuselage. Each nacelle contains a complete propulsion unit consisting of a core engine, two fixed pitch fans with variable inlet guide vanes, and associated inlets and nozzles (Figure 1). The fans are located ahead of the core engine and are mounted co-axially with the engine. Small fan diameters result from the use of two fans in each nacelle. A vectoring nozzle for the front fan and an inlet for the aft fan are incorporated between the two fans. Flow through the two fans is maintained separate at all times. The core engine is located immediately behind the fan and is supercharged by it. The core and aft fans flows are mixed and discharged through a vectoring nozzle.

Flow paths through the Tandem Fan nacelle are shown in Figure 2. During conventional flight, fan flows are vectored directly aft. For VTOL, nozzles are repositioned as shown to vector thrust vertically. Intermediate thrust vector angles are achieved by corresponding intermediate positions of each nozzle. Thrust vector response is rapid and smooth transitions are achieved by the control forces achievable through combined thrust modulation and vectoring.

Both inlets face directly forward throughout the transition maneuver to help expand aircraft descent boundaries during approaches to short or vertical landings.

The inlets have been designed to provide good performance and low distortion in a minimum length. Large inlet lip radii are used for good takeoff and V-Mode performance and to reduce inlet flow distortion. The forward inlet incorporates a close coupled inlet, fan and nose cap for improved angle-of-attack performance. The top inlet has been arranged to benefit from the favorable flow field of the front inlet and to integrate well into the nacelle. Low diffusion rates and turning of the flow through the bend to the aft fan has been provided to reduce losses and flow distortion.

The nozzles are designed to provide high thrust coefficients and efficient turning of the flow over a range of deflection angles from 0^{o} (cruise) to 110^{o} (V/STOL). The forward nozzle, which is two-dimensional for good integration with the nacelle and ease in vectoring, uses a simple two-piece deflector to vector thrust. Variation of nozzle area in cruise is achieved with a small flap mounted on the nacelle surface. The aft nozzle, which vectors mixed flow from the core engine and the aft fan, is two-dimensional for ease in vectoring the flow. The nozzle deflector is hinged along the lower portion of the nacelle and is rotated downward for V/STOL. A rotating lower flap is used to achieve the nozzle areas required for cruise.

Several years ago NASA Lewis Research Center and the Vought Corporation began a research effort to develop a broad data base for the design of the inlet and nozzle systems that will contribute to an effective, efficient, lightweight low drag Tandem Fan propulsion system that operates satisfactorily at the conditions applicable to the Navy Type A V/STOL aircraft.

This report covers the design and fabrication of an aft-mounted Tandem Fan inlet model by Vought as part of contract NAS3-21468 (Reference 1) and the subsequent performance evaluation by NASA Lewis in the 10-by-10 foot (3.048-by 3.048 meter) wind tunnel.

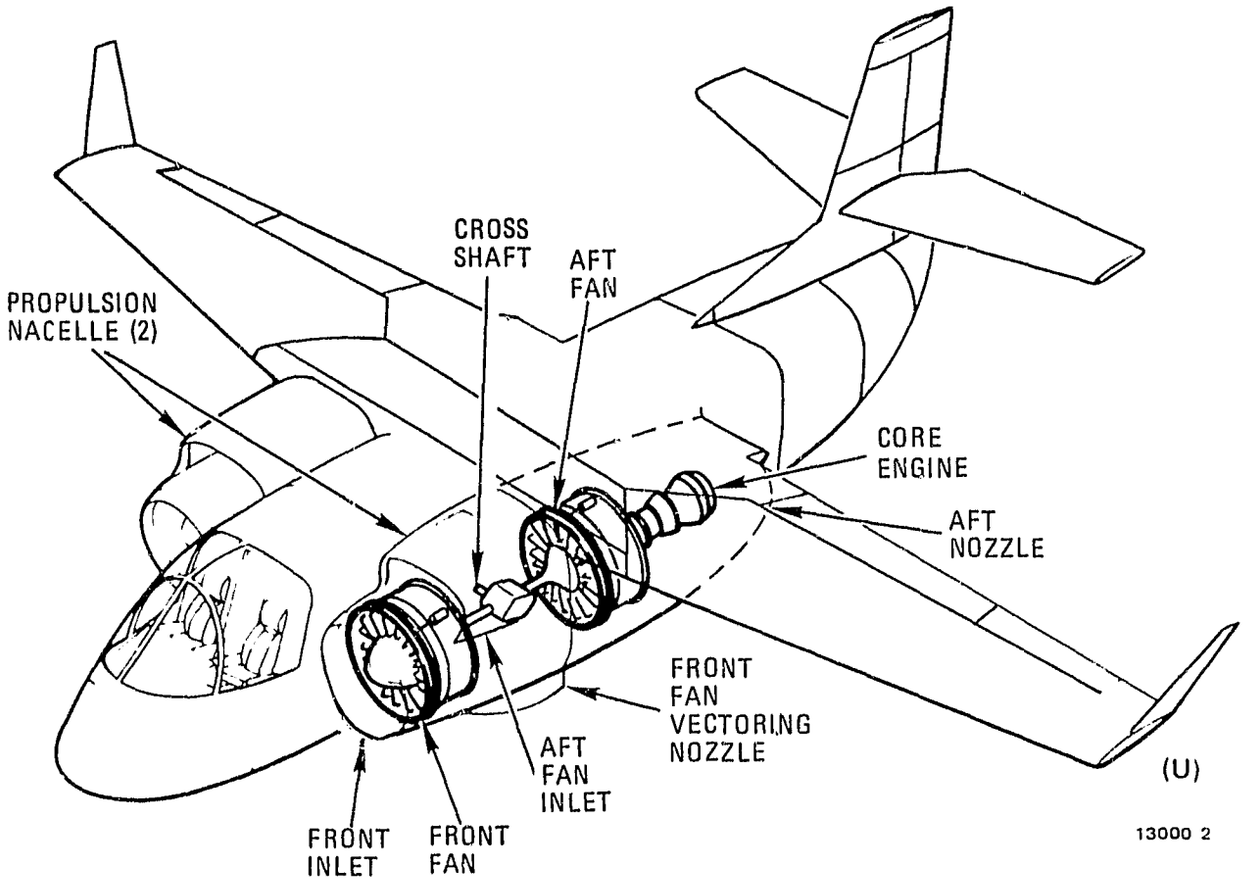

FIGURE 1 V/STOL TYPE "A" TANDEM FAN POWERED AIRCRAFT

A. – CONVENTIONAL FLIGHT

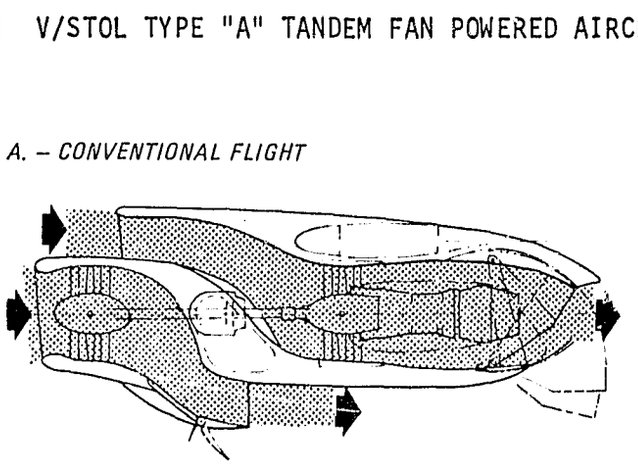

B. – VTOL FLIGHT

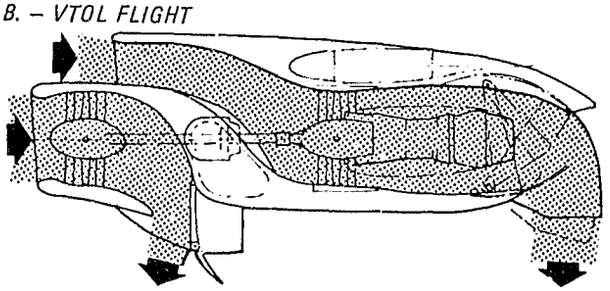

FIGURE 2 SINGLE STAGE TANDEM FAN NACELLE

3.0 SYMBOLS AND ABBREVIATIONS

A_{CAP}	Capture area
A_E	Fan exit area
A_{HI}	Hilite area
A_{MAX}	Area at maximum cowl diameter
A_{TH}	Throat area
BID	Blow-in door
DC60	Inlet Distortion Index (Ref.8)
D_{HI}	Hilite equivalent diameter
D_{MAX}	Maximum inlet equivalent diamter
D_{PT}	Maximum minus minimum total pressure at fan rake station
D_{SPILL}	Inlet spillage drag
D_{TH}	Throat equivalent diameter
H.L.	Hilite
IDC	Inlet distortion index (Ref. 8)
IDR	Inlet distortion index (Ref. 8)
KD_2	Inlet distortion index (Ref. 8)
$K\theta$	Inlet distortion index (Ref. 8)
LNG	Long
m	Inlet airflow
m_o	Airflow based on free stream conditions
MAX-MIN	Inlet distortion index. PTMAX-PTMIN/PTAV
M_{FAN}	Fan face mach number
M_o	Freestream mach number
M_{TH}	Throat mach number (MTHROAT)
P_s	Individual tap static pressure

P_T	Individual probe total pressure
P_{TAV}	Average total pressure at fan rake station
P_{TFAN}	Fan face total pressure
P_{TMAX}	Maximum total pressure probe reading at fan face
P_{TMIN}	Minimum total pressure probe reading at fan face
P_{TO}	Free stream total pressure
q_o	Free stream dynamic pressure
REC	Inlet total pressure recovery, PTAV/PTO
RMS	Root mean square pressure level
RPMC	Fan corrected RPM, $N/\sqrt{\theta}$
S	Surface distance along inlet wall measured from hilite
SHF	Shaft Simulator
VG	Vortex generator
V_o	Free stream velocity
W	Inlet airflow to fan
X	Inlet axial distance
Y	Inlet vertical distance
α	Angle of attack, also ALPHA, degrees
δ	Ratio of total pressure to sea leavel static pressure
Θ	Ratio of total temperature to standard data temperature, or equivalent diffuser conical half angle, degrees
ψ	Angle of yaw, degrees

SUBSCRIPTS

dd	Drag divergence
FAN	Fan
HI	Hilite
MAX	Maximum

0	Freestream
S	Static
T	Total
TH	Throat
2	Fan Discharge

4.0 PROGRAM OBJECTIVES AND DESCRIPTION

The objectives of this test program were to develop a broad data base for the design of aft inlet systems that will contribute to an efficient, lightweight, low drag Tandem Fan propulsion system that operates satisfactorily at the conditions applicable to the Navy Type A V/STOL aircraft.

Areas of investigation were:

- o close coupling of the fan with the inlet system
- o the rapid turning and large duct off-set of the aft fan inlet
- o inlet angle of attack

Specific objectives of this effort were the design and manufacture of model hardware and testing of an aft inlet model representative of the aft inlet arrangement of the Tandem Fan propulsion system.

The model hardware was designed to be compatible with installation in the NASA Lewis Research Center wind tunnels. Inlet testing was conducted using a government-furnished 12-inch (.3048 meter) diameter Tech Development tip turbine fan.

Aft inlet model was tested over a range of flight speeds from 0 to 240 knots. Angle of attack was varied from -10° to 40°. Inlet flow rates corresponding to throat Mach numbers up to 0.5 were evaluated at the above tunnel conditions. Configuration variables included a fan shaft simulator, duct vortex generators and blow-in doors.

The inlet configurations were evaluated in terms of engine face total pressure recovery and distortion, inlet angle of attack and separation limits. Recovery and distortion were evaluated with a multitube total pressure rake located at the fan face station with the 12-inch (.3048 meter) fan simulator located downstream of the fan face station. Both steady state and dynamic pressure measurements were obtained. Separation limits were determined from lip and diffuser surface static pressure measurements and the engine face total pressures.

5.0 TEST APPARATUS

This section describes the Tandem Fan nacelle model and the associated instrumentation. In addition, the NASA Lewis wind tunnel test facility, test conditions and procedures and data reduction requirements are also described.

5.1 Model Description

The nacelle model is an approximately 0.25 scale geometric representation of the full scale Tandem Fan nacelle and consists of an Aft-mounted inlet with a faired over front inlet and a tip turbine drive-turbofan simulator. Appropriate cowlings and fairings were designed and fabricated into a wind tunnel test article. A photograph of the complete nacelle is shown in Figure 3.

Aft Inlet

The aft inlet model for this program was designed by Vought to conform to the Vought V-530 Tandem Fan configuration. This inlet configuration, along with the front inlet was designed to produce maximum performance during vertical takeoff, while minimizing drag penalties during cruise and loiter. The inlet design conditions corresponding to takeoff, landing and transition are presented in Table I.

TABLE I

INLET DESIGN CONDITIONS

	Vertical Operation	Transition Flight
M_{FAN}	0.5	0.2 - 0.6
α_{MAX}	---	30^{o}
ψ_{MAX} (35 Kt crosswind)	90^{o}	90^{o}
V_o	---	0 - 150 Kts (0 - 77.2 m/s)

NASA
C-79-1907

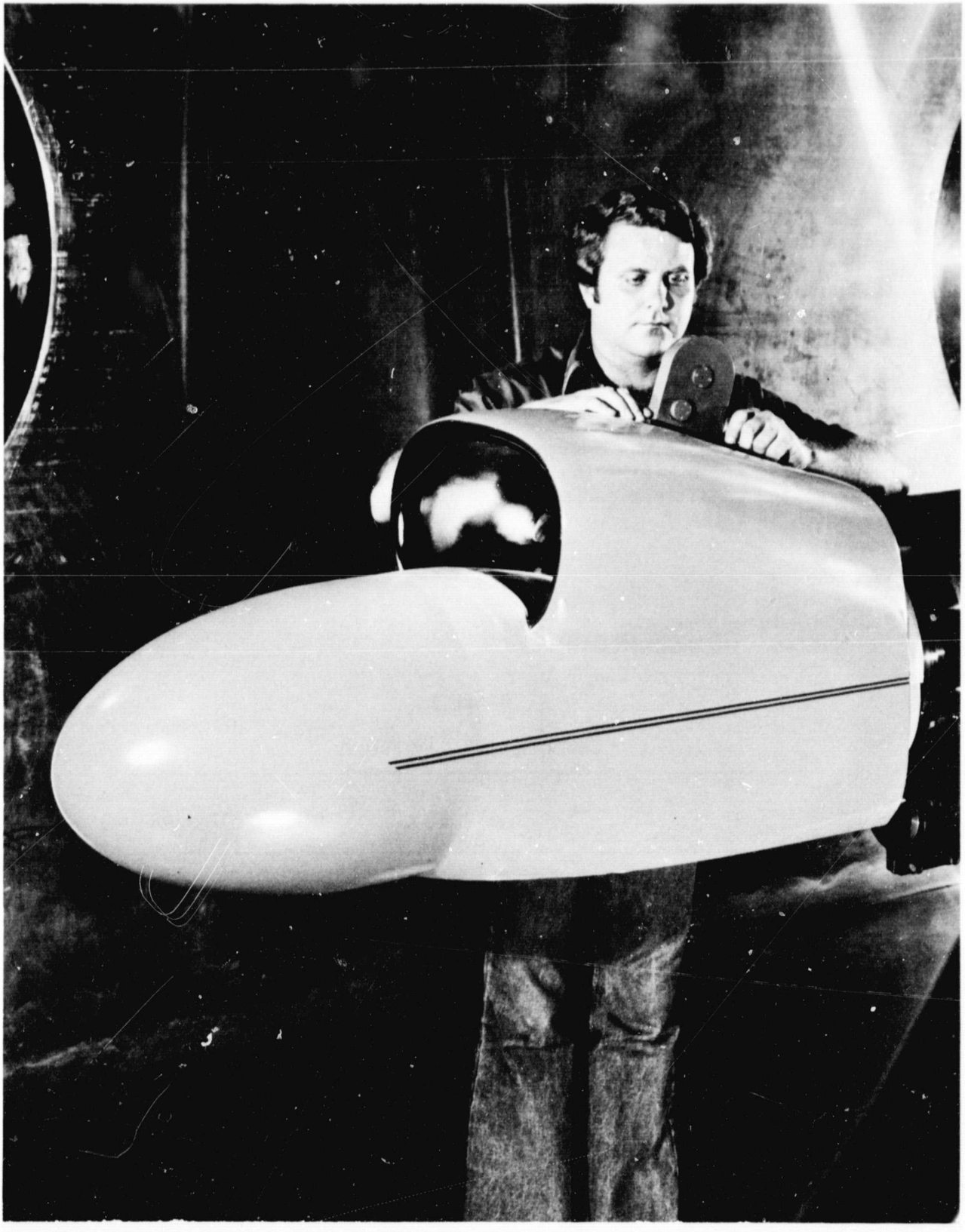

FIGURE 3 TANDEM FAN AFT INLET MODEL INSTALLED IN NASA LEWIS RESEARCH CENTER 10-by-10 FOOT (3.048-by-3.048) WIND TUNNEL

To meet the design conditions of Table I, the Aft inlet shape was defined in terms of contraction ratio, lip geometry and shape, and throat area. Preliminary inlet design studies, using existing test data of references 2 and 3 indicated a contraction ratio (A_{HI}/A_{TH}) of 1.46 was required to satisfy the low speed requirements, specifically the cross-wind conditions of Table I. However, for high speed operation a lower contraction ratio, and thinner lip, was desired to minimize inlet cruise and loiter drag. Thus, blow-in door passages were provided in the diffuser duct during V/STOL operation to reduce the inlet throat Mach number and hence the lip loading and allow a lower contraction ratio to be used. Blow-in door passages (equivalent to 30% of the throat flow area) were provided in the Aft inlet model. This allowed an inlet contraction ratio of 1.30 to be selected for model design. Lip shape studies were next performed using the test data of References 2 and 3. Several selected lip shapes meeting the V/STOL requirements of Table I were then evaluated in terms of high speed cruise and loiter drag levels based on the data in references 4 and 5.

Figure 4 identifies the external lip area ratio, A_{MAX}/A_{HI}, of 1.22, forebody diameter ratio, D_{HI}/D_{MAX}, of 0.91 and forebody length ratio, X/D_{MAX} of 0.3 selected and their relation to high speed mass flow and drag divergence levels. Figure 5 illustrates the predicted inlet spillage drag levels as a function of mass flow ratio and Mach number for an external lip area ratio of 1.22. The cruise power mass flow ratio and spillage drag are shown in the figure for reference. With the inlet contraction ratio and lip geometry selected, the inlet throat area was sized to provide maximum airflow during cruise flight at approximately a 0.65 throat Mach number. The overall diffuser lines were then established through analysis by using the combined potential and viscous flow routine developed by NASA Lewis Research Center and Vought (reference 6). Figure 6 shows a schematic of the basic inlet lines while Figure 7 shows the diffuser area distributions selected for the model.

The blow-in door passages were provided in the upper surfaces of the aft inlet cowl. A description of the blow-in door passages is included in Figure 8. The basic configuration was tested with the blow-in door passages plugged. The plugs were removed from the cowl when the effects of blow-in door operation were evaluated.

Vortex generators were also fabricated for the aft inlet diffuser duct. Characteristic geometry of these generators are shown in Figure 9. The generators were made to be removable so that the model could be tested with and without them.

Figure 10 shows a schematic of the aft inlet/nacelle model assembly. For this test entry, the front inlet has been replaced by a forebody cap so that the performance of the aft inlet alone could be obtained. Future tests will evaluate combined front and aft inlet operation. Figure 10 also shows the other variables (blow-in doors, vortex generator and a simulated fan shaft) provided for aft fan inlet evaluation.

The front fan of the V/STOL Type "A" Tandem fan powered aircraft is to be driven by a shaft that extends from the aft fan, through the aft inlet duct, to the front fan assembly to test the influence of such a shaft. A stationary shaft was installed in the aft inlet model duct. The diameter of the shaft simulator was .08 the diameter of the aft fan simulator or 1 inch(2.54 cm). The size of the shaft was scaled from the full size shaft dimensions which were developed during the V/STOL "A" tandem fan transmission sizing studies.

LIP FOREBODY LENGTH RATIO, X/D_{MAX} = .3,

(increased to obtain higher drag divergence)

A_{MAX}/A_{HI} = 1.22 (same as Front Inlet)

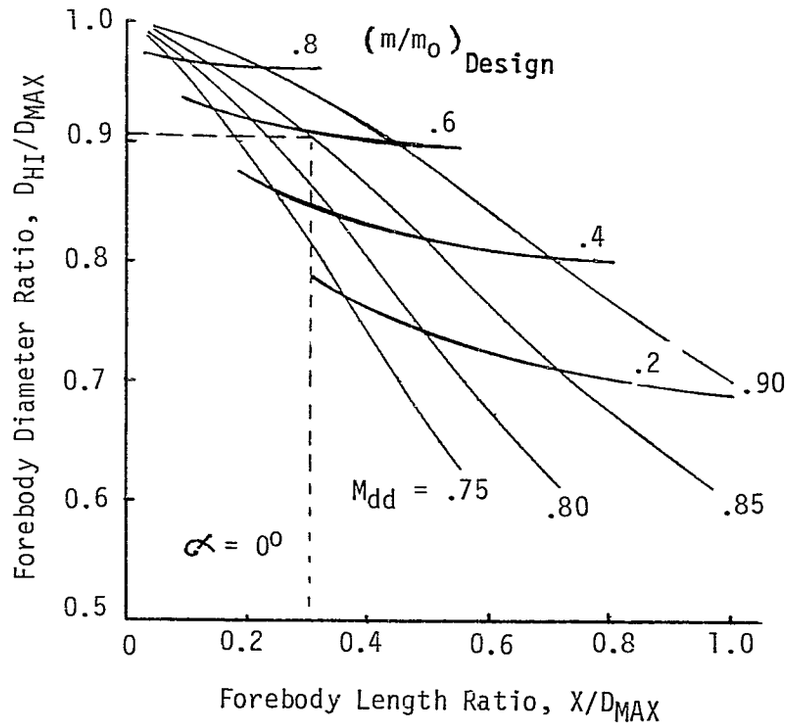

FIGURE 4 AFT INLET EXTERNAL LIP CHARACTERISTICS

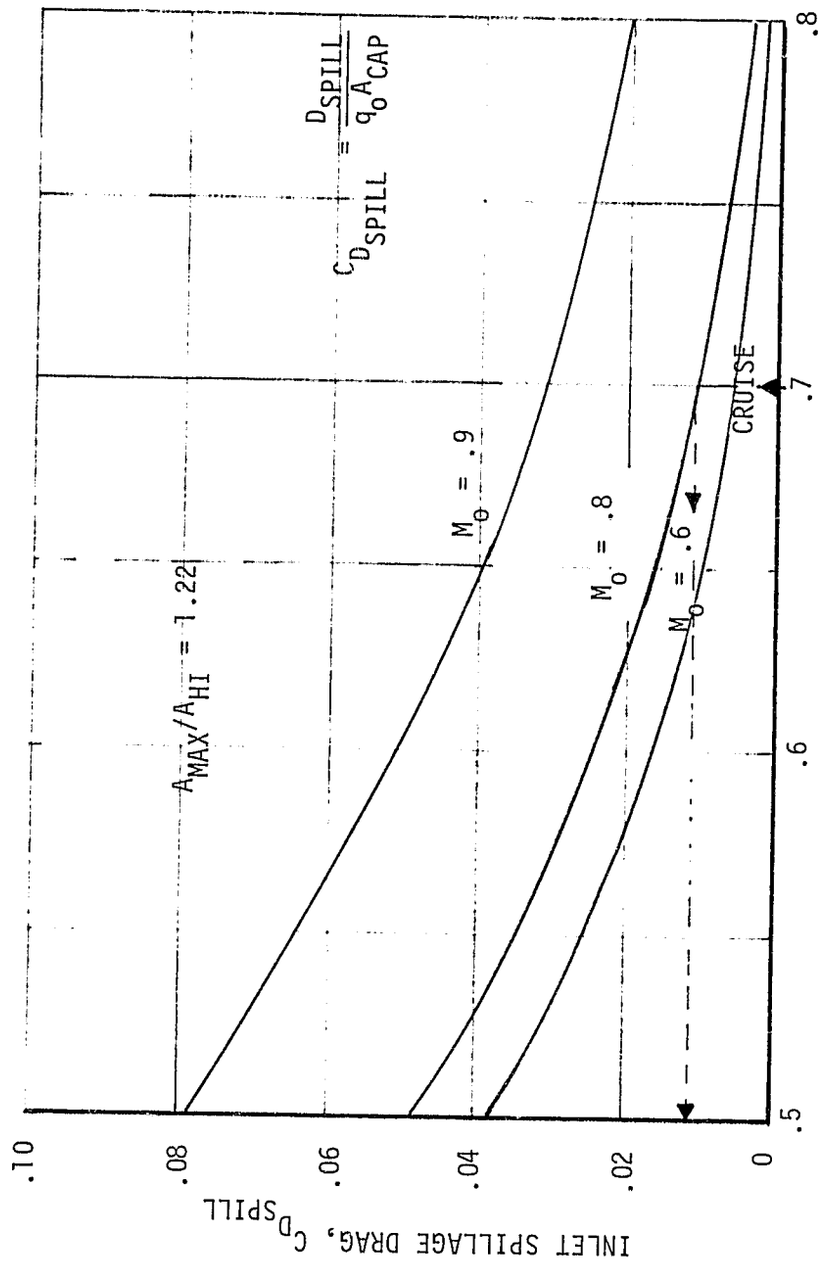

FIGURE 5 AFT INLET SPILLAGE DRAG CHARACTERISTICS

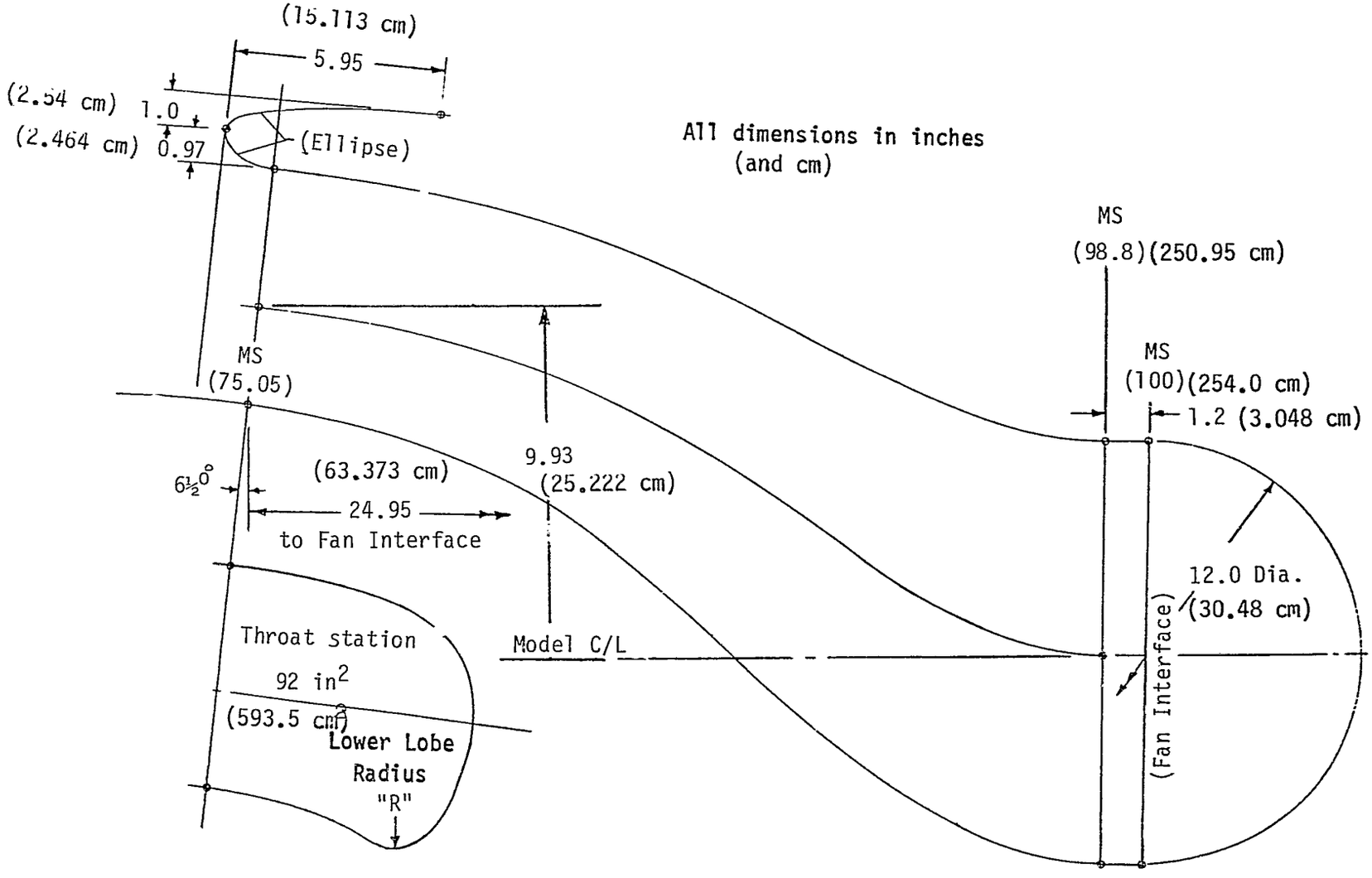

FIGURE 6 AFT INLET LINES

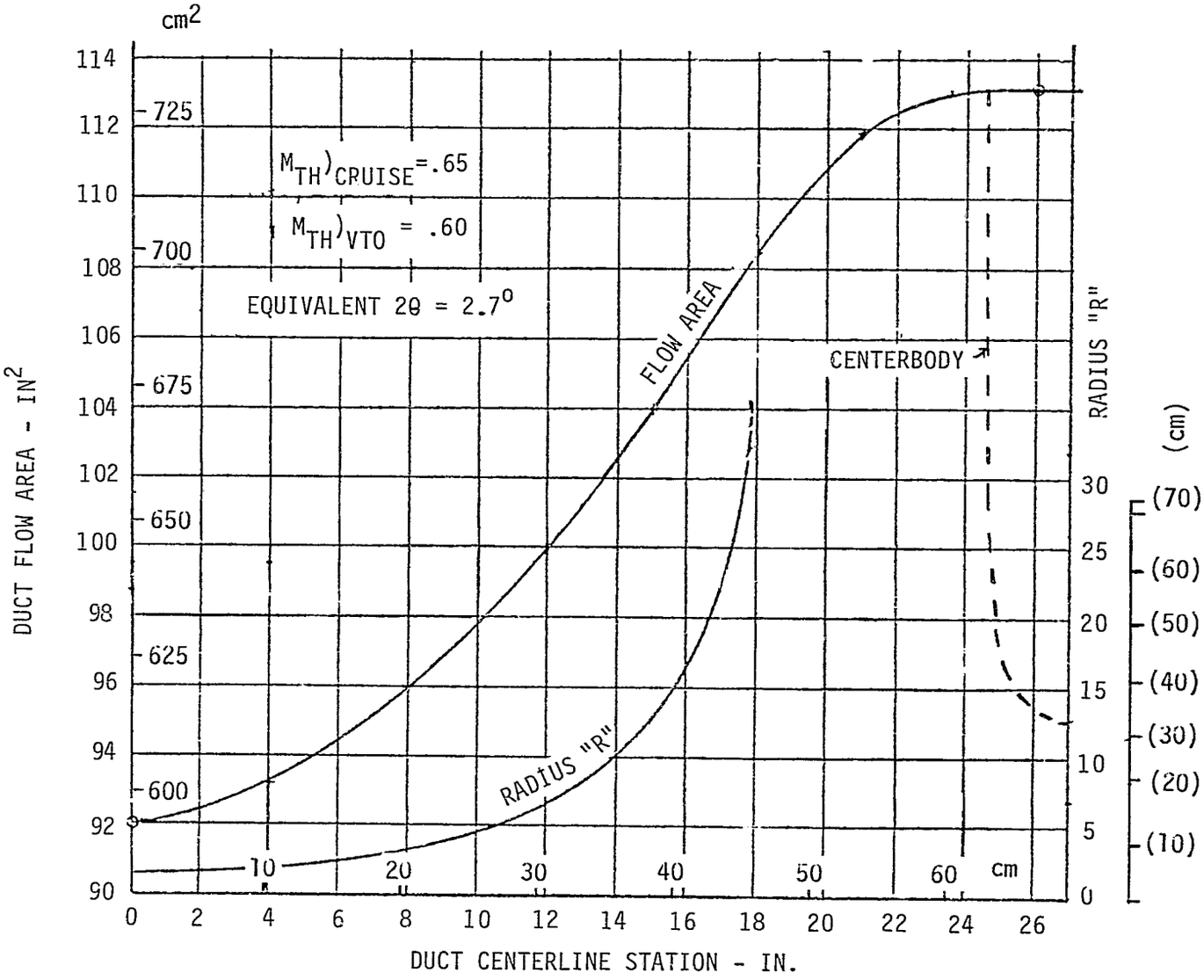

FIGURE 7 AFT INLET DIFFUSER DESIGN

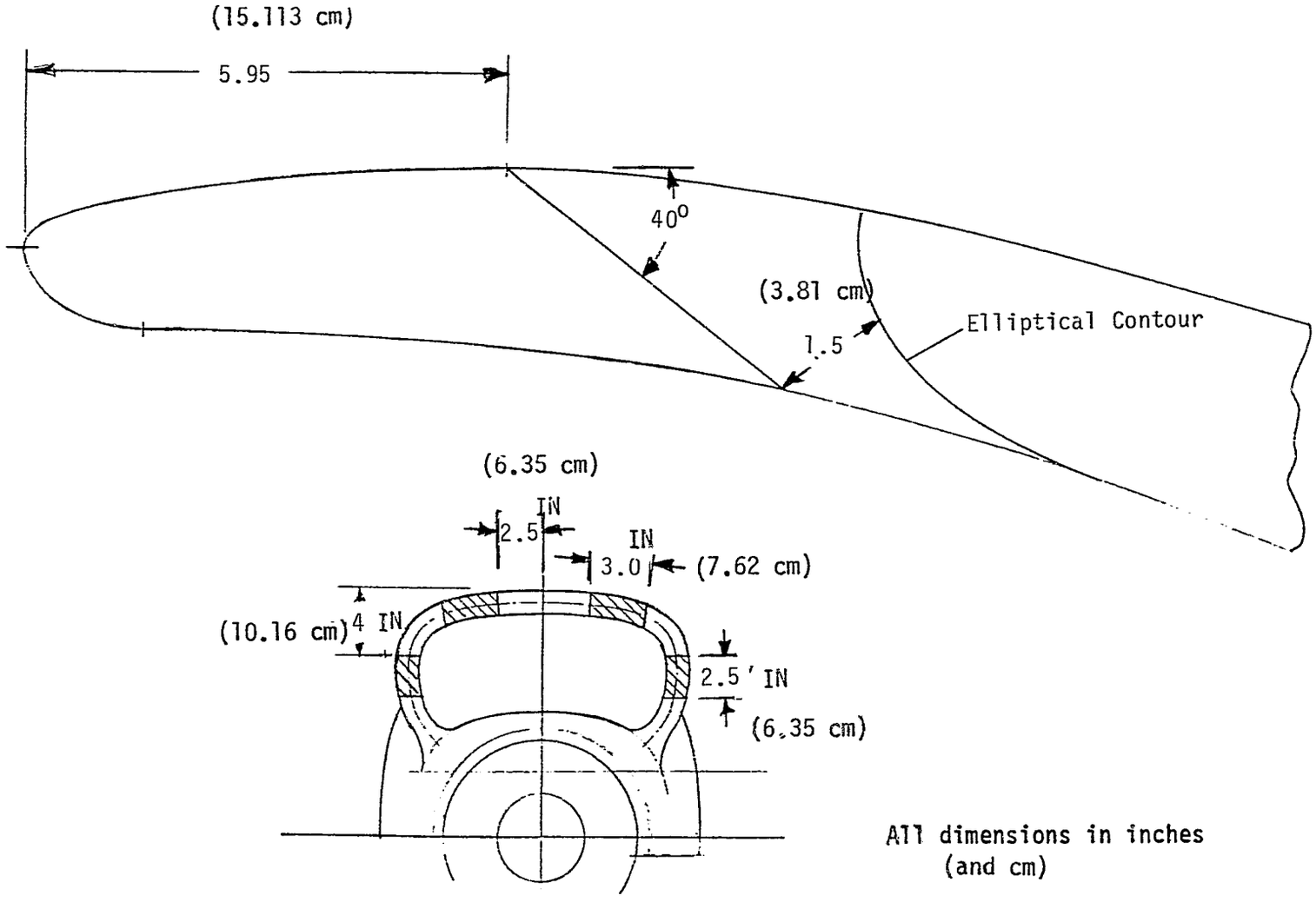

FIGURE 8 BLOW-IN DOOR GEOMETRY

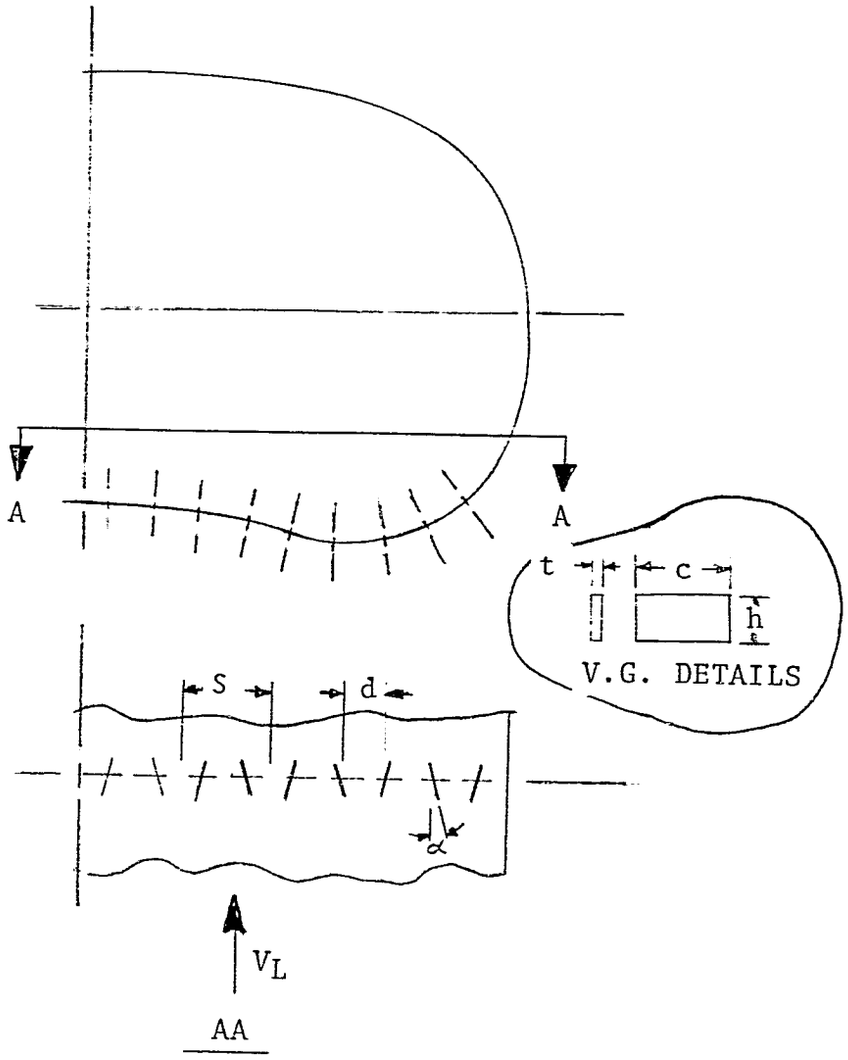

SELECTION OF V.G. LOCATION

- REGION OF MAX DUCT CURVITURE
- UPSTREAM OF MAX DUCT DIFFUSION

CONFIGURATION DETAILS

- HEIGHT ≈ LOCAL BOUNDARY LAYER HEIGHT
  $h = .25"$ (0.635 cm)
- UNIFORM SPACING
  $d/h = 3, S/d = 2$
- ANGLE OF ATTACK
  $\alpha = 16^{o}$
- RECTANGULAR SHAPE
  $c/h = 2$
- FLAT PLATE CONTOUR
  $t/c = .04$

FIGURE 9 VORTEX GENERATOR CONFIGURATION

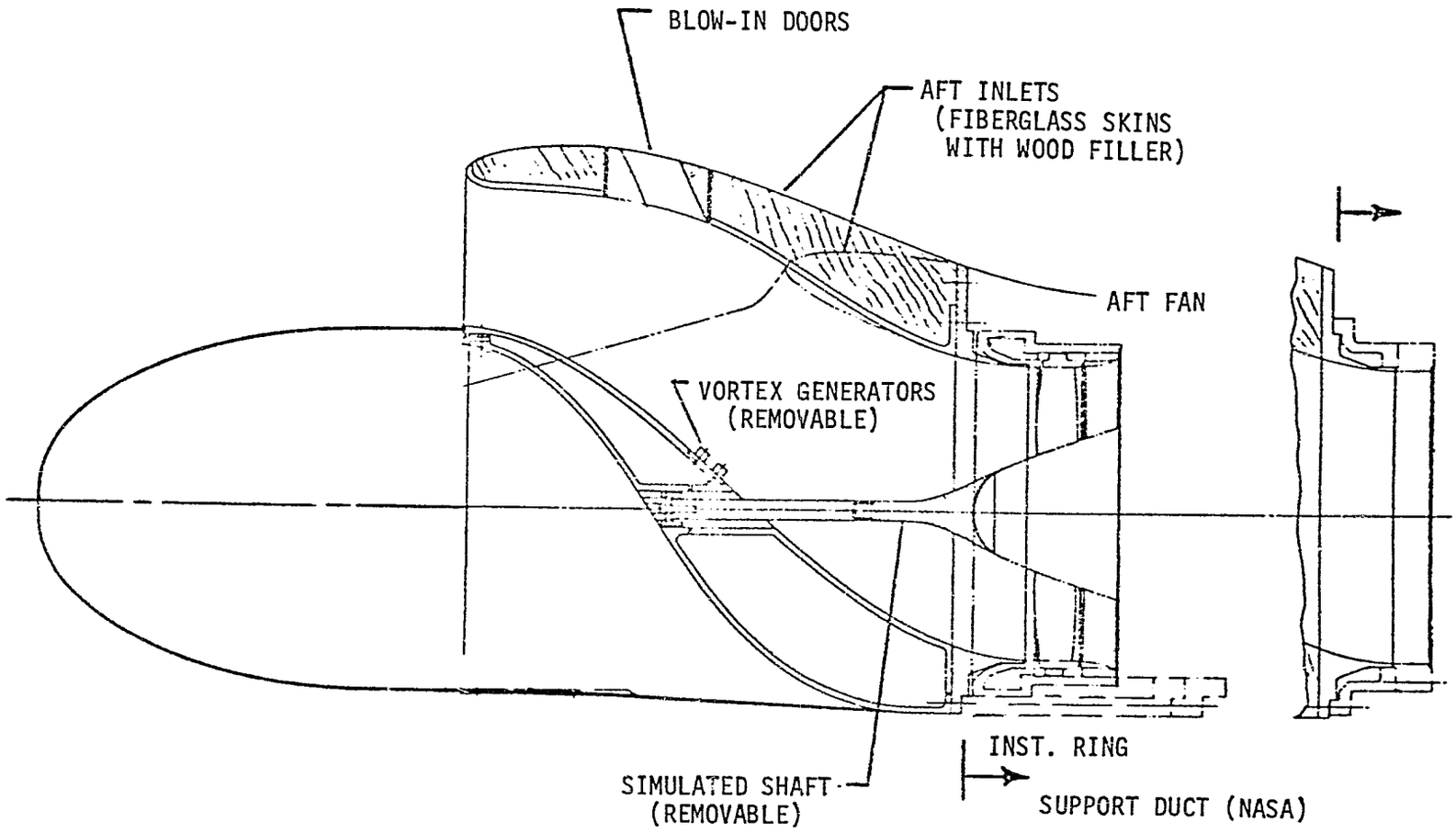

FIGURE 10 TANDEM FAN AFT INLET MODEL ASSEMBLY

Short Aft Inlet

An alternate aft inlet configuration was also fabricated for this test program. This inlet design incorporated a cut-back cowl which was developed as a means to reduce the nacelle profile drag and to improve pilot visibility over the wing and nacelle.

This inlet was also optimized to meet the design requirements of Table I and the high speed flight regime using a procedure similar to the one described for the long aft inlet. A contraction ratio (A_{HI}/A_{TH}) of 1.46 was required to satisfy the low speed requirements without blow-in door passages.

Lip shape studies were next performed using the data of references 2 and 3. These studies showed that the external lip shape and geometry should be the same as the long aft inlet design, namely: A forebody length ratio (X/D_{MAX}) of 0.3, a forebody diameter ratio (D_{HI}/D_{MAX}) of 0.91 and an external lip area ratio (A_{MAX}/A_{HI}) of 1.22. Figure 11 illustrates the predicted spillage drag levels of this inlet as a function of cruise mass flow ratio and Mach number for an external lip area ratio of 1.22. The cruise power mass flow ratio and spillage drag are shown in the figure for reference.

With the inlet contraction ratio and lip geometry selected, the inlet throat area was sized to provide maximum airflow during cruise flight at approximately a 0.57 throat mach number.

The overall diffuser lines for the aft inlet were established through analysis using the combined inlet flow analysis routine (reference 6). Figure 12 shows a schematic of the basic inlet lines. Figure 12 also shows the diffuser area distributions derived for the model.

Configuration Definition

Table II identified the various configurations which were tested by NASA Lewis Research Center. Configuration No. 1, without the simulated fan shaft, vortex generators and blow-in door passages, was defined as the baseline geometry for the evaluation.

TABLE II

AFT INLET CONFIGURATION DEFINITION

Configuration No.	Long Inlet	Short Inlet	Support Shaft	Vortex Generators	Blow-in Doors
1	X				
2	X				X
3	X			X	
4	X		X	X	
5		X			

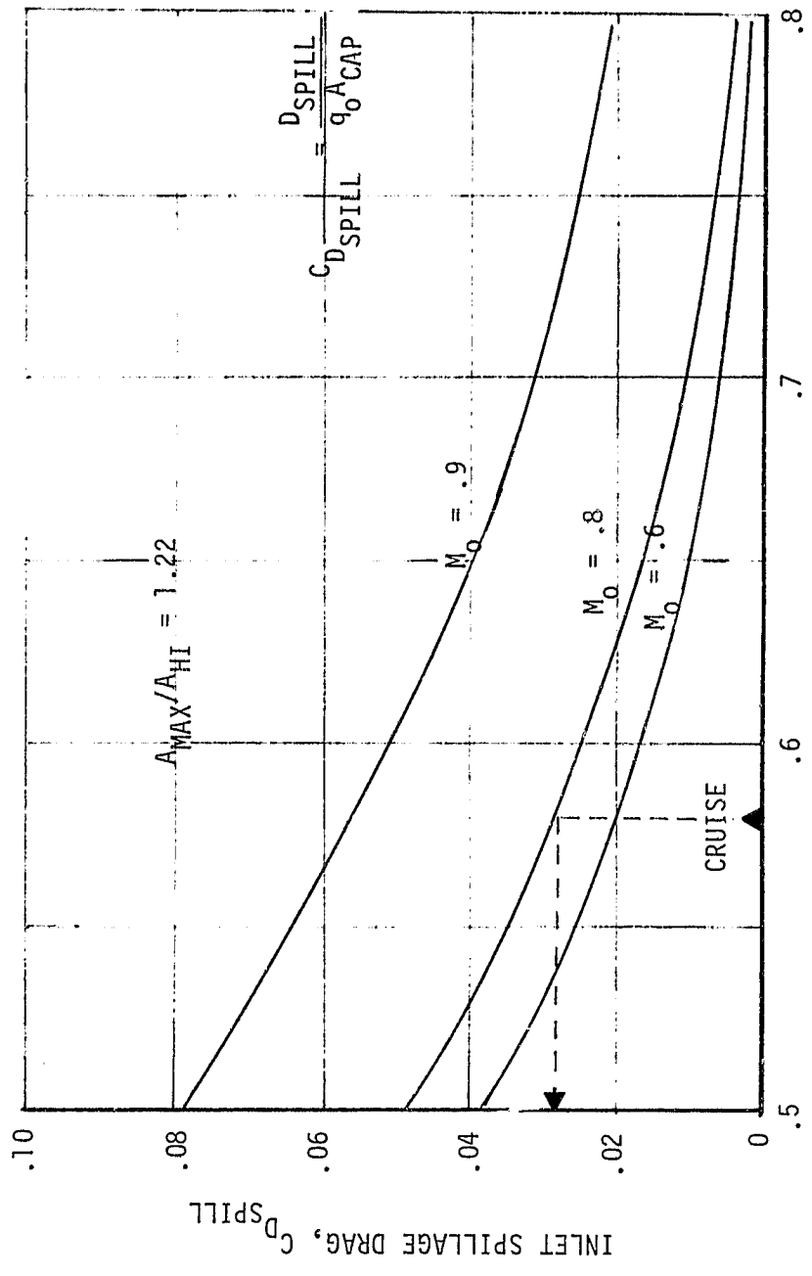

FIGURE 11 SHORT AFT INLET SPILLAGE DRAG CHARACTERISTICS

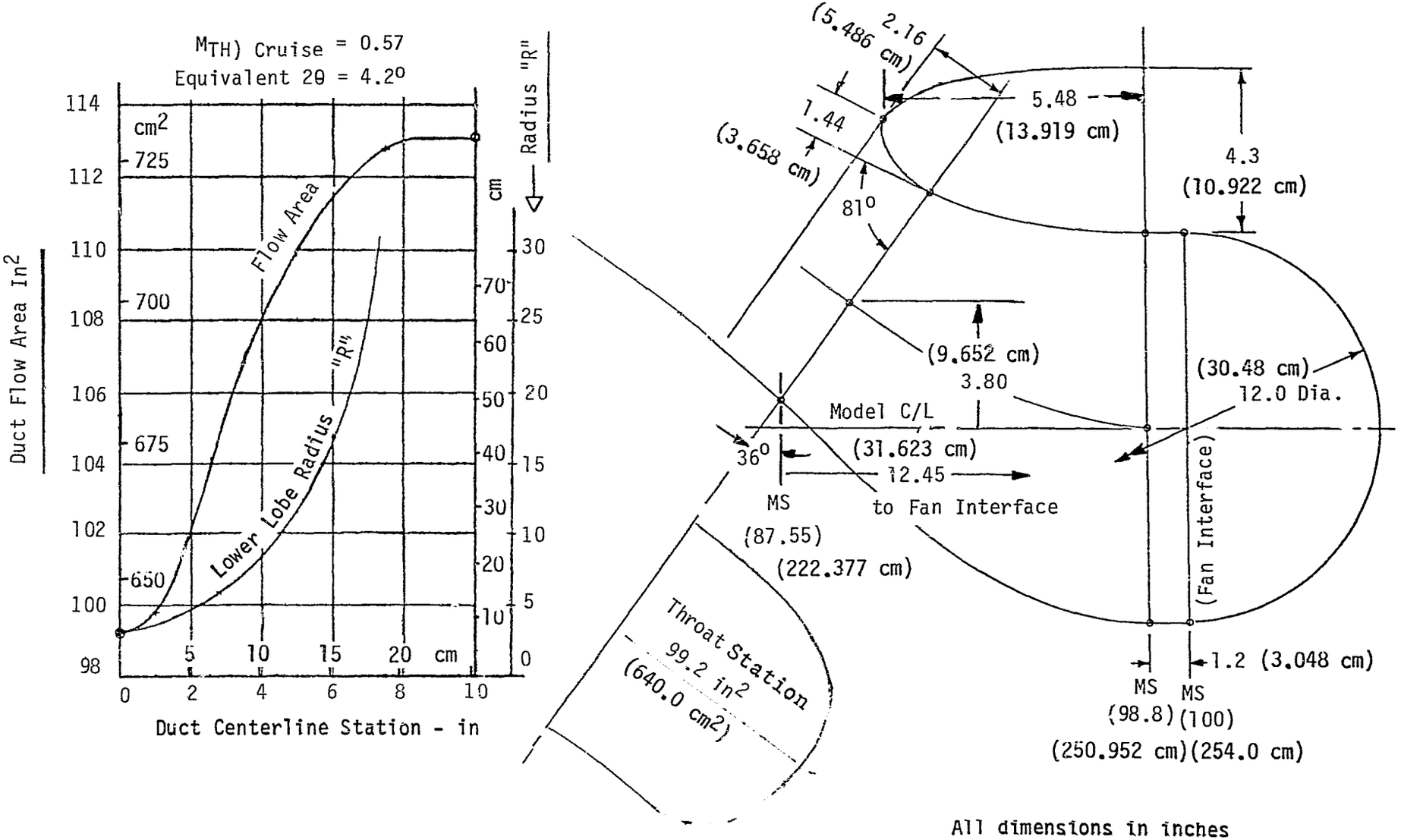

FIGURE 12 SHORT AFT INLET LINES AND DIFFUSER DESIGN

Turbofan Simulator

Fan engine airflow simulation was provided to the model by a 12 inch (.3048 meter) diameter, tip-driven, warm-air powered, turbofan which was designed and fabricated by Tech Development Inc. (Reference 2). Fan speed is controlled by the drive air to the tip turbine while fan back pressure is controlled by a variable exit area consisting of a hydraulically translated conical plug inside a fixed nozzle ring. The turbofan simulator, shown in Figure 13, was calibrated in the 10-by-10 foot (3.048-by-3.048 meter) wind tunnel during March of 1979. Figure 14 shows the fan performance as a function of fan pressure ratio, fan flow rate, fan corrected speed and exit area.

To conduct the aft inlet testing in the 10-by-10 foot (3.048-by-3.048 meter) tunnel an exit area (A_e) of 85 square inches (548.39 cm^2) was selected. Variations in fan flow rate (and inlet throat mach number) were obtained by varying fan corrected speed.

5.2 Instrumentation

The test model was instrumented extensively to provide detailed inlet aerodynamic performance data and to ensure safe operation of the propulsive nacelle. This section describes the model performance instrumentation which includes inlet and turbofan simulator parameters.

5.2.1 Inlet Instrumentation

The aft inlet cowl lip is provided with seven surface static taps at the top (0^0) and seven along the side (90^0) as shown in Figure 15. Diffuser static pressure instrumentation includes three rows of static taps equally spaced from the throat to the fan face, at the top (0^0), on the side (90^0) and along the bottom (180^0). In addition, four static pressure taps are located on the inlet cowl lip hilite as shown in Figure 15.

The short aft inlet configuration is provided with eight surface static taps at the top (0^0) and eight along the side (90^0) as shown in Figure 16. Diffuser instrumentation includes one tap in the duct at the top (0^0), two taps in the duct at 90^0;instrumentation along the bottom (180^0) consists of 8 static taps (5 taps located ahead of inlet throat and 3 taps equally spaced from throat to the fan face.) Three additional pressure taps are located on the cowl lip highlight as shown in Figure 16 .

5.2.2 Fan Instrumentation

The fan face rake has 8 arms spaced 45^0 apart. Each rake arm is provided with total pressure probes for measurement of steady state and dynamic pressures and flow angularity. Static pressure taps are located on the hub and tip surfaces alongside each rake arm. Figure 17 illustrates the fan face rake instrumentation for the 12-inch (30,48 cm) fan simulator.

Other fan simulator instrumentation recorded included fan exit total pressures and temperatures, fan exit static pressure and nozzle plug position, fan speed and stator pressure, fan drive air pressure and temperature. Turbine drive instrumentation included turbine exit total pressures, total temperature and static pressures.

COURTESY TECH DEV (REF 7)

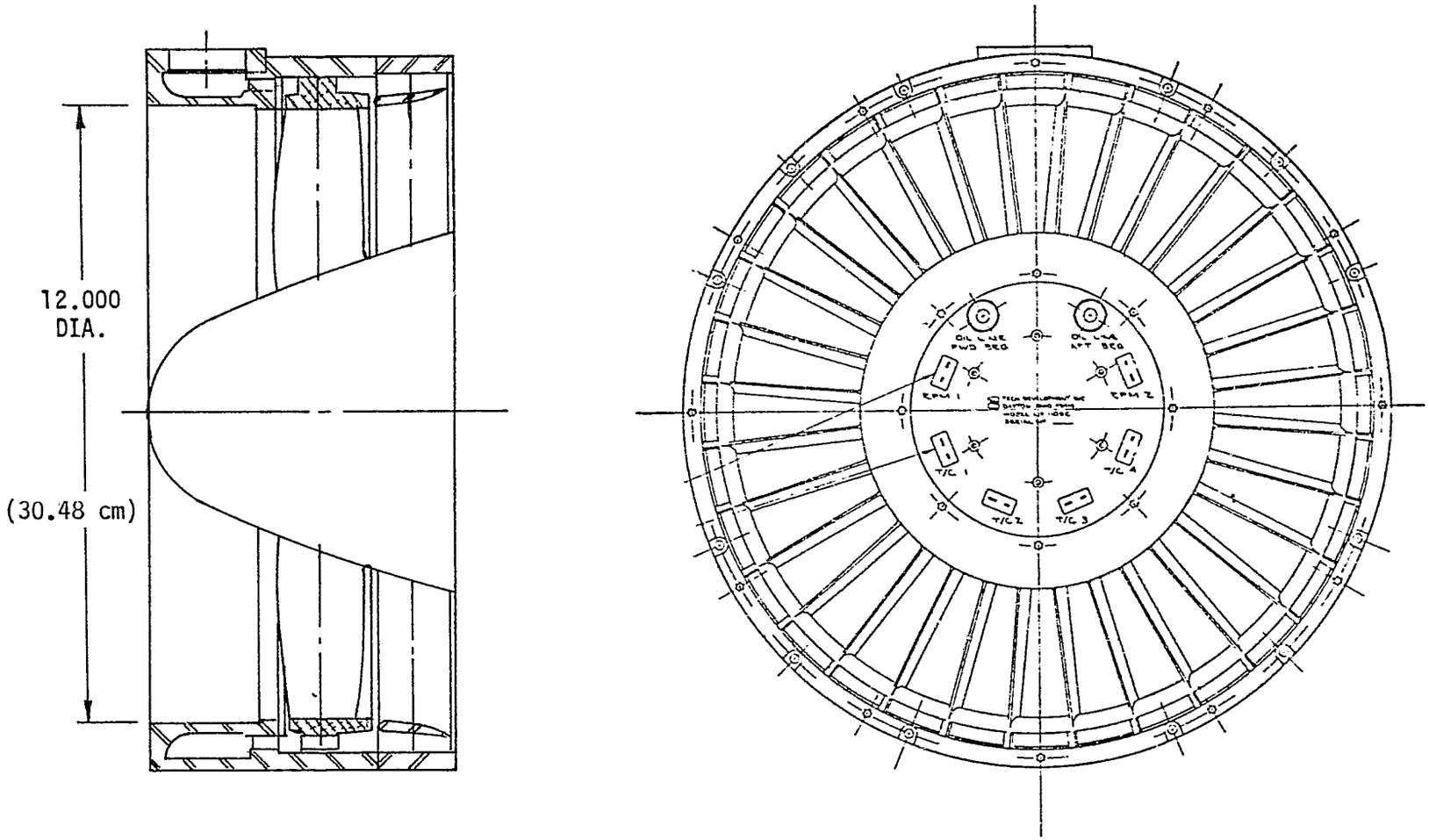

FIGURE 13 TWELVE-INCH POWERED SIMULATOR ASSEMBLY

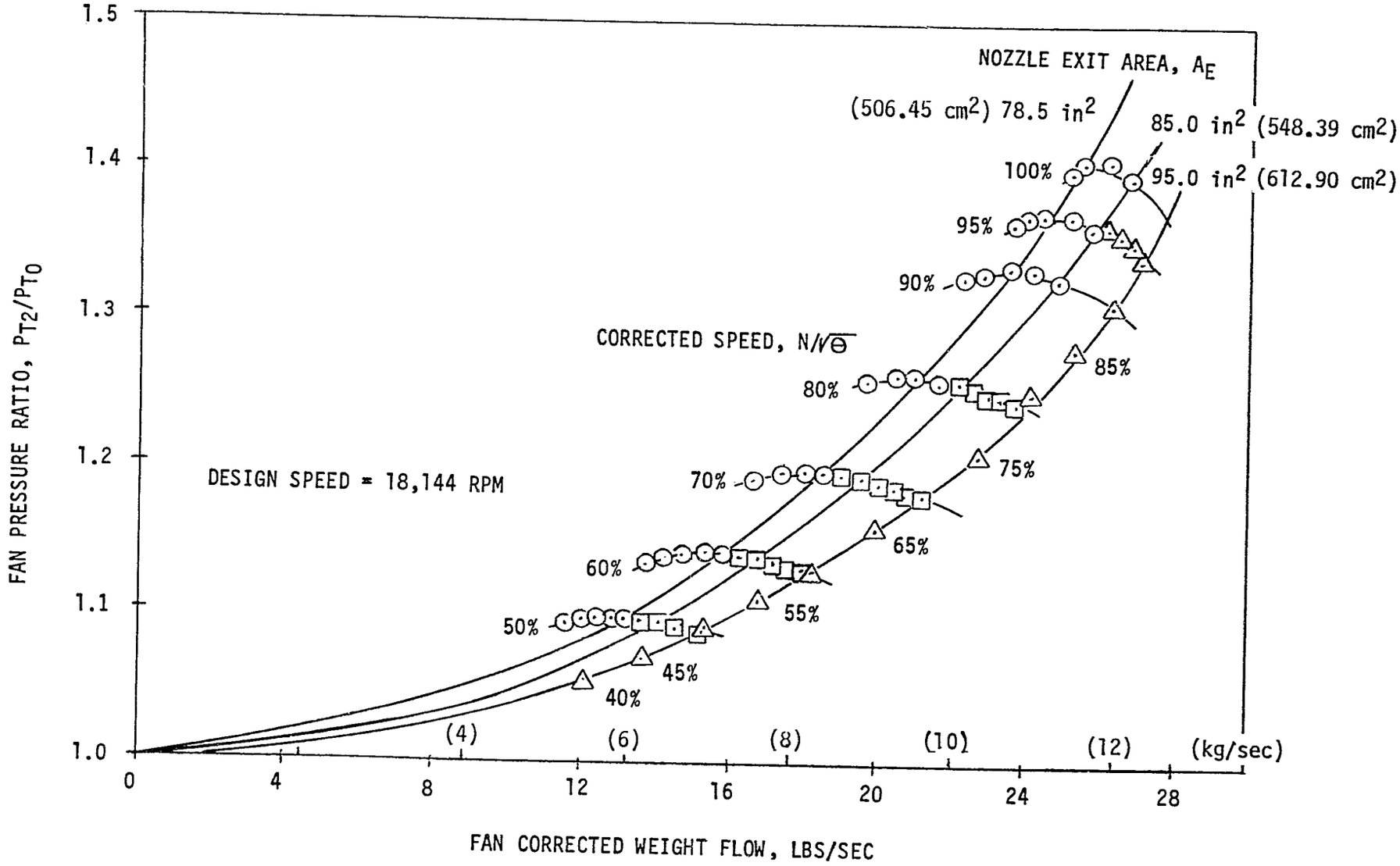

FIGURE 14 TWELVE-INCH POWERED FAN SIMULATOR CALIBRATION

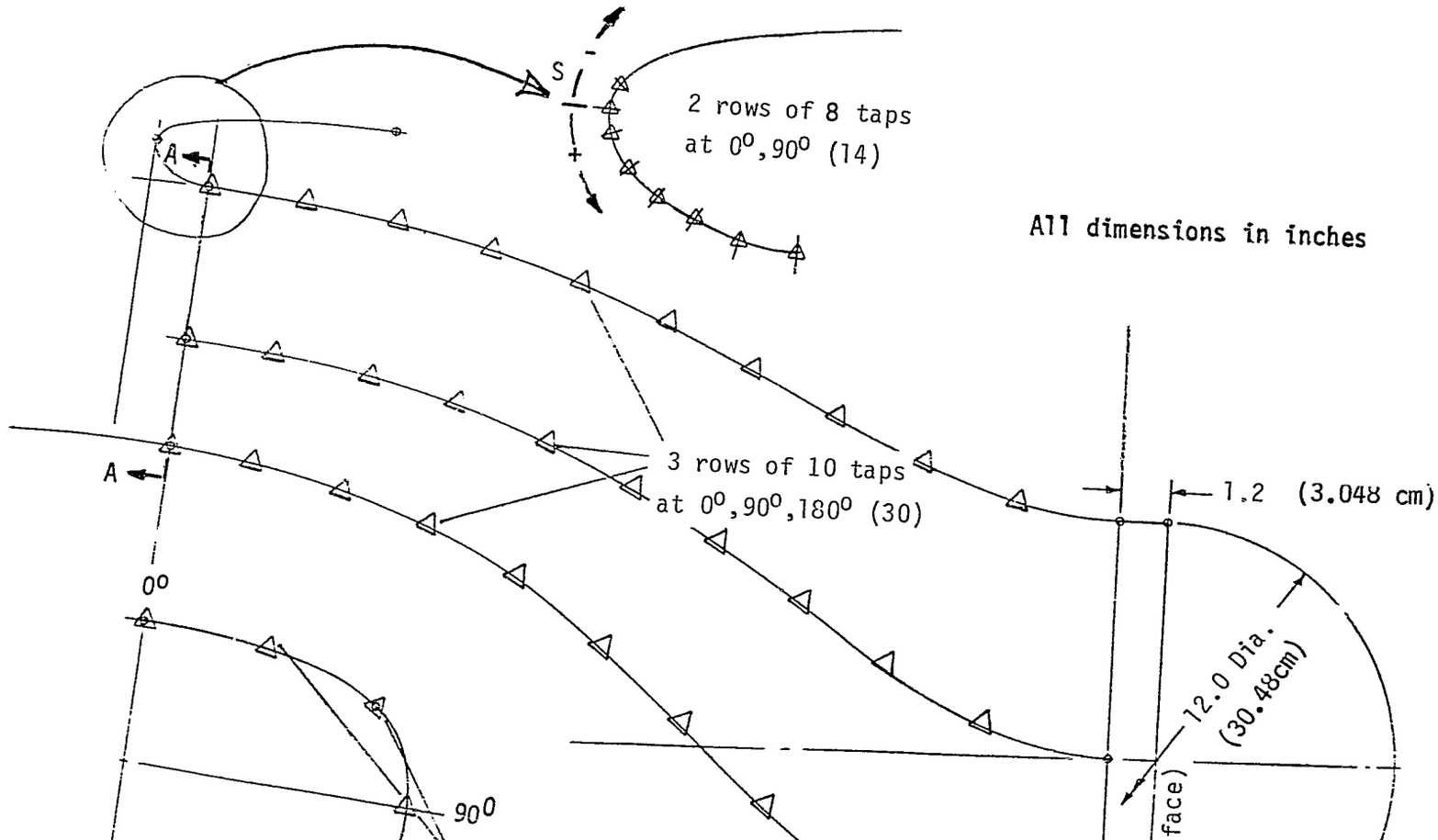

FIGURE 15 AFT INLET PRESSURE TAP LOCATIONS

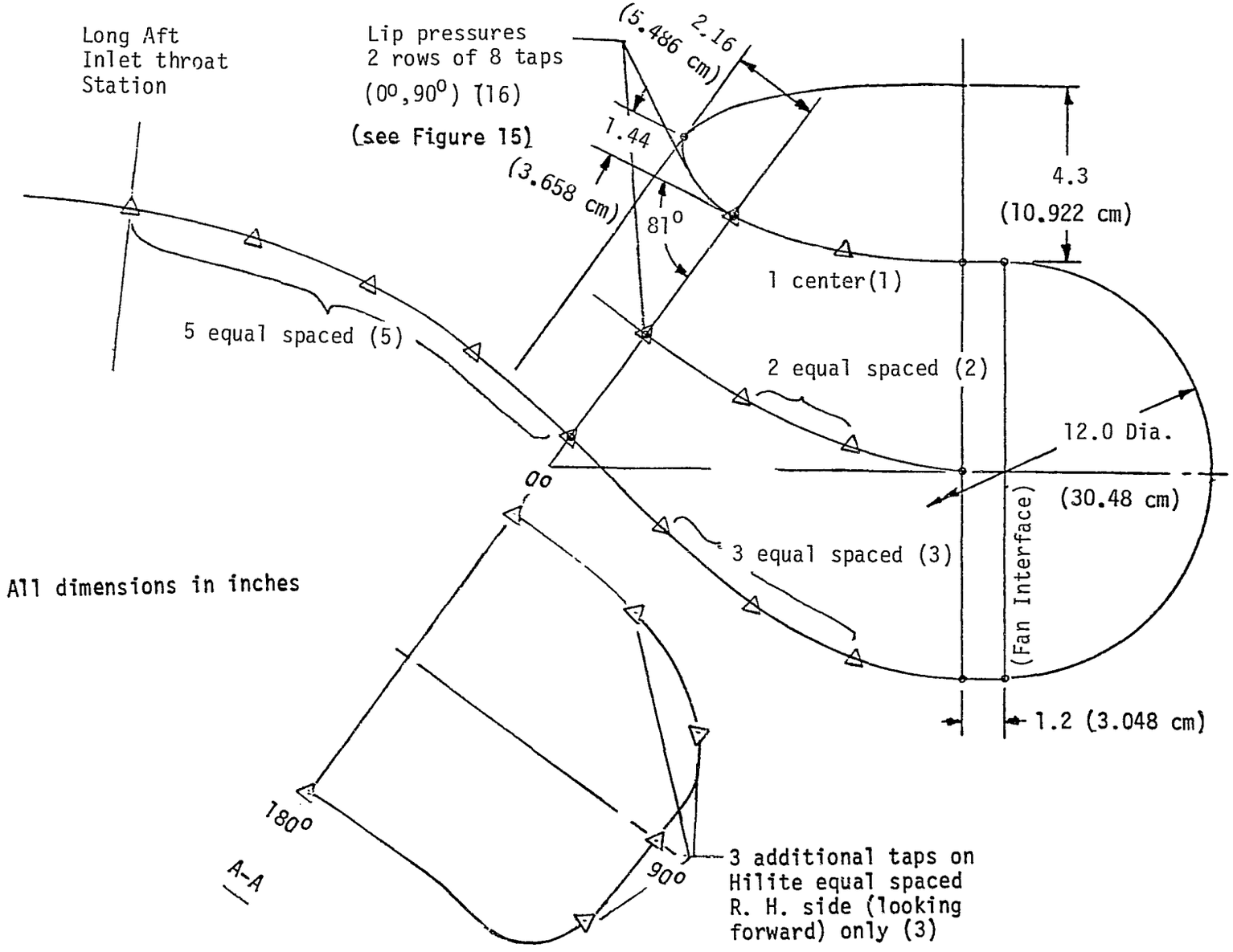

FIGURE 16 SHORT AFT INLET PRESSURE TAP LOCATIONS

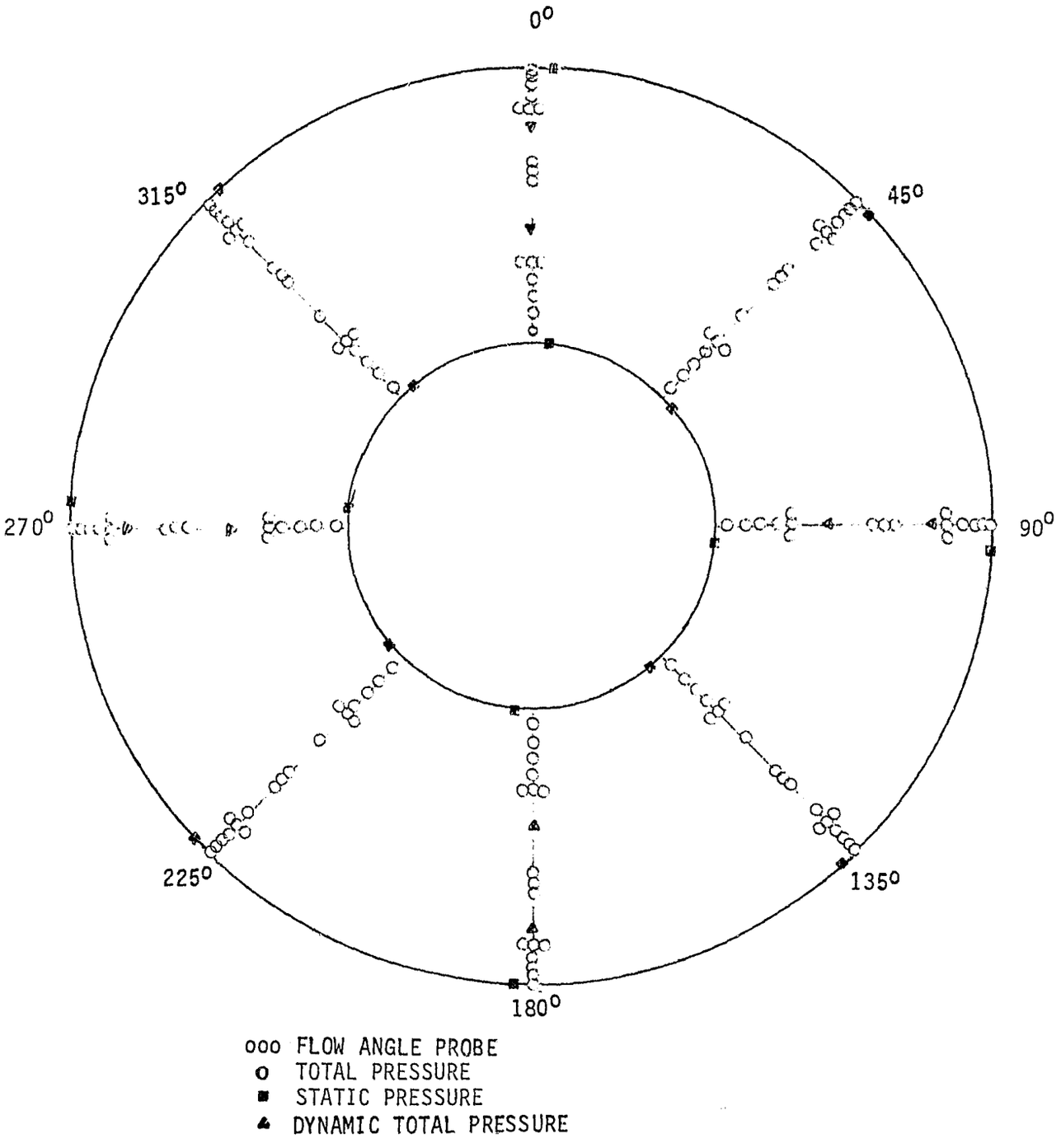

FIGURE 17 TWELVE-INCH FAN SIMULATOR INSTRUMENTATION RAKE AT FAN FACE

5.3 Test Facility

The test program was conducted in the NASA Lewis Research Center 10-by-10 foot (3.049-by-3.048 meter)wind tunnel. A schematic of the model installed in the test section is shown in Figure 18. As shown in the figure the model was cantilevered on the end of the support sting which in turn was attached to the tunnel main support strut. The sting rotation point was located so that the forward part of the nacelle model was always visible, even at angle of attack. The nacelle model was mounted upside down for testing to minimize interference with the flow adjacent to the tunnel walls.

5.4 Test Conditions and Prodedures

Nacelle operating conditions simulated during this test are summarized in Table III in terms of tunnel velocity, nacelle angle of attack, and aft inlet throat Mach number and configuration.

TABLE III

TANDEM FAN NACELLE TEST CONDITIONS

Aft Inlet Configuration Number	Tunnel Velocity V_o - Kts	Nacelle Angle of Attack α - degrees	Aft Inlet Throat Mach Number, M_{TH}
1, 2, 3, 4, 5	0	0	.2, .3, .4, .5, .6
1, 2, 3, 4, 5	35	-10	.2, .3, .4, .5, .6
1, 2, 3, 4, 5	(18 m/s)	0	.2, .3, .4, .5, .6
1, 2, 3, 5		10	.2, .3, .4, .5, .6
1, 2, 3, 4, 5		20	.2, .3, .4, .5, .6
1, 2, 3, 5		30	.2, .3, .4, .5, .6
1, 2, 3, 4, 5		40	.2, .3, .4, .5, .6
1, 2, 3, 4, 5	85	-10	.2, .3, .4, .5, .6
1, 2, 3, 4, 5	(43.7 m/s)	0	.2, .3, .4, .5, .6
1, 2, 3, 5		10	.2, .3, .4, .5, .6
1, 2, 3, 4, 5		20	.2, .3, .4, .5, .6
1, 2, 3, 5		30	.2, .3, .4, .5, .6
1, 2, 3, 4, 5		40	.2, .3, .4, .5, .6
1, 2, 3, 4, 5	135 (69.5 m/s)	-10	.2, .3, .4, .5, .6
1, 2, 3, 4, 5		0	.2, .3, .4, .5, .6
1, 2, 3, 5		10	.2, .3, .4, .5, .6
1, 2, 3, 4, 5		20	.2, .3, .4, .5, .6
1, 2, 3, 5		30	.2, .3, .4, .5, .6
1, 2, 3, 4, 5		40	.2, .3, .4, .5, .6
4	240 (123.5 m/s)	0	.27 to .44 @ ΔMth - .015
5	240 (123.5 m/s)	0	.23 to .40 @ ΔMth - .015

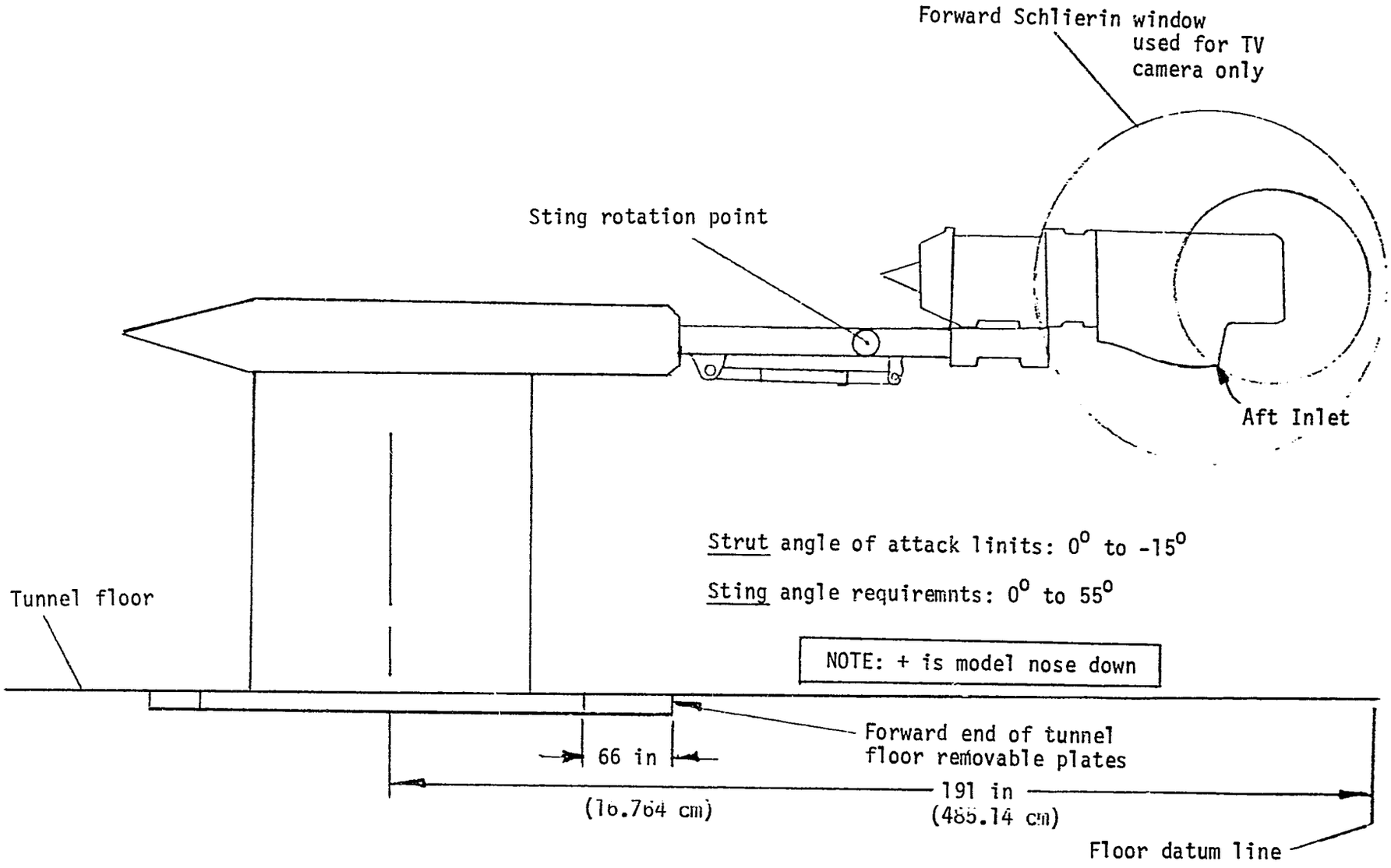

FIGURE 18 TANDEM FAN MODEL TUNNEL INSTALLATION

The test was conducted using the following procedure:

(1) The Tandem Fan nacelle model was assembled to form configuration No. 1.

(2) The wind tunnel flow conditions were established.

(3) The model was pitched to the desired angle of attack.

(4) The turbofan simulator was operated at various fan speeds and pressure ratios necessary to establish the desired inlet flow rates (throat Mach numbers) and data was recorded.

(5) Steps (3) and (4) were repeated at each angle of attack.

(6) Steps (2), (3), (4), (5) were then repeated for each tunnel condition required.

(7) Steps (1) through (7) were repeated for configurations 2, 3, 4 and 5.

5.5 Data Reduction and Presentation

Model and simulator instrumentation data were recorded by the Lewis Research Center's Central Automatic Digital Data encoder and simultaneously recorded and analyzed by a time-sharing digital computer system. A large amount of pressure data was recorded by the digital data encoder using eight automatic scanning valves each having 48 ports.

On-line data consisted digital displays to monitor and ensure safe operation of the fan simulator.

Quick-Look off-line data were processed on the Lewis computer to provide maximum test visibility and test performance. Final data and computer plots were processed at Lewis on the computer.

The data recorded from the test was reduced by the computer to the following parameters:

Inlet

- Surface static pressure ratio and Mach number distributions
- Weight flow and throat Mach number

Fan

- Fan face total pressure ratios and pressure recovery
- Fan face weight flow and Mach number
- Fan face total pressure distortion (MAX - MIN, KD_2, $K\Theta$, IDC, IDR, DC60)

- Fan face flow angles
- Fan face total pressure contour plots
- Fan corrected speed, pressure ratio and horsepower

Turbine

- Turbine weight flow, pressure ratio and turbine horsepower.

6.0 TEST RESULTS

The following paragraphs present the inlet performance data obtained from the test. The first paragraphs (6.1 through 6.5) describe the test results for the individual configurations in terms of total pressure recovery, steady state pressure distortion, RMS pressure levels, fan face total pressure contour maps, and static pressure distributions in the inlet as a function of tunnel speed, model attitude and inlet flow rate. Paragraph 6.6 presents the performance comparisons of the five configurations in terms of pressure recovery, steady state pressure distortion and RMS pressure levels as a function of tunnel speed, model attitude and inlet flow rate. A summary of the fan face pressure recovery and steady state distortion levels for the various configurations is contained in Table IV.

Individual inlet performance levels for the aft inlet configuration are presented in Figures 19 to 40. The total pressure recovery (P_{TAV}/P_{TO}) in the figures is the area weighted average pressure computed from the 40 probe rake at the fan face station, Section 5.2 divided by the freestream total pressure. The distortion level (DPT/PTAV) is computed as the difference between the maximum and minimum pressures in the 40 probe array divided by the average. The turbulence level (RMS/PTAV) is defined as the arithmetic average of root-mean-square values from the eight dynamic probes (Section 5.2 divided by the average total pressure. These data are plotted as functions of inlet throat Mach number and (inlet mass flow rate) which were controlled by the turbofan simulator.

The static pressure distribution along three inlet "streamlines" are also presented for two inlet throat mach numbers. The pressure ratio is formed by dividing the local static pressure by the freestream total pressure. The pressure ratios are plotted as a function of the surface distance from the inlet lip hilite, with positive being downstream. The three streamlines begin at the inlet outer (top) lip, the side lip, and along the lower ramp surface.

Fan face station total pressure contour plots are presented for the same tunnel and inlet conditions as the static pressure distributions. These plots are oriented with the inlet on top looking downstream.

Fan face flow angularity data when plotted for the same inlet and tunnel conditions as the other data showed no particular trends and only a few plots are included in the reported results.

6.1 Long Aft Inlet

The inlet performance for the basic long aft inlet design is presented in Figures 19 through 22, for freestream velocities of 0, 35, 85, and 135 Kts.(0,18, 43.7, and 69.5 m/s). Fan face pressure contours and inlet static pressure distributions are presented for throat Mach numbers of .490 and .296 in Figure 19 and V_o=0 kts and α= 0°, Note the scale change in the static pressure distributions. The highest velocity at the inlet highlight occurs along the side wall streamline. The flow along the lower ramp surface initially accelerates and then diffuses as it approaches the fan face. The flow along the top surface diffuses rapidly just downstream of the lip and then accelerates slightly just in front of the fan face station. The side surface streamline falls in between the other two streamline distributions.

TABLE IV

DATA SUMMARY - RECOVERY/DISTORTION
FOR TANDEM FAN AFT INLET (ISOLATED)

Flight Condition			Long Aft Inlet				Short Aft Inlet (5)
Freestream Velocity Kts	Angle of Attack Deg.	Throat Mach No.	Basic (1)	Blow-in Door (2)	Vortex Generator (3)	V.G.+ Shaft (4)	
0 (0 m/s)	0	.5	.989/.048	.982/.061	.988/.049	.988/.049	.998/.013
		.3	.994/.019	.992/.025	.995/.019	.994/.020	.999/.004
35 (18 m/s)	0	.5	.988/.050	.983/.055	.989/.048	.988/.048	.997/.014
	40		.989/.048	.982/.056	.988/.055	.987/.056	.994/.041
85 (43.7 m/s)	0	.5	.984/.066*	.983/.055	.989/.049	.988/.046	.996/.030
	40	.5	.987/.055	.982/.064	.986/.057	.985/.053	.985/.095
135 (69.5 m/s)	0	.5	.989/.045	.983/.053	.990/.050	.989/.046	.997/.025
	40	.5	.981/.069	.977/.065	.978/.066	.978/.072	.979/.111
240 (123.5 m/s)	0	.4				.993/.037	.996/.042

*M_{TH} = .588

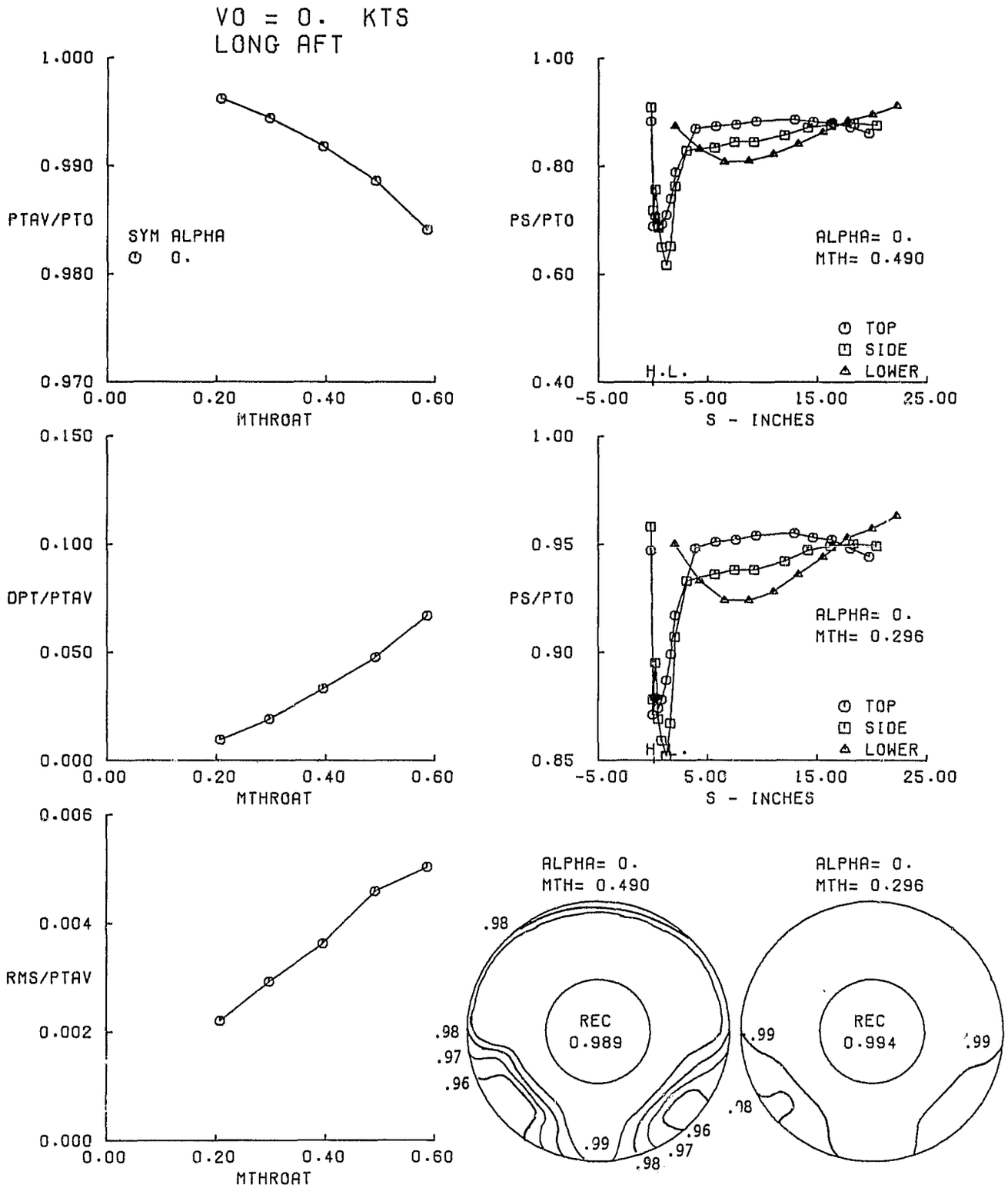

FIGURE 19 LONG AFT INLET PERFORMANCE AT V_o = 0 KNOTS

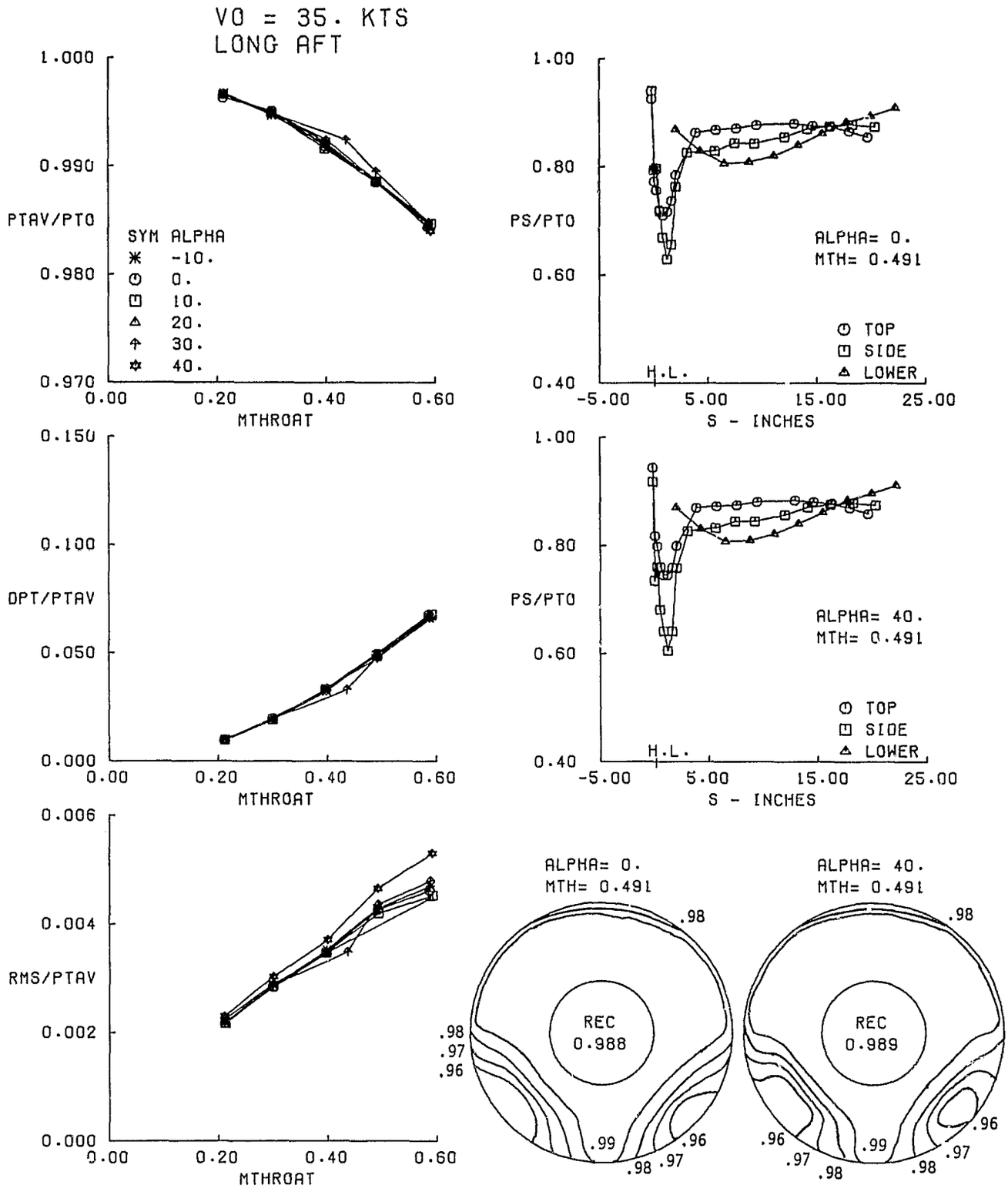

FIGURE 20 LONG AFT INLET PERFORMANCE AT V_0 = 35 KNOTS

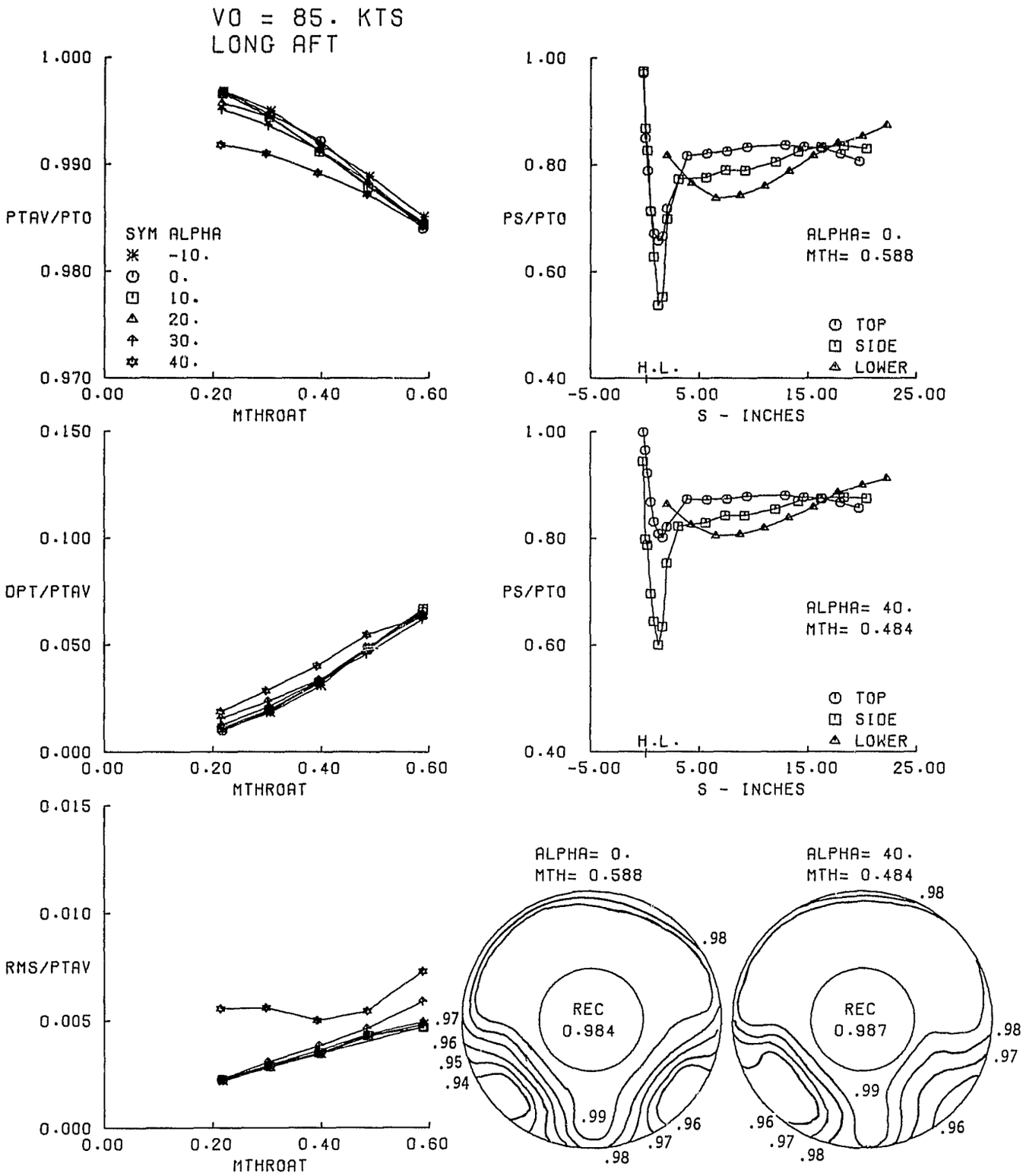

FIGURE 21 LONG AFT INLET PERFORMANCE AT V_o = 85 KNOTS

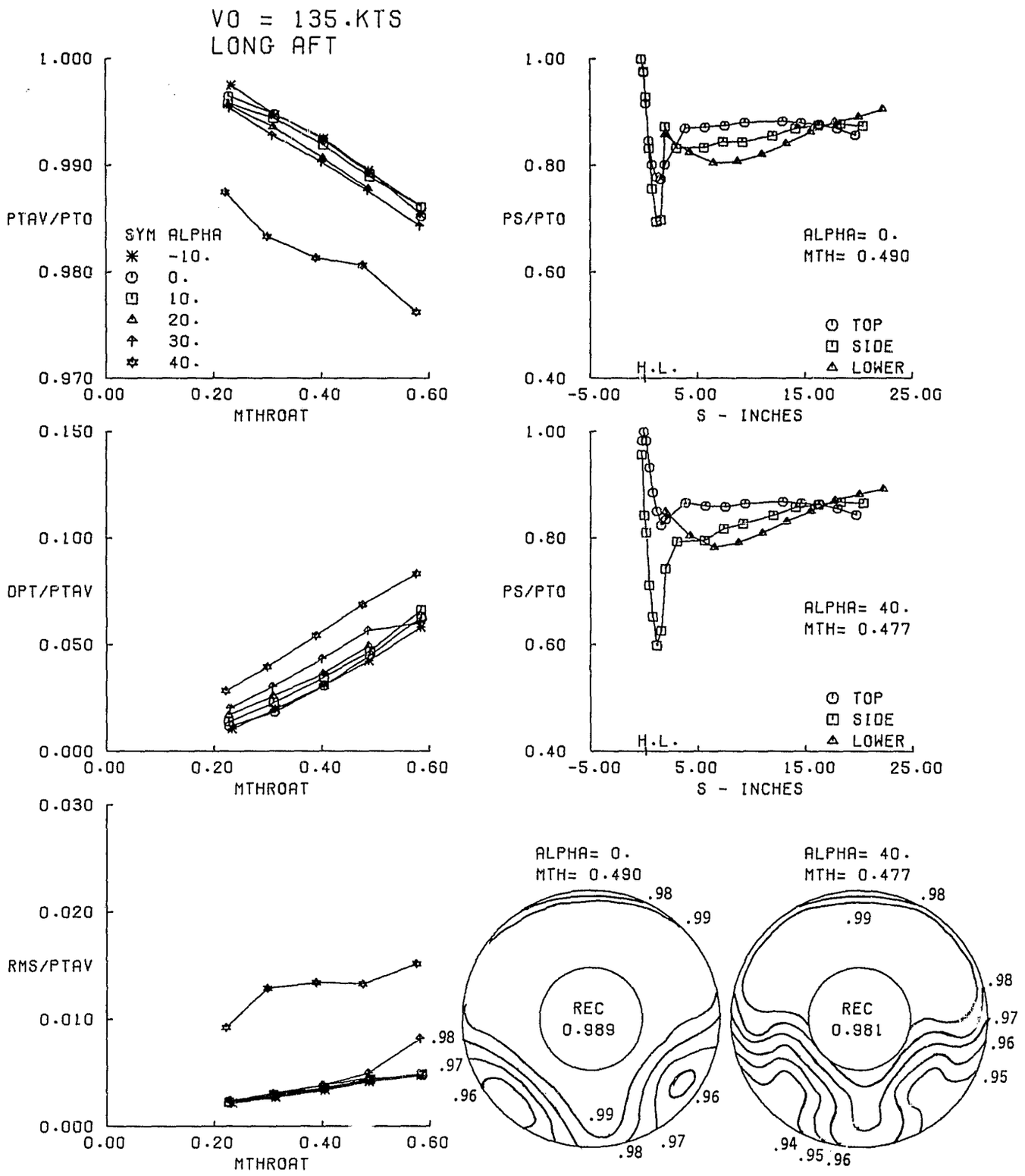

FIGURE 22 LONG AFT INLET PERFORMANCE AT V_0 = 135 KNOTS

The recovery levels remain essentially unchanged as forward speed was increased to 35 Kts (18 m/s), 85 Kts (43.7 m/s) and 135 Kts (69.4 m/s), Figures 20, 21 and 22, and angle of attack was increased to 10°, 20° and then 30°. At an angle of attack of 40° however, the pressure recovery decreases and the distortion and turbulence level increase at forward speeds of 85 Kts (43.7 m/s) and 135 Kts (69.5 m/s), Figures 21 and 22.

Note also that at the $\alpha = 40°$ condition the velocity at the inlet lip increases at the side and decreases at the top. The distortion pattern at the fan face remains essentially unchanged, increasing only slightly in pressure decay.

6.2 Long Aft Inlet with Blow-in Doors

The test results for the long aft inlet with the four blow-in door passages open are shown in Figures 23, 24, 25, and 26. The pressure recovery levels are slightly (0.1%) lower than for the basic long aft inlet and the distortion levels are slightly greater. Also note that the regions of low recovery extend further along the sides, and a small low pressure region at the top has also appeared. The presence of the blow-in door passages is also reflected in the static pressure distributions. The velocity at the inlet lip is more uniform between the top and side at $\alpha = 0°$ than for the basic long aft inlet. The blockage in the duct caused by the auxilary air entering through the door passages generates higher static pressures on the top and side upstream of the door locations and also causes higher velocities downstream of the door locations when compared to the basic long inlet pressure distributions. At $\alpha = 40°$, the velocity at the inlet lip along the side is higher than along the top of the inlet lip, which also was observed with the door passages closed (basic long aft inlet). The static pressure distributions in Figure 23 through 26 all show a reduction in lip velocity (lip loading) when compared to the basic aft inlet distributions which is indicative of blow-in door configurations.

6.3 Long Aft Inlet with Vortex Generators

Figures 27, 28, 29 and 30 show the basic performance data for the long aft inlet with the lower surface vortex generators installed. The principal effect of the vortex generators is to redistribute the low pressure region further up along the sides and reduce the extent from the outer wall. The static pressure distributions, remain essentially unaffected when vortex generators are installed.

6.4 Long Aft Inlet with Vortex Generators and Shaft

The front inlet fan is driven by a shaft that extends through the aft inlet duct. A stationary shaft was installed to simulate the front fan drive shaft, Figure 10. Test results for this long aft inlet configuration, including presence of vortex generators, are shown in Figures 31, 32, 33, 34, and 35. The pressure recovery and distortion levels are only slightly lower than for the basic long aft inlet. For the conditions shown in the Figures where throat mach number equals approximately 0.49, the low pressure region observed at the fan face of the basic long aft inlet has been modified so that it extends to the fan centerbody below the shaft. Note that this condition does not exist at the lower throat mach

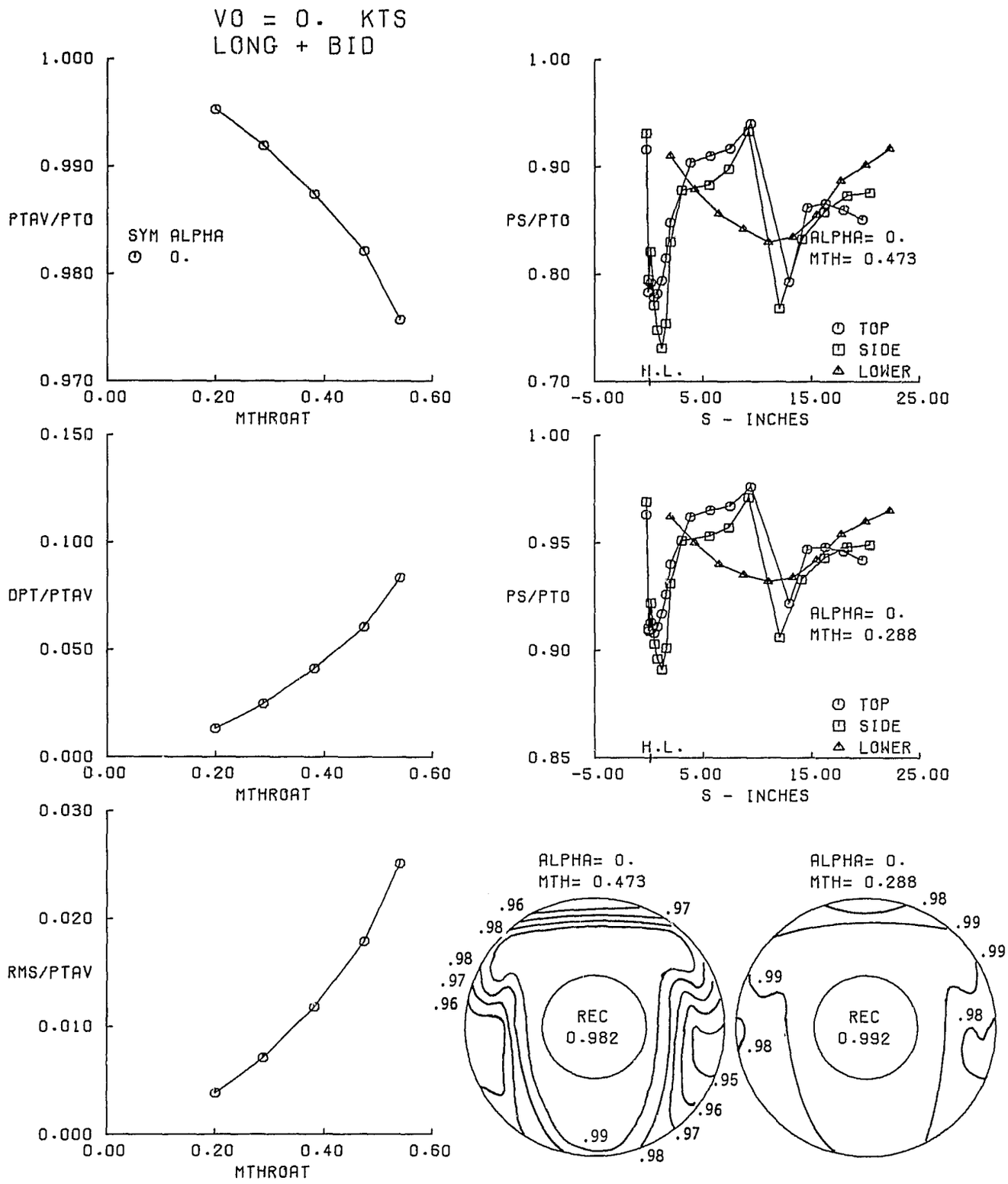

FIGURE 23 LONG AFT INLET WITH BLOW-IN DOORS PERFORMANCE AT V_o = 0 KNOTS

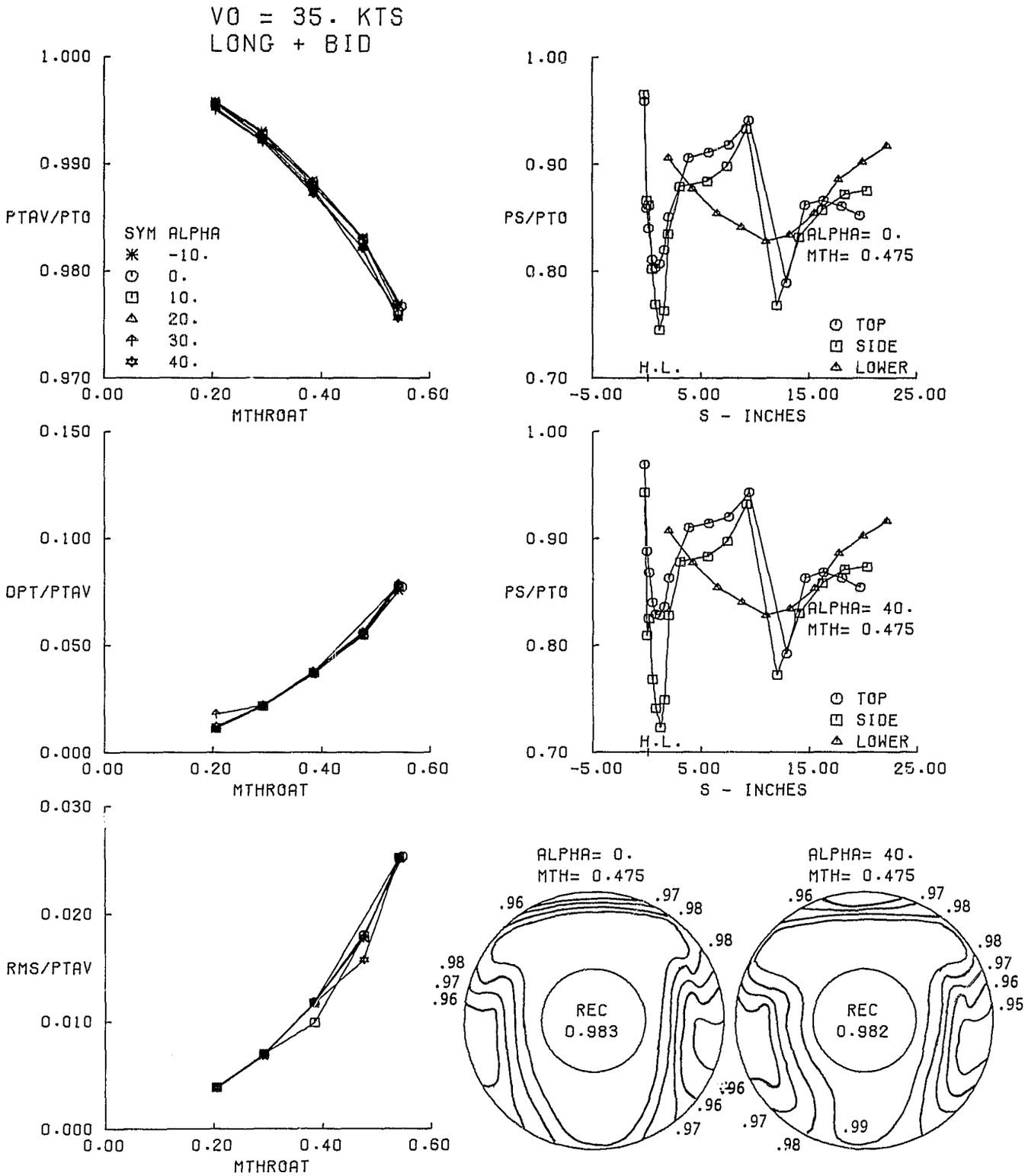

FIGURE 24 LONG AFT INLET WITH BLOW-IN DOORS PERFORMANCE AT V_0 = 35 KNOTS

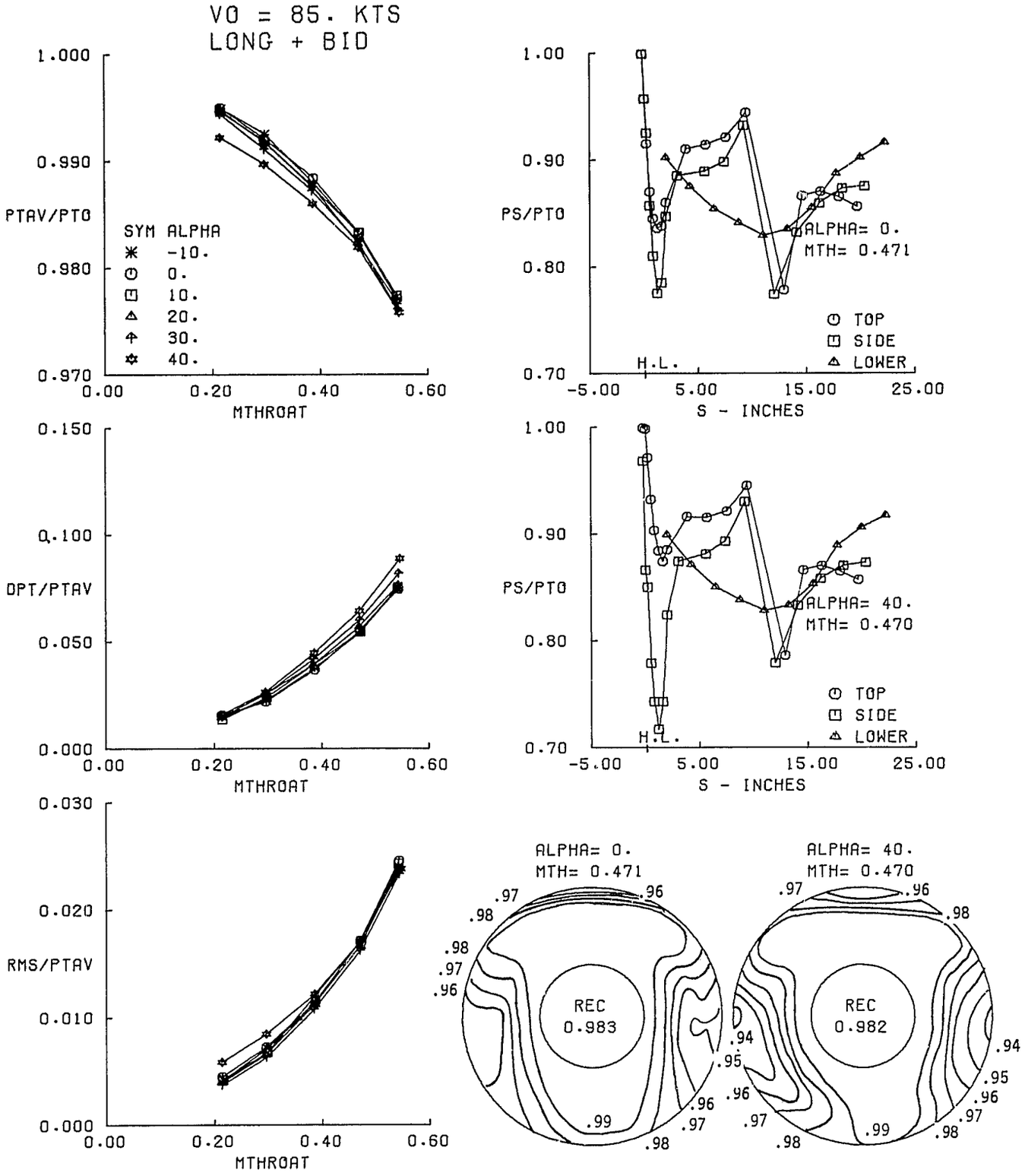

FIGURE 25 LONG AFT INLET WITH BLOW-IN DOORS PERFORMANCE AT V_0 = 85 KNOTS

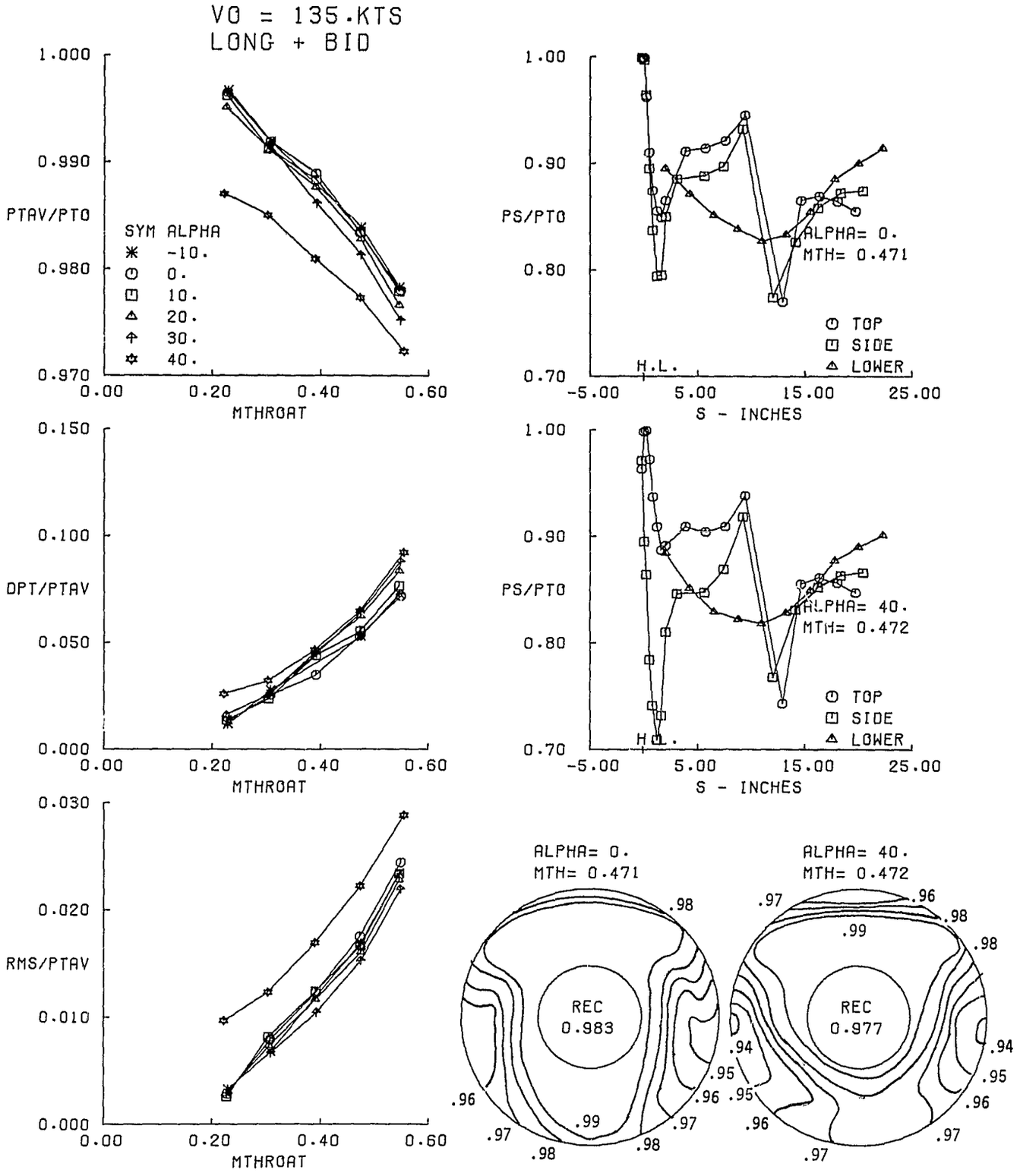

FIGURE 26 LONG AFT INLET WITH BLOW-IN DOORS PERFORMANCE AT V_0 = 135 KNOTS

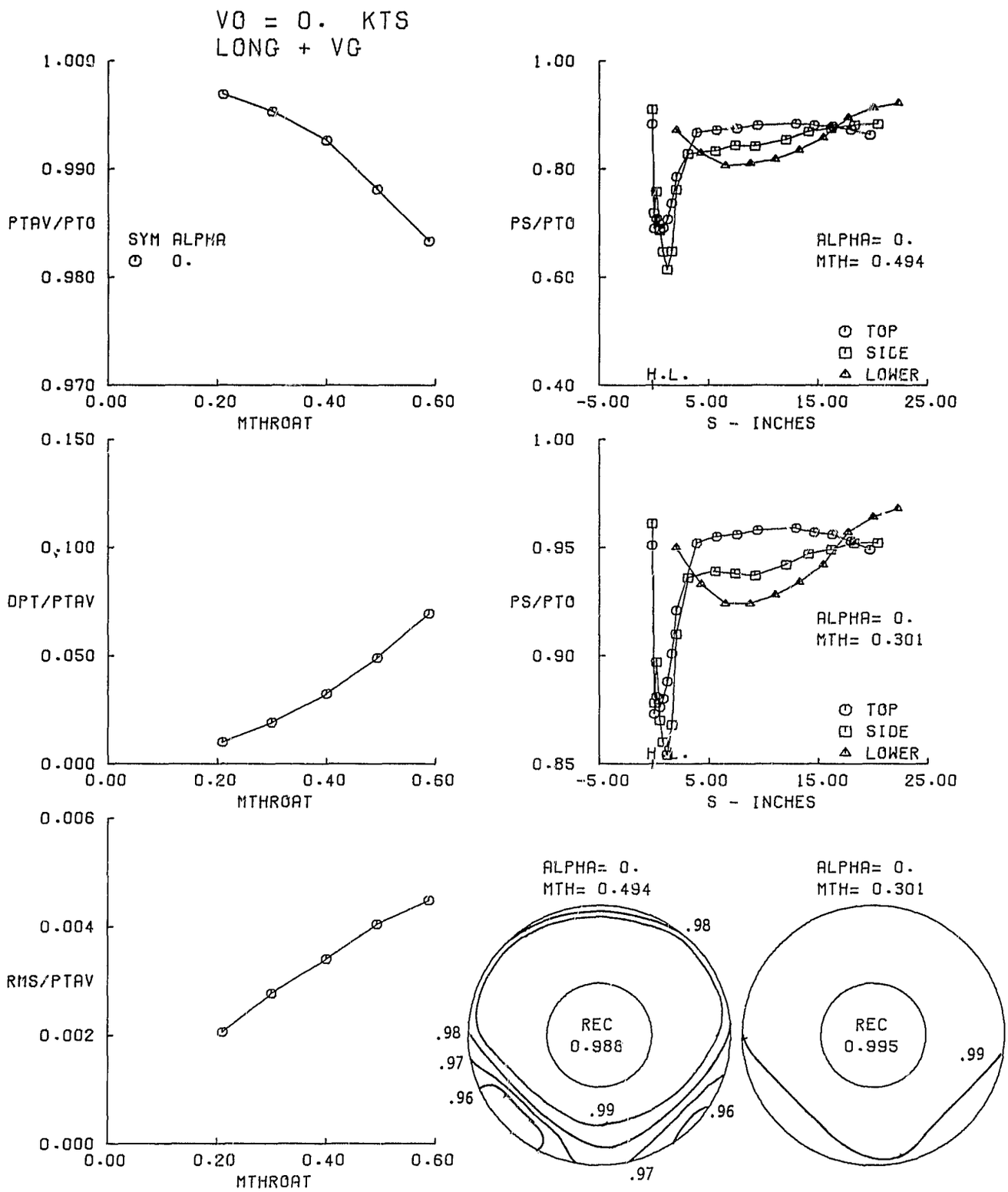

FIGURE 27 LONG AFT INLET WITH VORTEX GENERATORS PERFORMANCE AT V_0 = 0 KNOTS

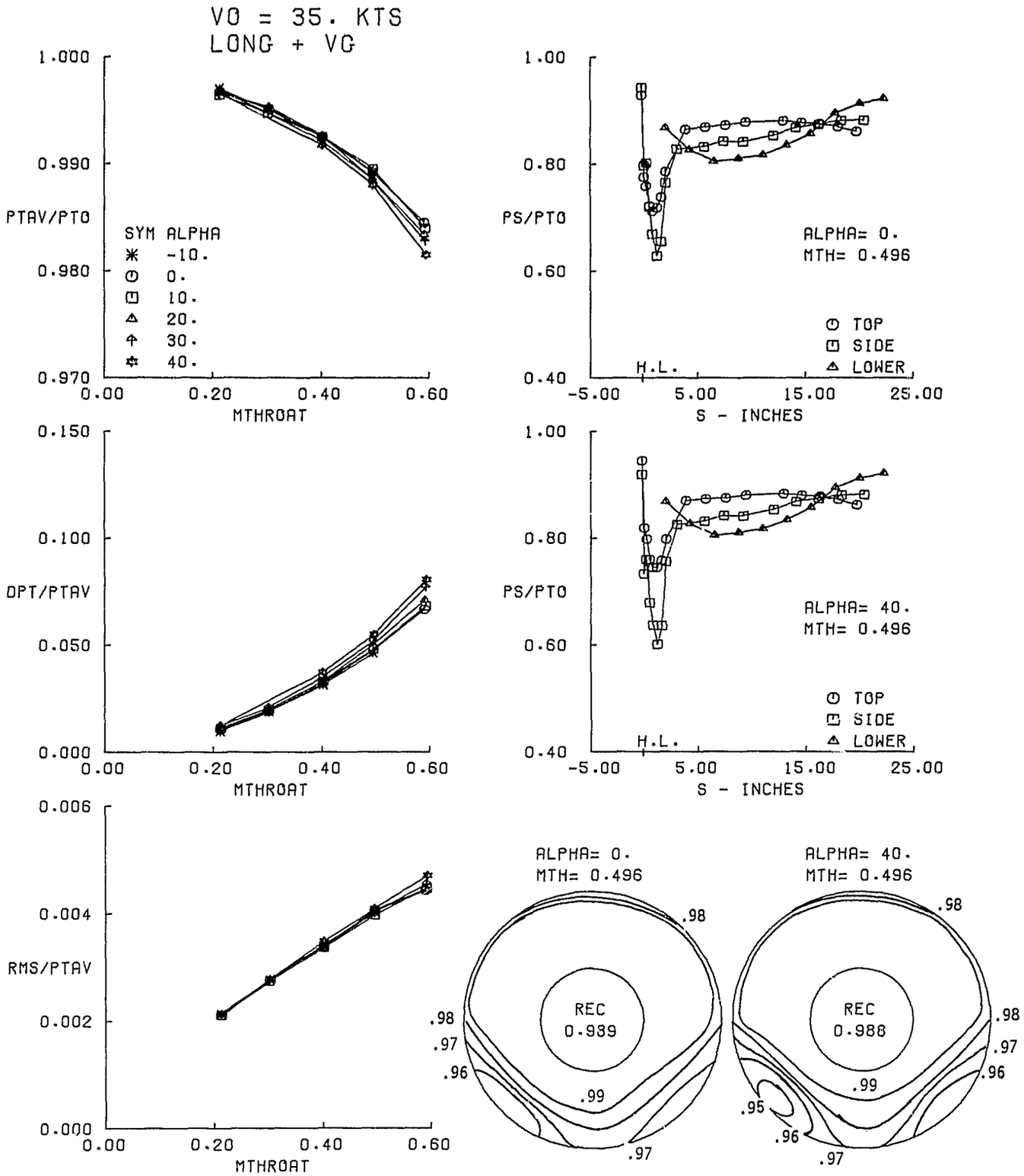

FIGURE 28 LONG AFT INLET WITH VORTEX GENERATORS PERFORMANCE AT V_0 = 35 KNOTS

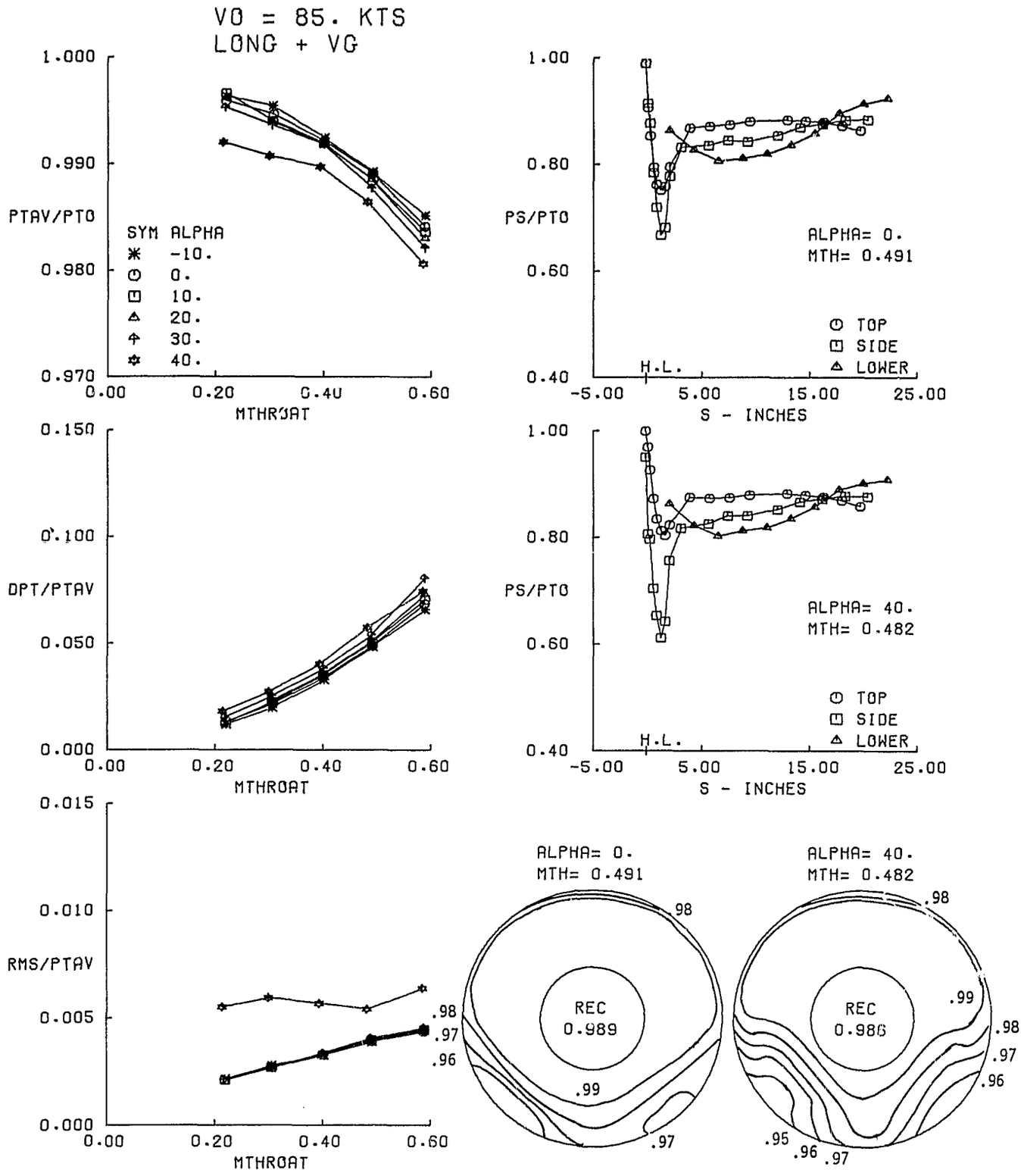

FIGURE 29 LONG AFT INLET WITH VORTEX GENERATORS PERFORMANCE AT V_o = 85 KNOTS

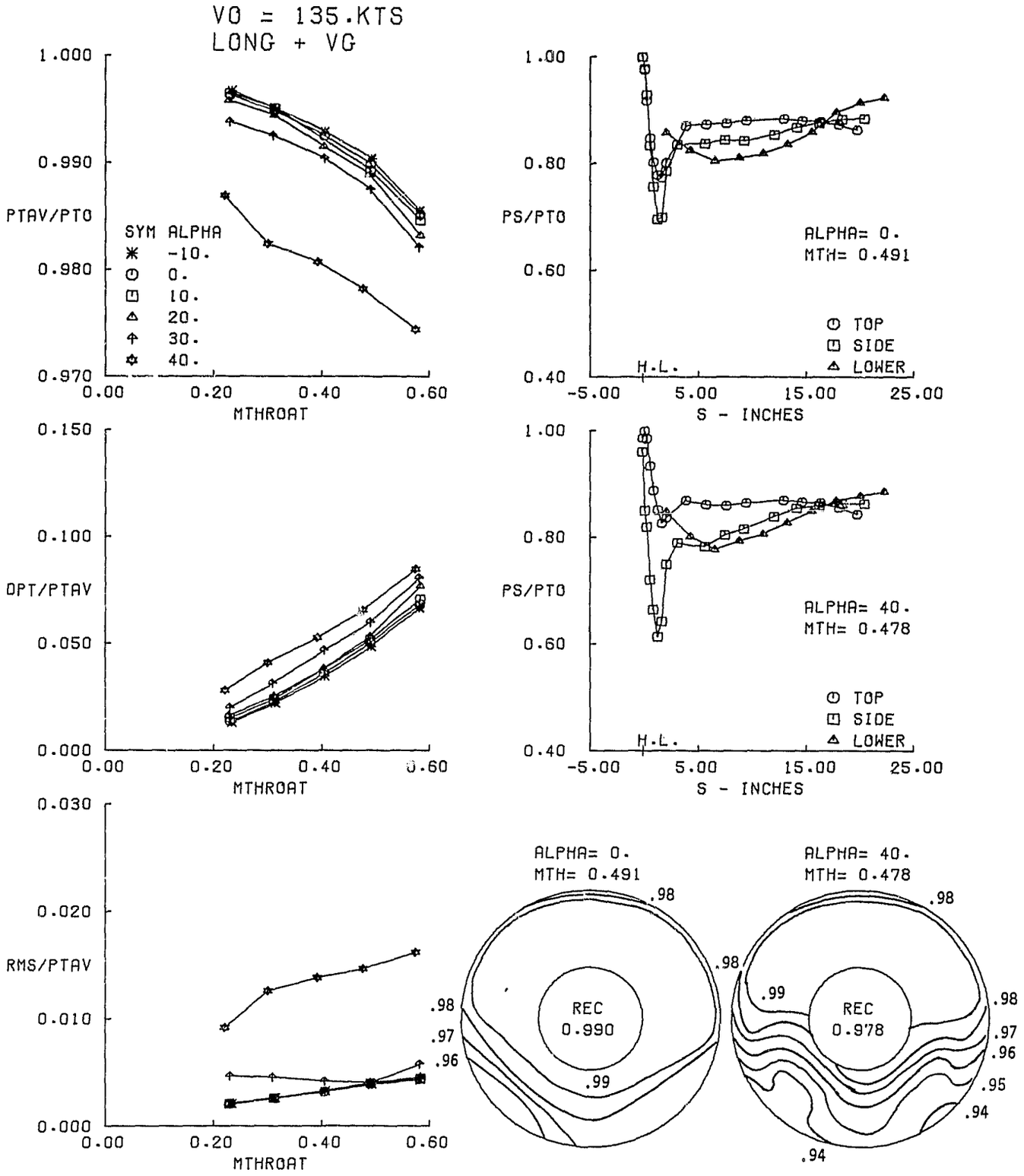

FIGURE 30 LONG AFT INLET WITH VORTEX GENERATORS PERFORMANCE AT V_0 = 135 KNOTS

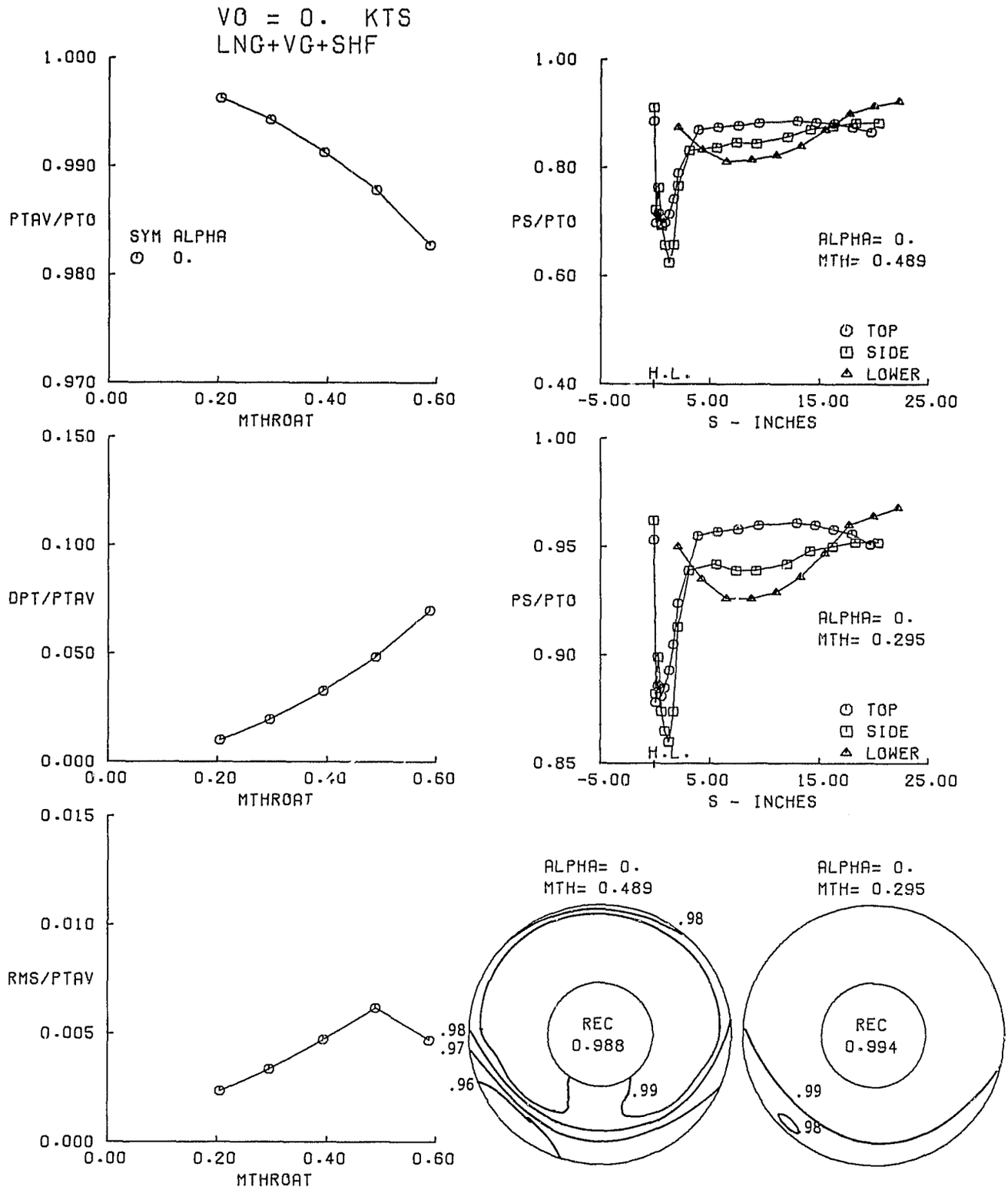

FIGURE 31 LONG AFT INLET WITH VORTEX GENERATORS AND SHAFT SIMULATOR. PERFORMANCE AT V_o = 0 KNOTS

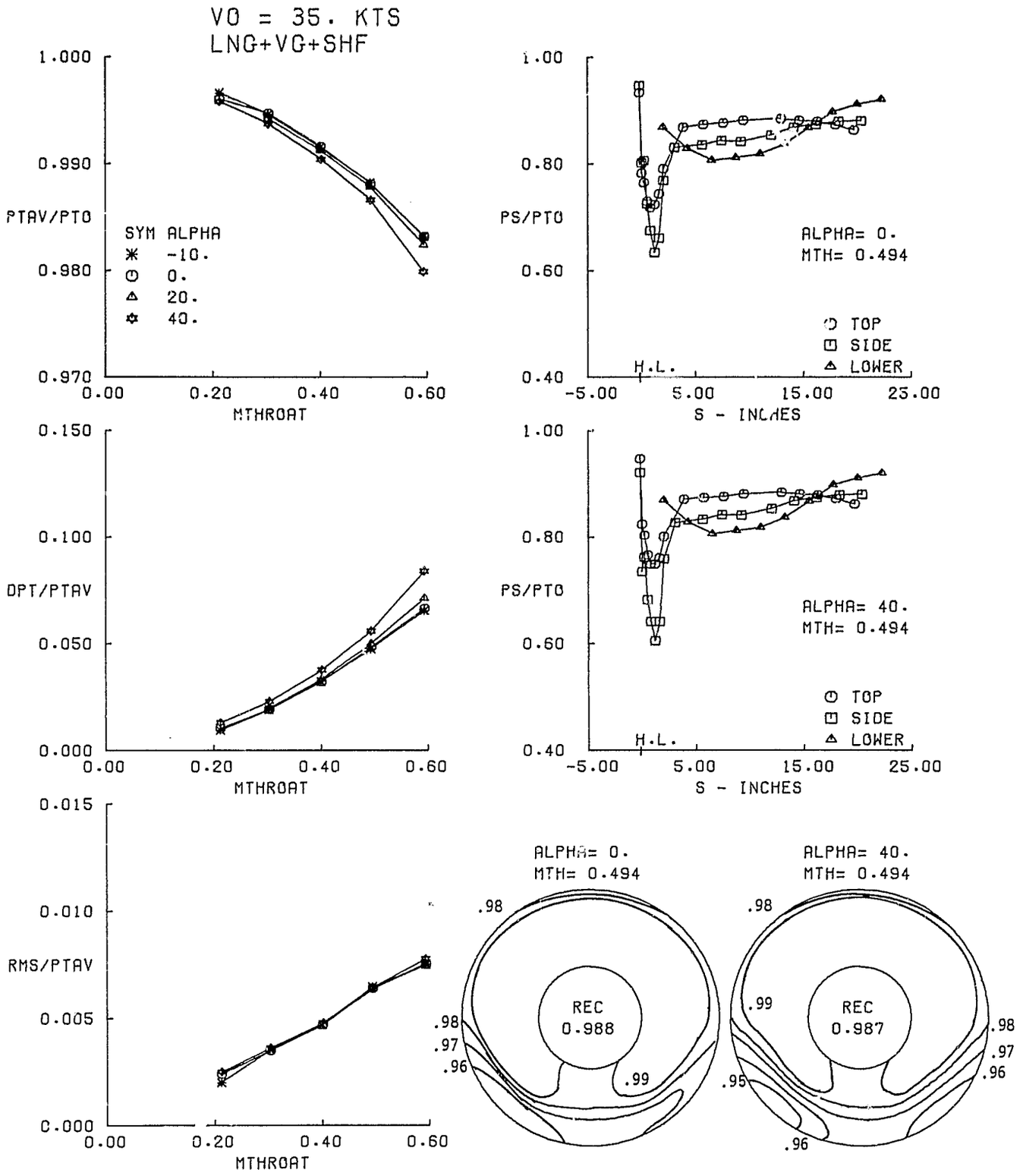

FIGURE 32 LONG AFT INLET WITH VORTEX GENERATORS AND SHAFT SIMULATOR PERFORMANCE AT V_o = 35 KNOTS

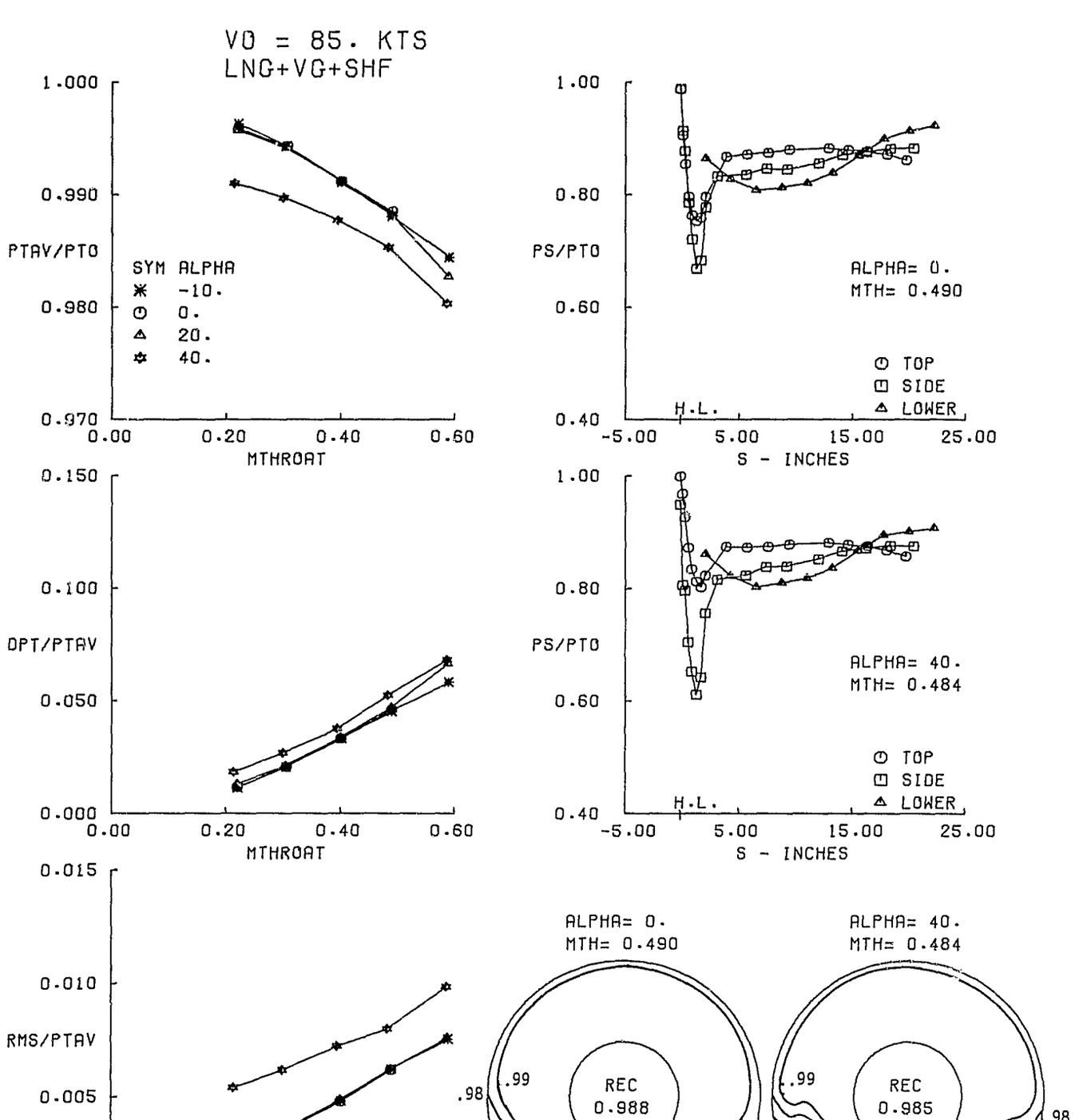

FIGURE 33 LONG AFT INLET WITH VORTEX GENERATORS AND SHAFT SIMULATOR PERFORMANCE AT V_o = 85 KNOTS

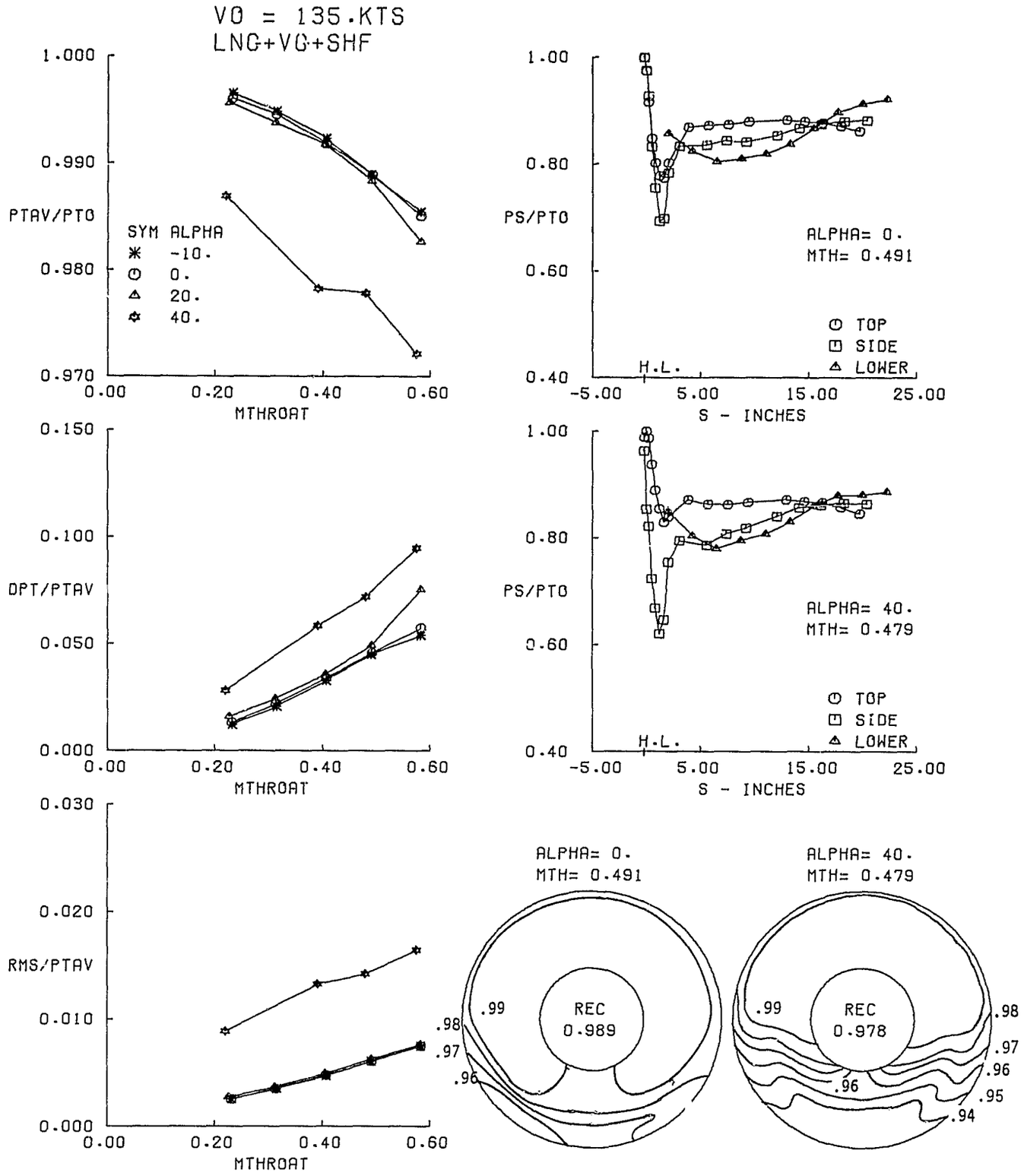

FIGURE 34 LONG AFT INLET WITH VORTEX GENERATORS AND SHAFT SIMULATOR PERFORMANCE AT V_o = 135 KNOTS

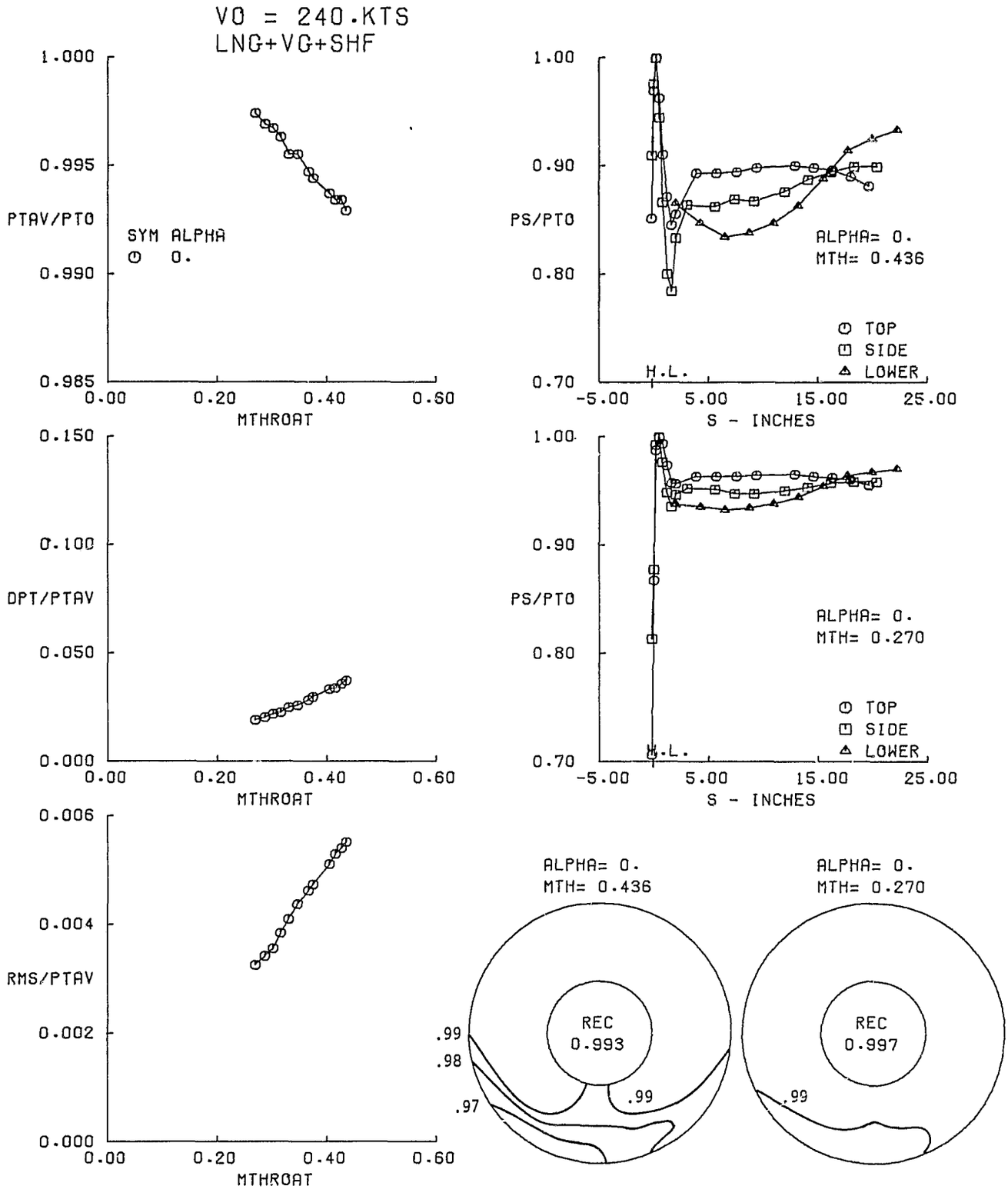

FIGURE 35 LONG AFT INLET WITH VORTEX GENERATORS AND SHAFT SIMULATOR PERFORMANCE AT V_o = 240 KNOTS

Mach numbers (.25 - .30) as shown in Figures 31 and 35. Figures 31, 32, 33, and 34 indicate through the plotted static pressure distributions that the stagnation point remains outside the inlet lip hilite at low speed. Figure 35, which presents results at 240 Kts (123.5 m/s), shows a throat mach number of .436. The stagnation point is very near the hilite, and at a throat mach number of .27, the stagnation point has shifted inside the lip.

6.5 Short Aft Inlet

The detailed inlet performance for the short aft inlet is presented in Figures 36, 37, 38, 39, and 40 for V_0 = 0, 35, 85, 135, and 240 Kts (0, 18, 43.7 69.5, and 123.5 m/s). The static pressure distributions are plotted as a function of surface distance from the lip highlight. For the lower ramp surface, the throat station was used as the reference point. The velocity at the lip is higher along the top streamline than along the side streamline, Figure 36 and 37 at low speed, but reverse at higher speeds, Figure 38 and 39. At V_0 = 0 Kts, the short aft inlet configuration exhibits a trend in which the recovery loss with increasing mass flow rate is less than the long aft inlet as shown in Figures 19 and 36. The short aft inlet recovery level is more dependent on angle of attack than the long aft inlet as shown in Figures 20 and 37, 21 and 38, 22 and 39 for V_0 = 35, 85 and 135 Kts (18, 43.7, and 69.5 m/s).

6.6 Configuration Comparisons

Comparisons in terms of total pressure recovery, distortion, and turbulence levels for the various aft inlet configurations are presented in Figures 41 to 47. These data include freestream conditions of V_0 = 0, 35, 85, and 135 Kts (0, 18.0, 43.7, and 69.5 m/s). Except for the static conditions, these comparisons include angles of attack of 0 and 40 degrees.

At $\alpha = 0^o$, the highest performance is obtained with the short aft inlet, and the lowest is achieved by the long inlet with blow-in door passages open. At $\alpha = 40^o$, the distortion and turbulence levels for the short aft inlet are higher.

For the static condition, Figure 41, the best performance is obtained with the short aft inlet. At the lower airflow rates, the use of the vortex generators with the long aft inlet design improves the pressure recovery level and the distortion and turbulence levels. Note that the presence of the front fan shaft simulator induces a very small performance detriment. The pressure recovery loss is greater with the blow-in doors open, although less than 1%. A redesign of the blow-in door geometry -- the flow passage contour and/or flow passage area distribution -- is needed to improve performance. Note that the short aft inlet is more insensitive to airflow variations than the long aft inlet configurations.

Figures 42 and 43 show configuration comparisons for V_0 = 35 (18.0 m/s) and $\alpha = 0^o$ and 40^o. The short aft inlet yields the best performance. For $\alpha = 40^o$, the distortion levels are slightly greater for the long aft inlet with vortex generators than without vortex generators. The turbulence level, however, is lower with the vortex generators. The presence of the shaft simulator increases slightly the turbulence level. The turbulence level is higher for the short aft inlet than for the long aft inlet, except with the blow-in doors open.

Similar results were obtained at V_0 = 85 Kts (43.7 m/s), Figures 44 and 45. Even at V_0 = 135 (69.5 m/s) and $\alpha = 0^o$, the short aft inlet design yields

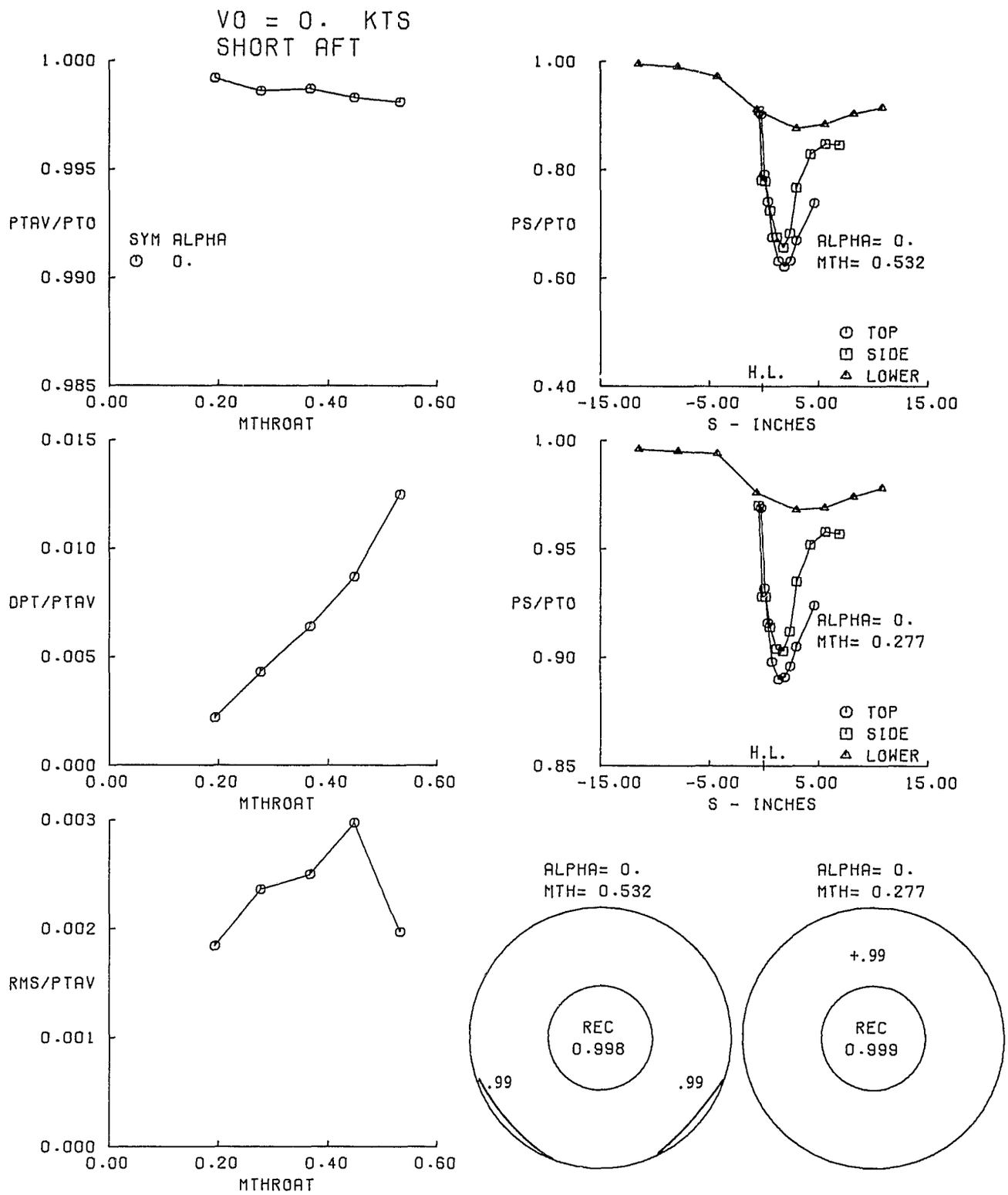

FIGURE 36 SHORT AFT INLET PERFORMANCE AT V_0 = 0 KNOTS

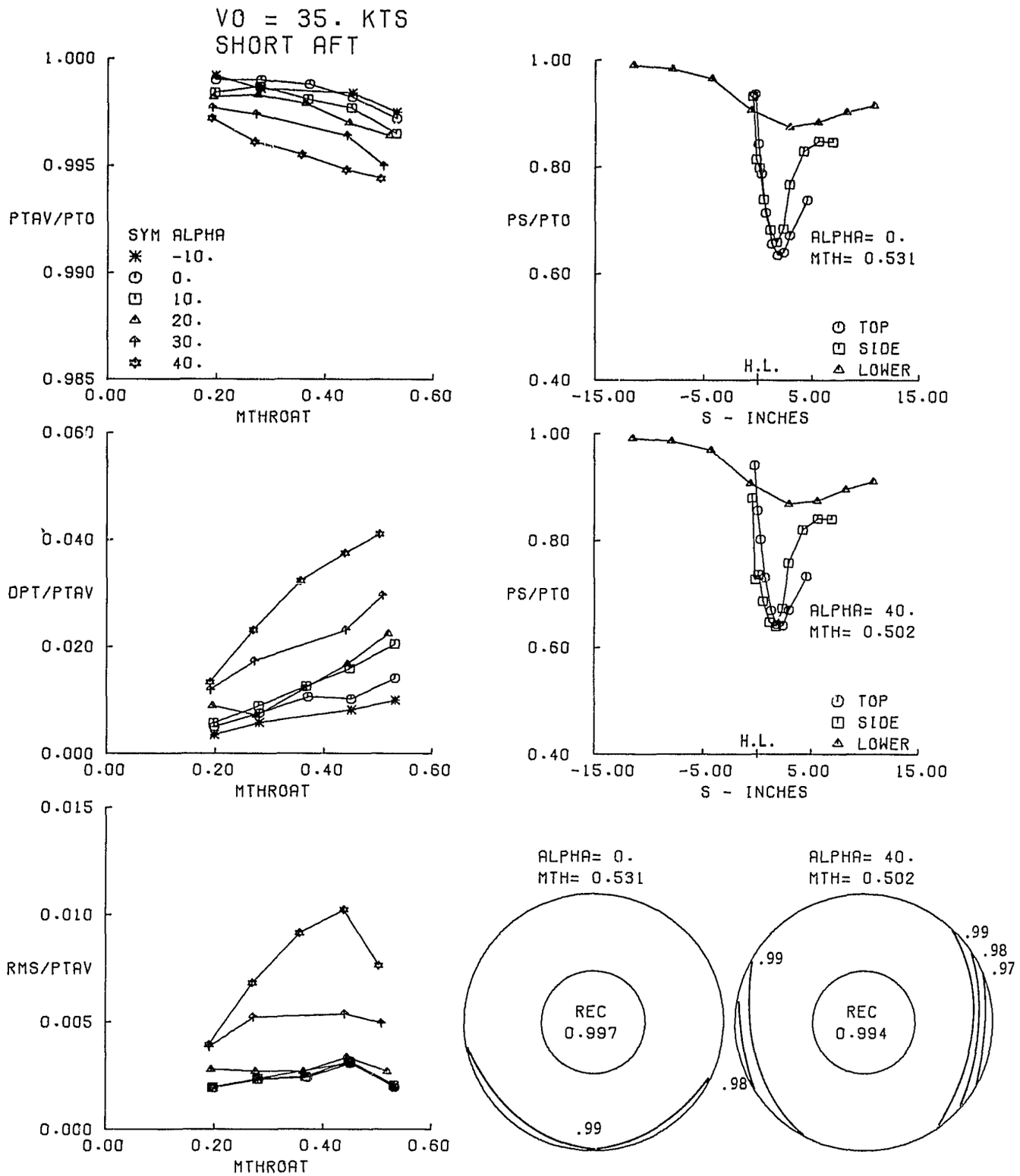

FIGURE 37 SHORT AFT INLET PERFORMANCE AT V_o = 35 KNOTS

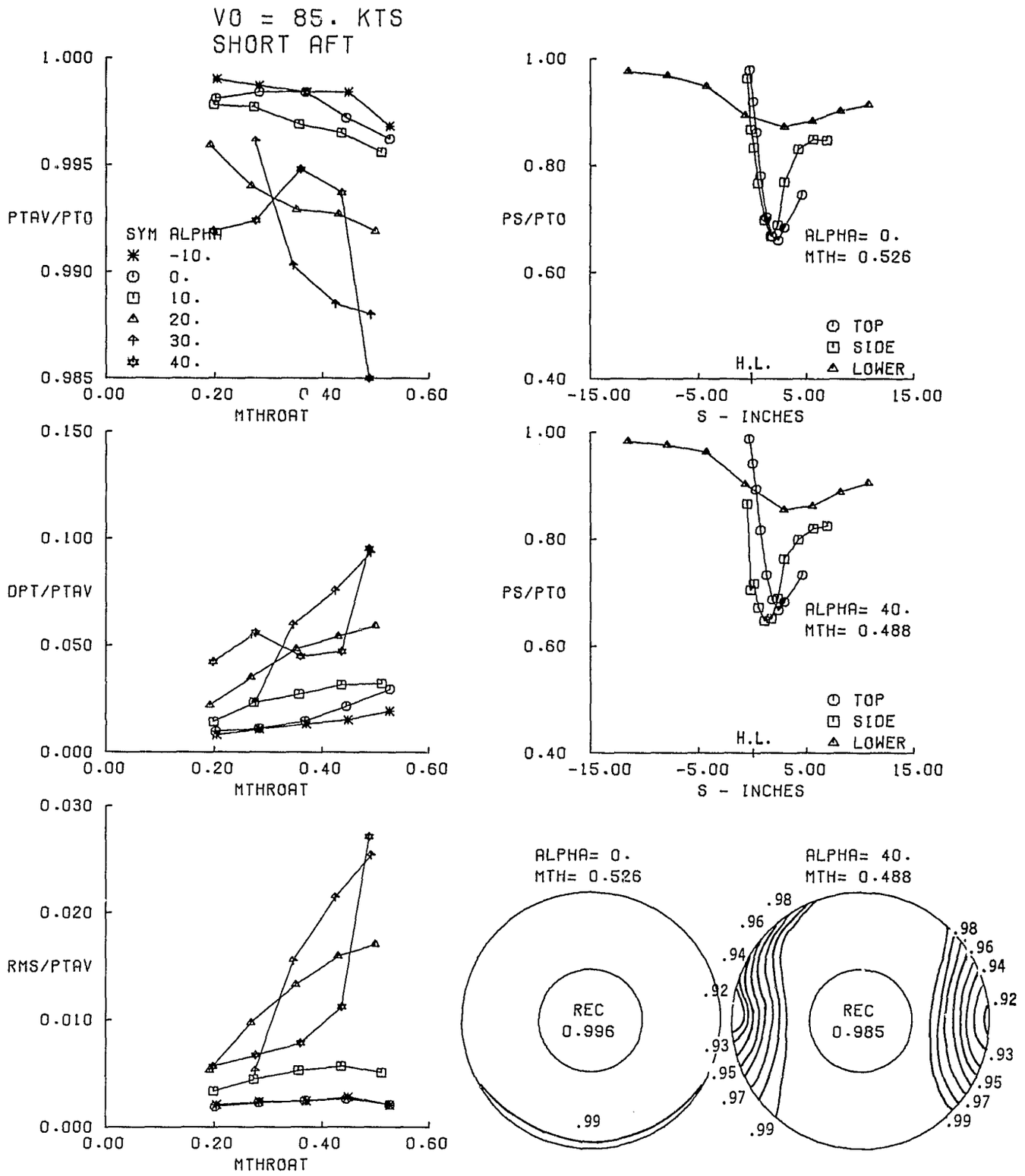

FIGURE 38 SHORT AFT INLET PERFORMANCE AT V_o = 85 KNOTS

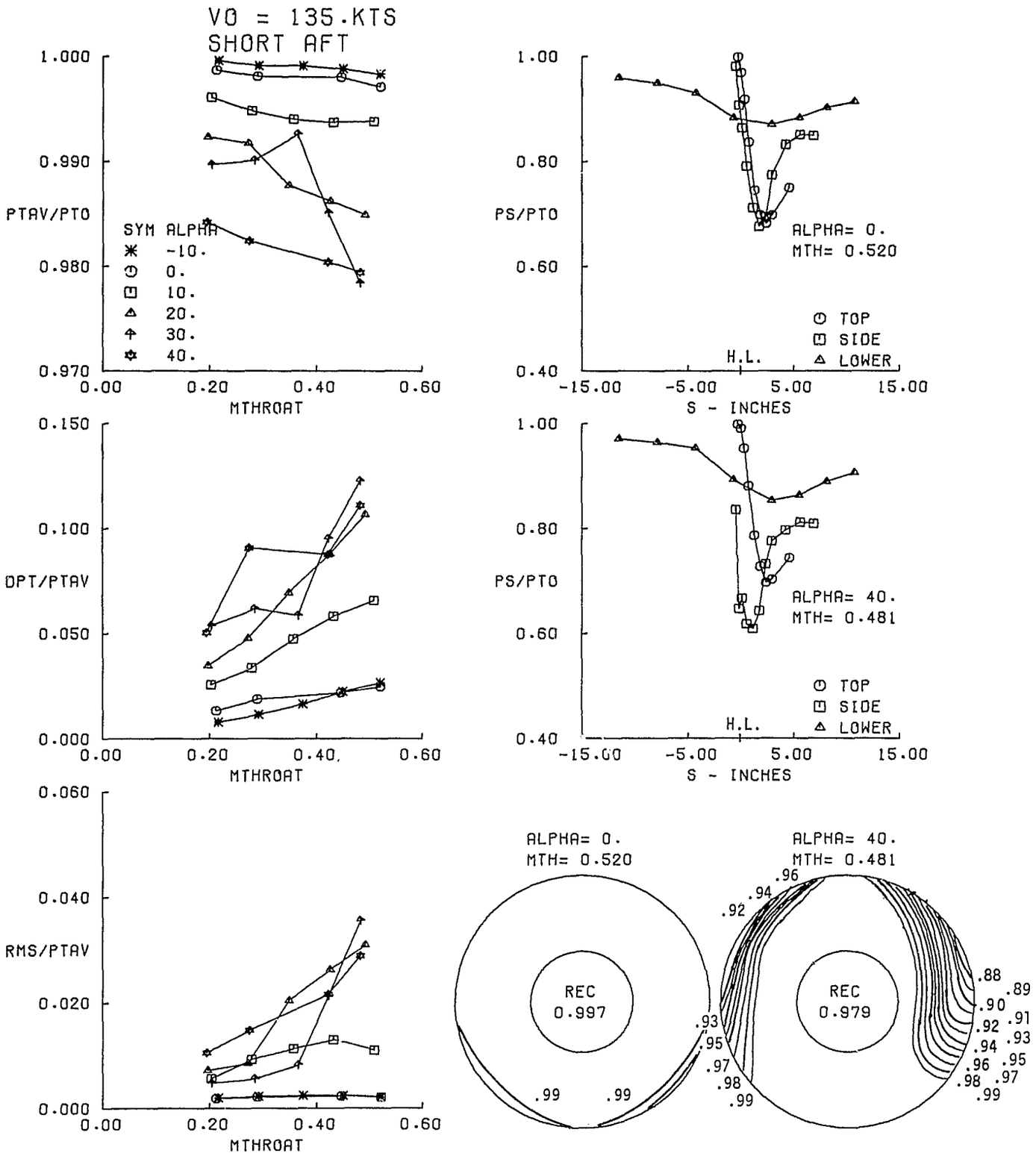

FIGURE 39 SHORT AFT INLET PERFORMANCE AT V_o = 135 KNOTS

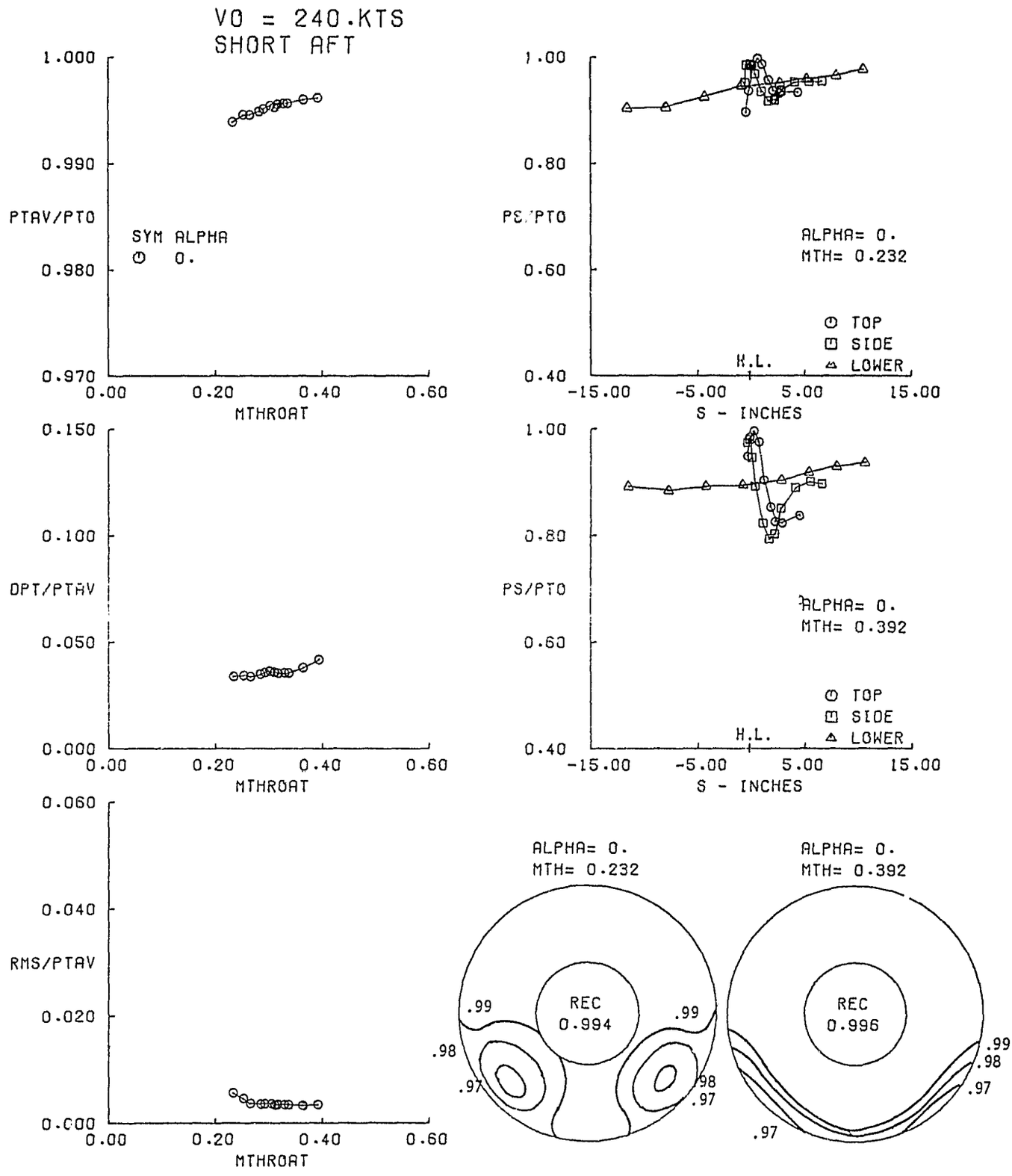

FIGURE 40 SHORT AFT INLET PERFORMANCE AT V_o = 240 KNOTS

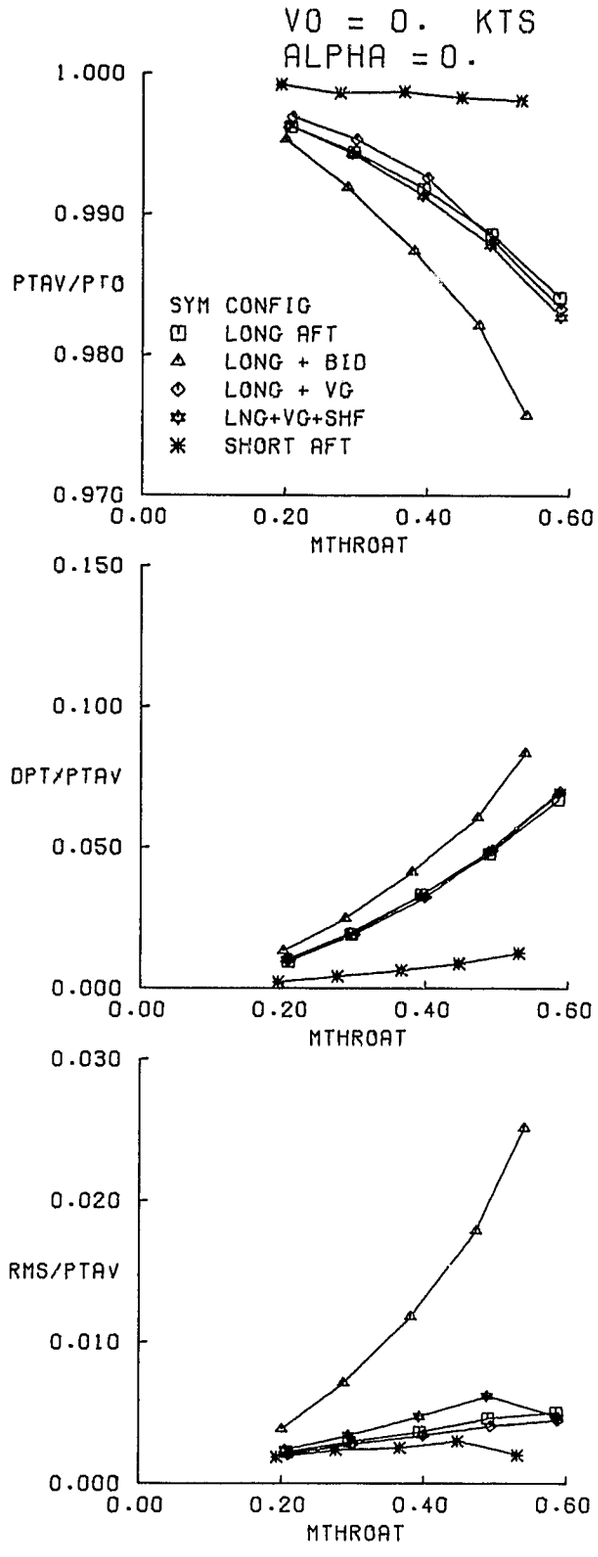

FIGURE 41 PERFORMANCE COMPARISONS AT V_0 = 0 KNOTS, α = 0^0

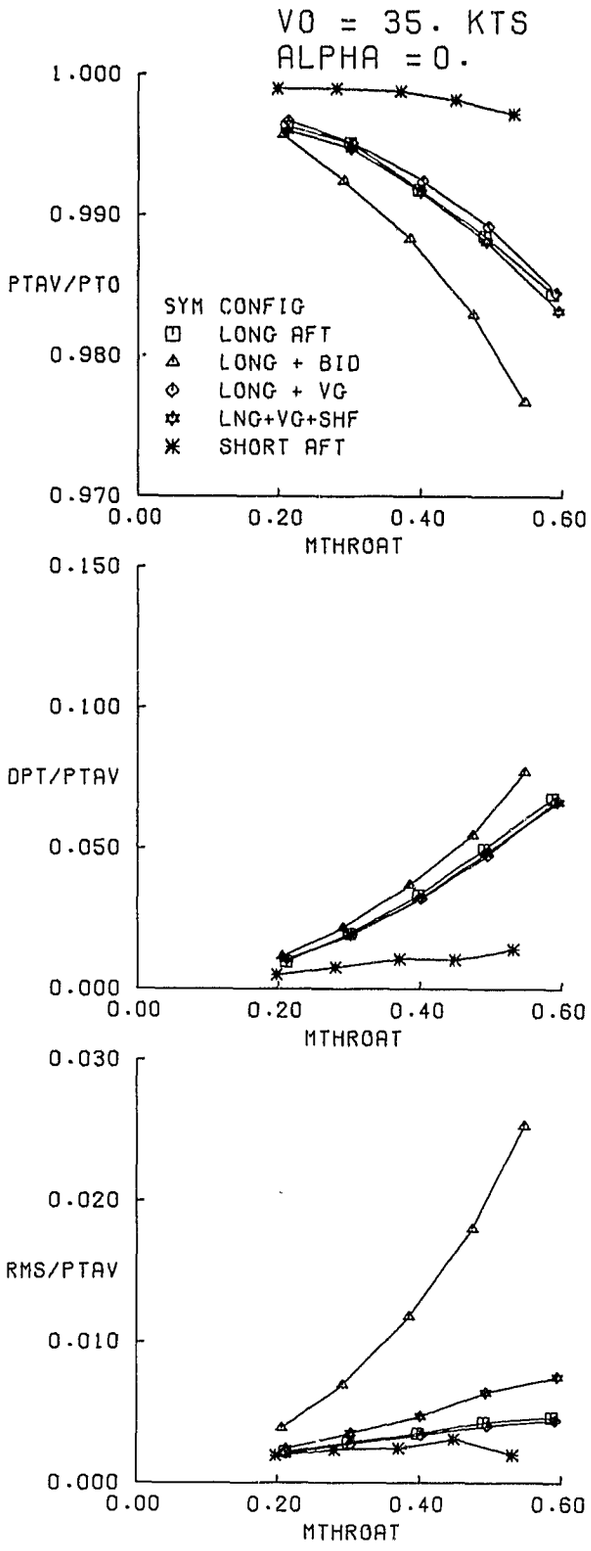

FIGURE 42 PERFORMANCE COMPARISONS AT V_0 = 35 KNOTS, $\alpha = 0^0$

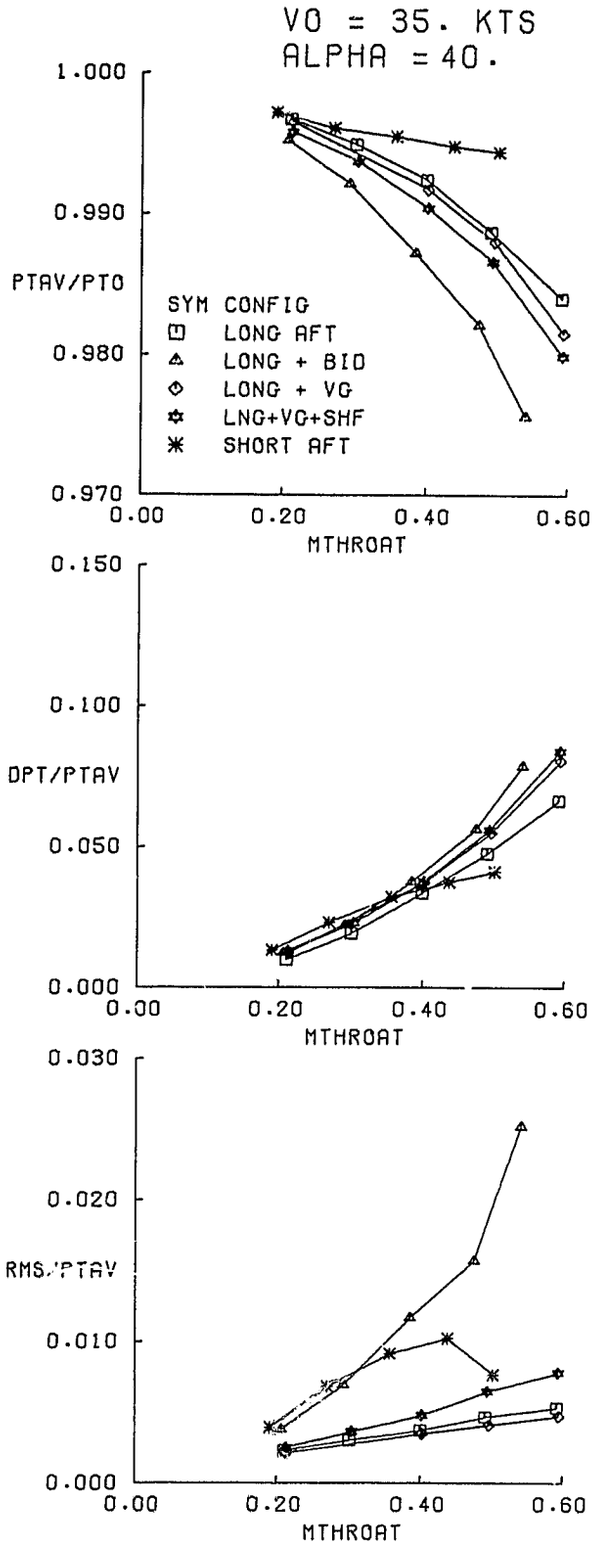

FIGURE 43 PERFORMANCE COMPARISONS AT V_0 = 35 KNOTS, α = 40°

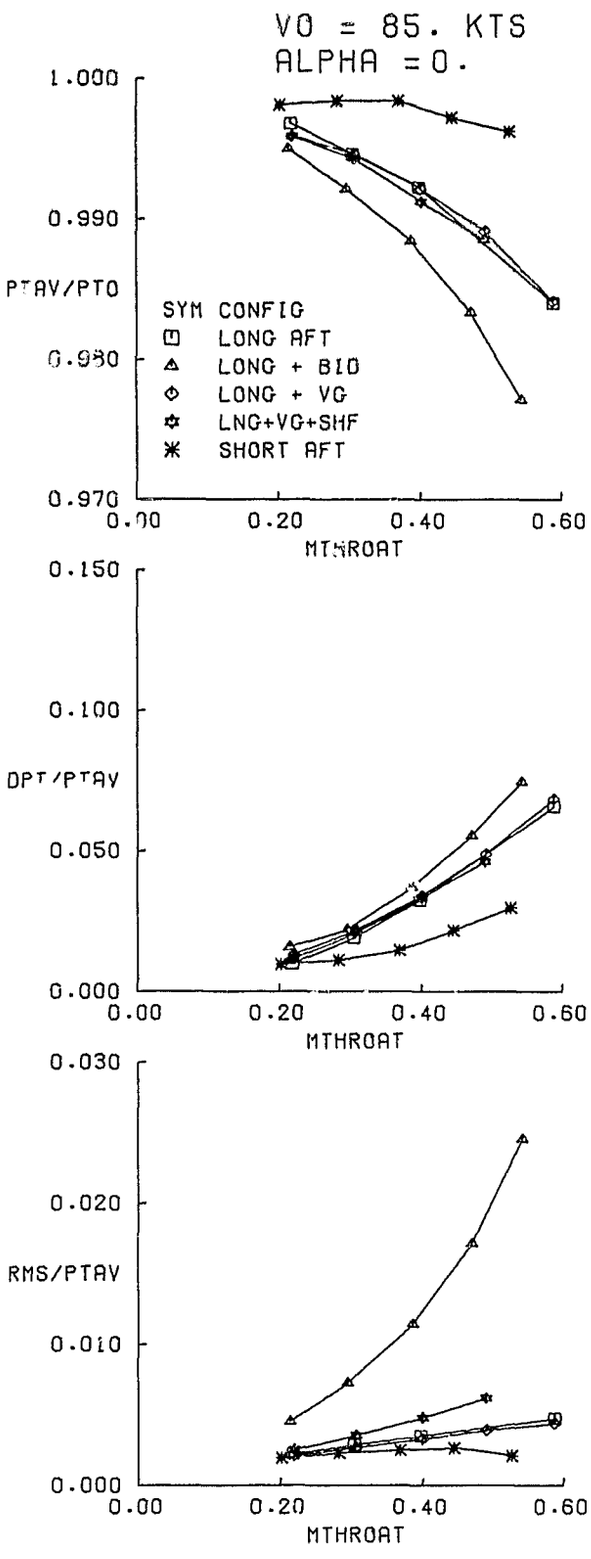

FIGURE 44 PERFORMANCE COMPARISONS AT V_o = 85 KNOTS, $\alpha = 0^o$

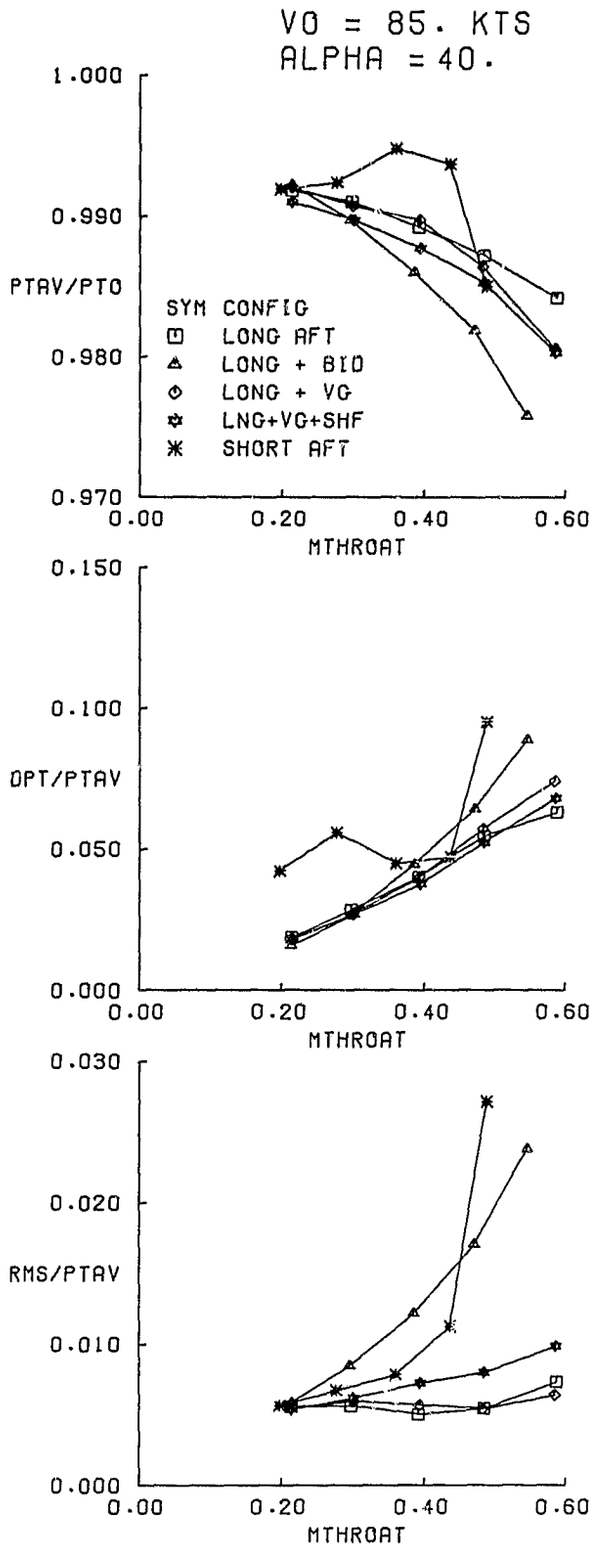

FIGURE 45 PERFORMANCE COMPARISONS AT V_o = 85 KNOTS, α = 40°

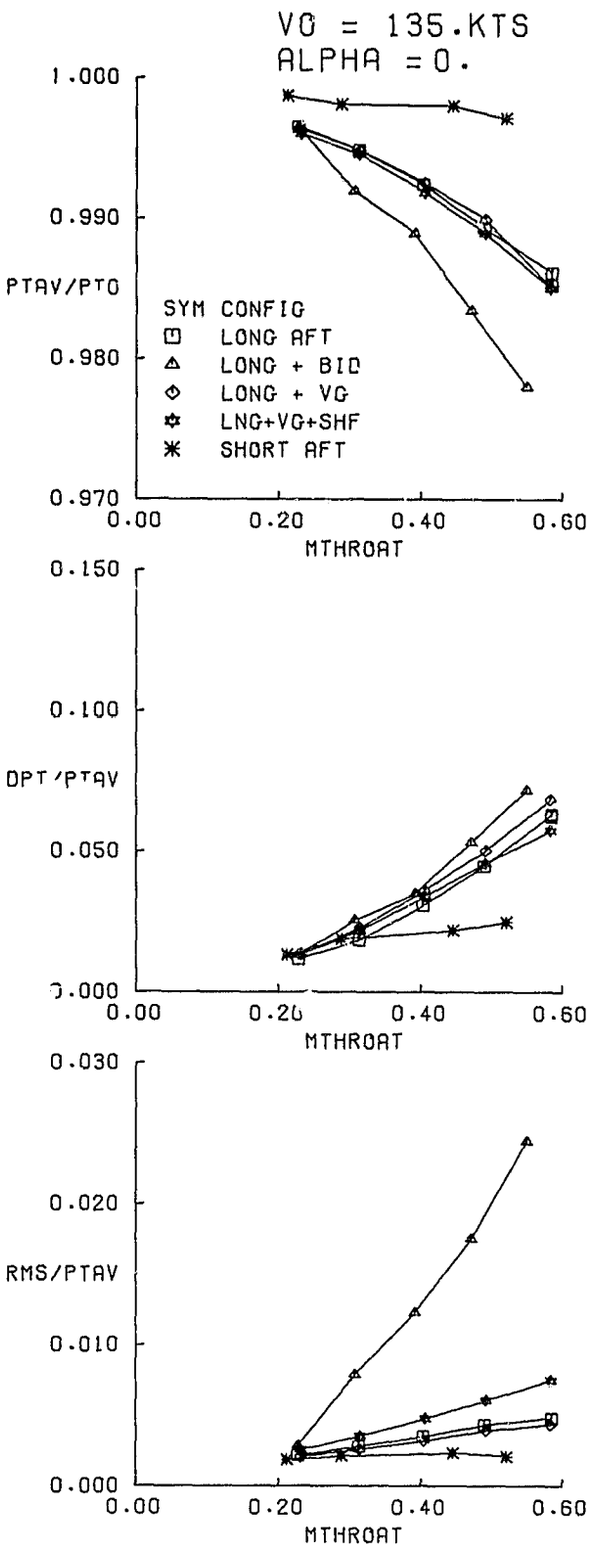

FIGURE 46 PERFORMANCE COMPARISONS AT V_o = 135 KNOTS, $\alpha = 0^o$

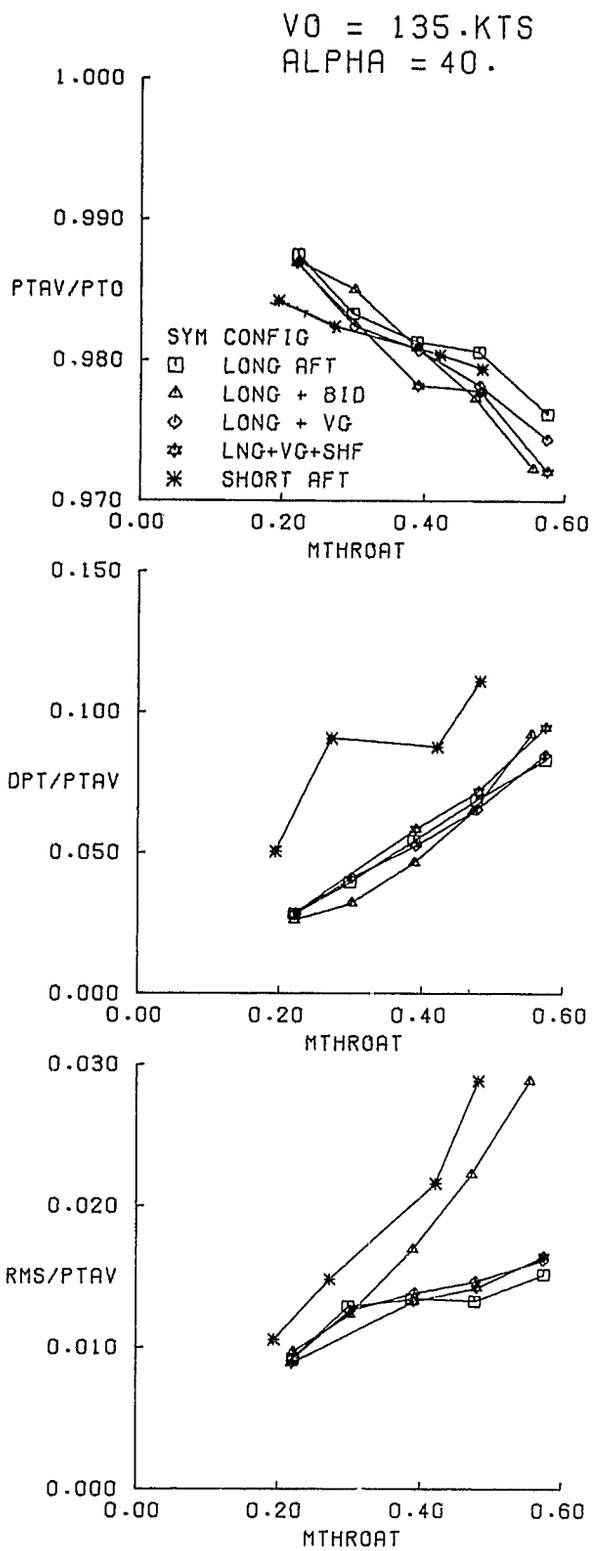

FIGURE 47 PERFORMANCE COMPARISONS AT V_o = 135 KNOTS, $\alpha = 40^o$

better performance, Figure 46. The degradation with angle of attack, however, is much more pronounced at $\alpha = 40^{o}$, Figure 47.

Figures 48 and 49 show comparisons of the static pressure circumferential distributions at the inlet lip and throat plane. Comparisons are presented between the long aft inlet (baseline configuration) and the short aft inlet at nearly identical flow conditions. Figure 48 includes data at $\alpha = 0^{o}$ for forward speeds of 0, 35, 85, and 135 Kts (0, 18.0, 43.7 and 69.5 m/s). Figure 49 includes data at $\alpha = 40^{o}$ for forward speeds of 35, 85, and 135 Kts (18.0, 43.7, and 69.5 m/s). The data are presented as the ratio of the local static pressure to the freestream total pressure plotted as a function of the angle measured clockwise from the top of the inlet as shown in the inset in Figures 48 and 49. The static pressure data for each condition include distributions along the inlet lip hilite and the inlet throat. For the static condition (V_o - 0 Kts) shown in Figure 48 the short aft inlet data are for approximately 6% higher flow rate. The throat static pressures are very similar except at the top ($\theta = 0^{o}$), where the short aft inlet indicate a higher local velocity. The hilite static pressures indicate that the velocity is almost constant around the long aft inlet lip, but the short aft inlet shows a definite gradient (increasing velocity) toward the top. Since the short aft inlet has a thicker lip shape, the velocities on the short inlet lip are lower than on the long aft inlet lip. With increasing forward speed (35, 85, 135 Kts) (18.0, 43.7, and 69.5 m/s) the mean level of the lip static pressures increase indicating a reduction in lip loading. In addition, increasing forward speed creates a pressure gradient around the lip whereby the higher velocities occur at the inlet lower lobe. This effect becomes more pronounced at $\alpha = 40^{o}$, see Figure 49. Also, note that the velocities on the short aft inlet lip hilite are higher at V_o = 85 and 135 Kts (43.7 and 69.5 m/s). The short aft inlet performances deteriorates more at $\alpha = 40^{o}$ that the long aft inlet performance.

6.7 FLOW ANGLE PROBE RESULTS

A total of 24 flow angle probes were located in the fan face instrumentation plane, as shown in figure 17. The probes were 3 tube, 2 dimensional types, as described in reference 9. The test results are shown qualitatively in figure 50. A computer graphic program generated arrows with size proportional to the flow angle. For both long and short inlets, a general downward flow is noted. In the long aft inlet, no vorticity was detectable despite the wide range of test conditions and configurations. However, the short aft inlet produced a vortex pair at extreme test conditions. High airspeed and angle-of-attack produce the vortex pair illustrated in figure 50-(g). These vortices become stronger at lower fan speeds. Direction of swirl is downwards near the centerbody, with centers in the upper quadrants.

The short aft inlet also produced a vortex pair at the condition of 240 knots, zero angle-of-attack,and low air flow, figure 50-(h). The swirl centers are at the lower quadrants. The center appear to move away from the centerbody as fan speed is increased.

The location of the vortices described above generally corresponds with the location of maximum total pressure loss, as shown in figures 39 and 40.

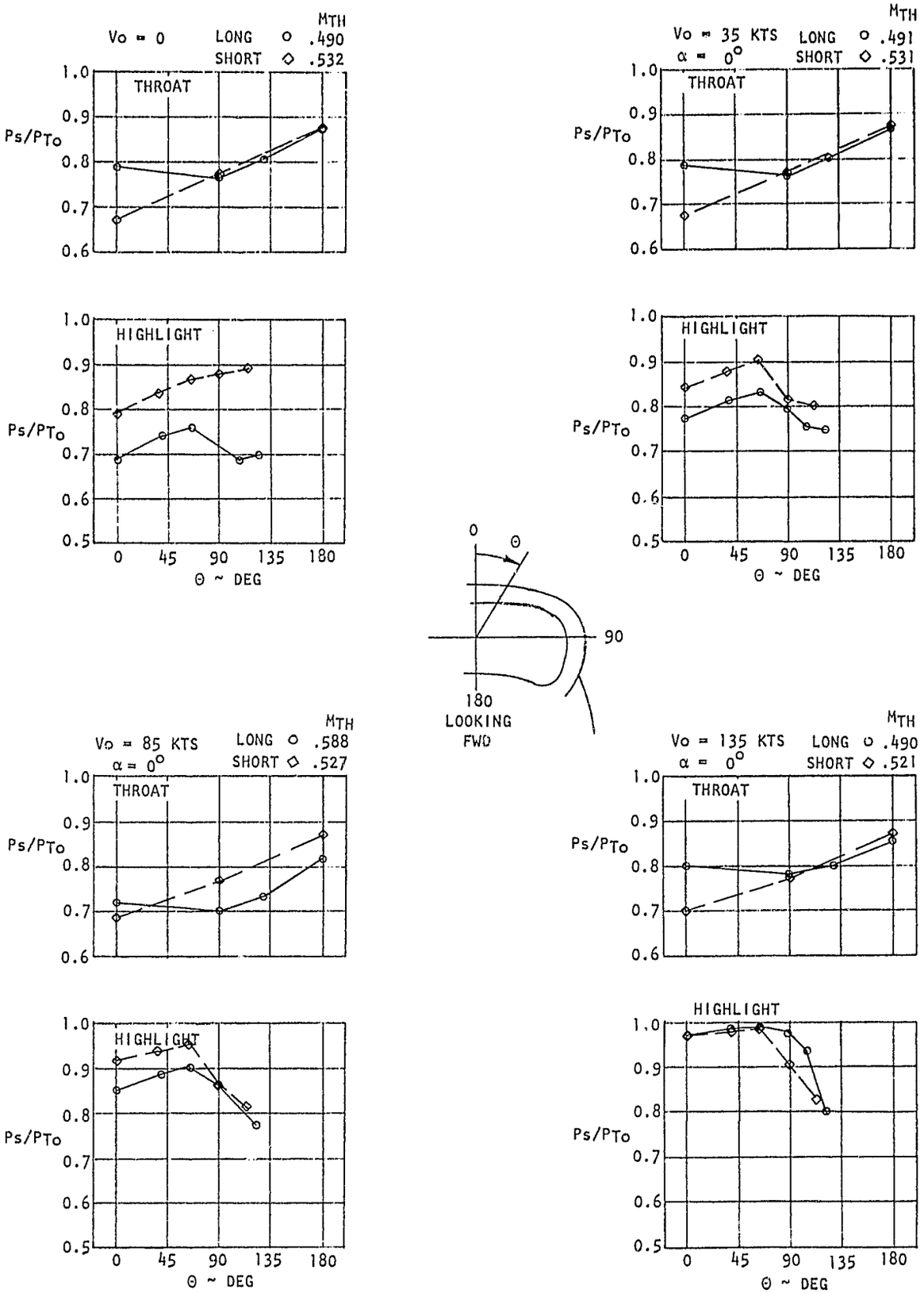

FIGURE 48. CIRCUMFERENTIAL STATIC PRESSURE COMPARISONS FOR LONG AND SHORT AFT INLETS, $\alpha = 0^{\circ}$

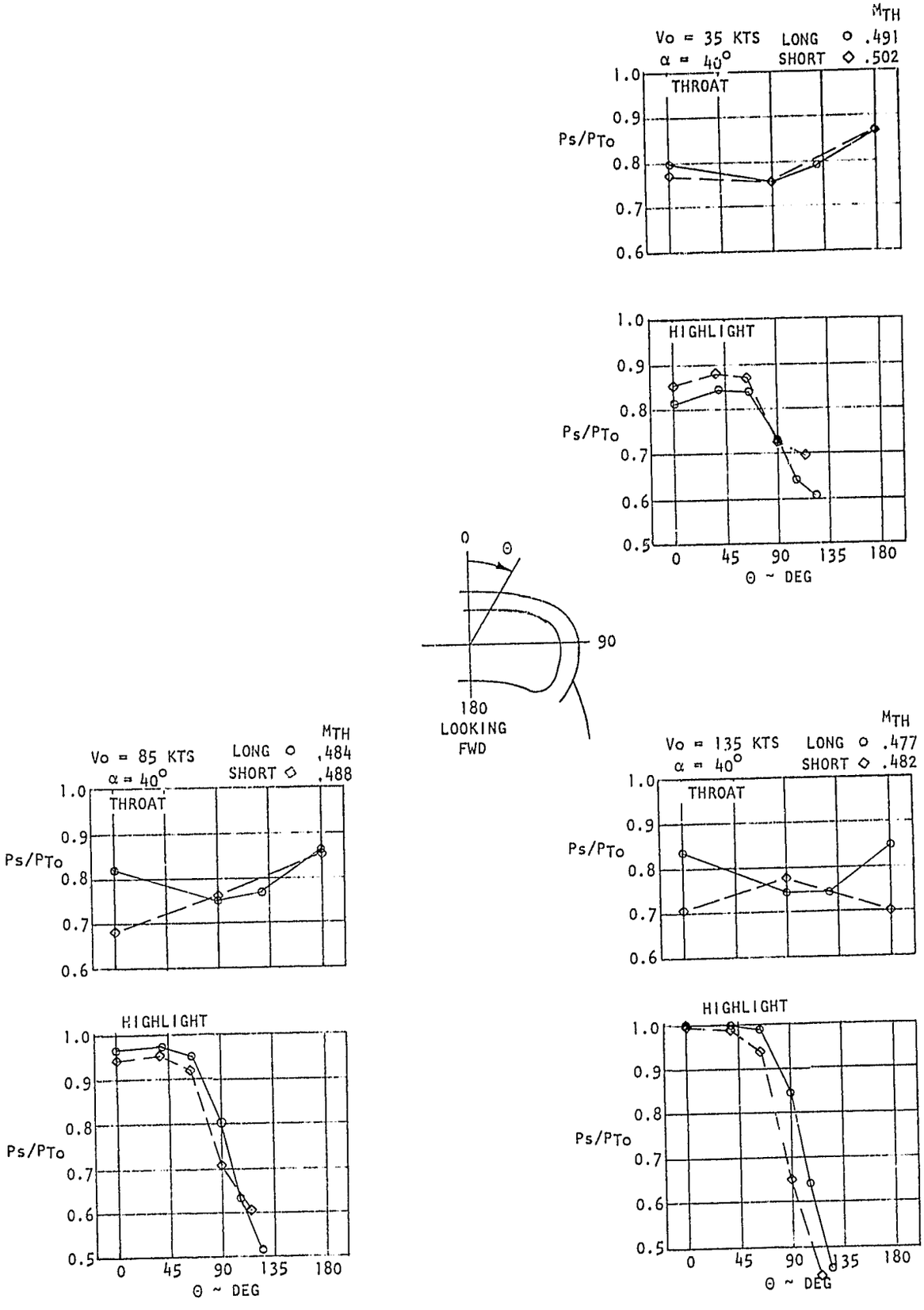

FIGURE 49. CIRCUMFERENTIAL STATIC PRESSURE COMPARISONS FOR LONG AND SHORT AFT INLETS, $\alpha = 40^{\circ}$

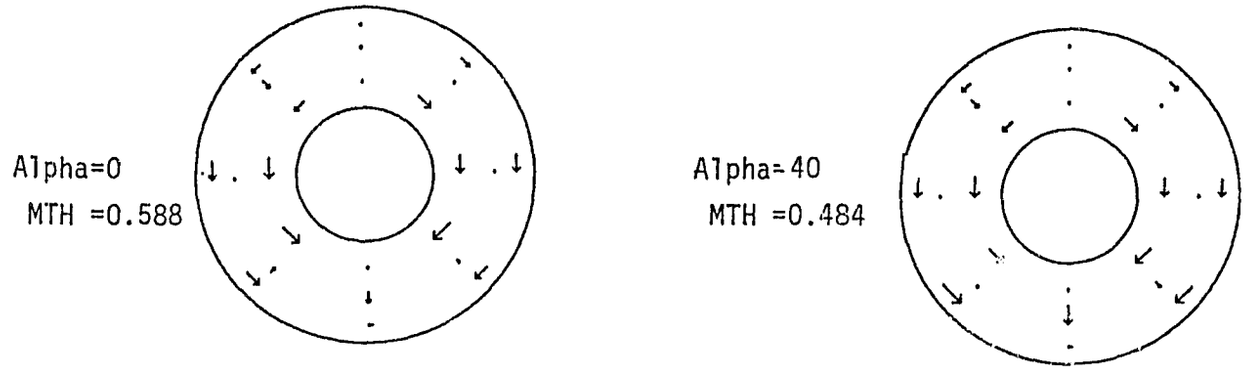

(a) Long Aft Inlet at Vo=85 knots

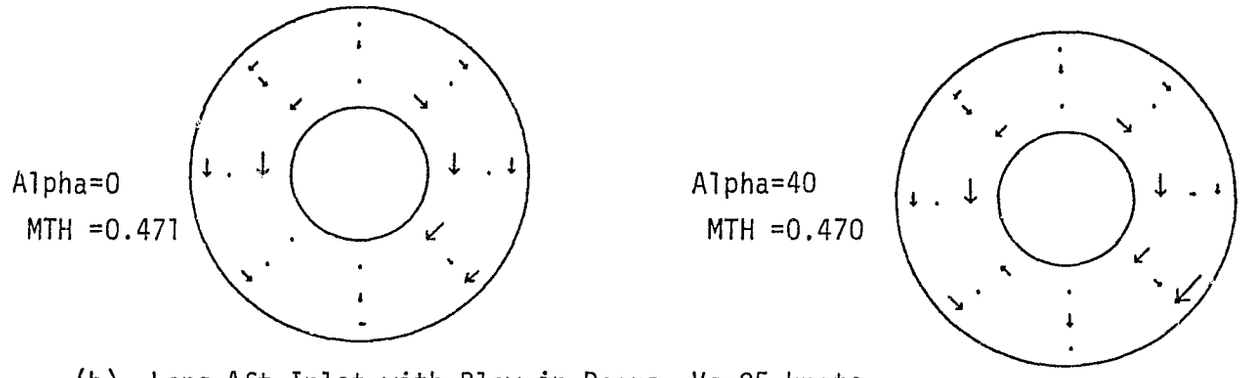

(b) Long Aft Inlet with Blow-in Doors, Vo=85 knots

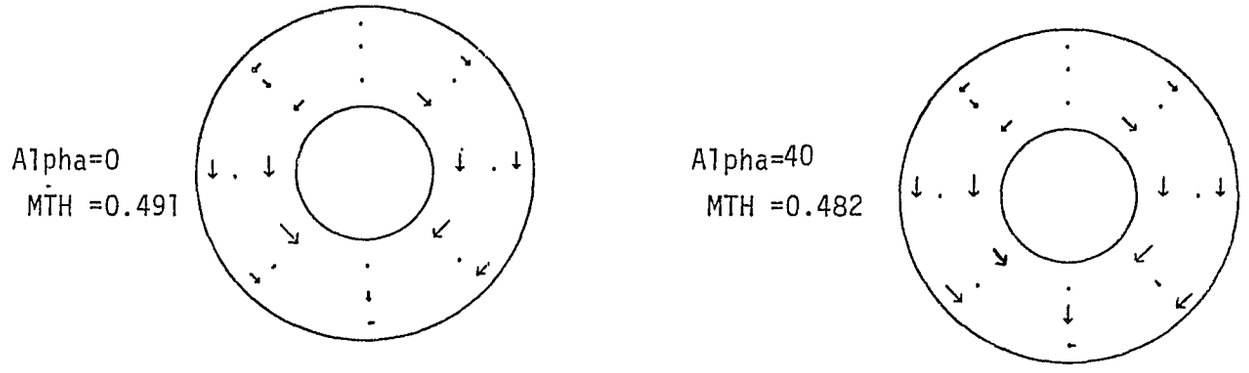

(c) Long Aft Inlet with Vortex Generators, Vo=85 knots

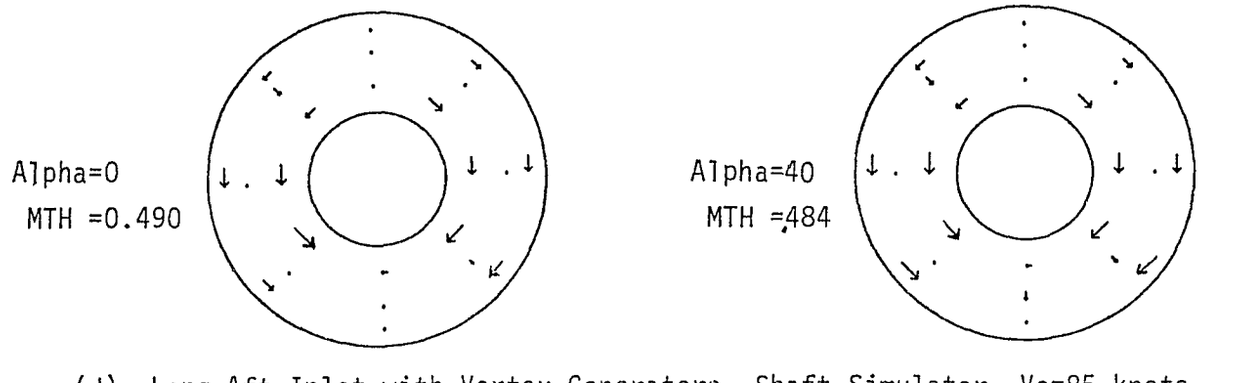

(d) Long Aft Inlet with Vortex Generators, Shaft Simulator, Vo=85 knots

FIGURE 50 FLOW ANGULARITY PROBE TEST RESULTS

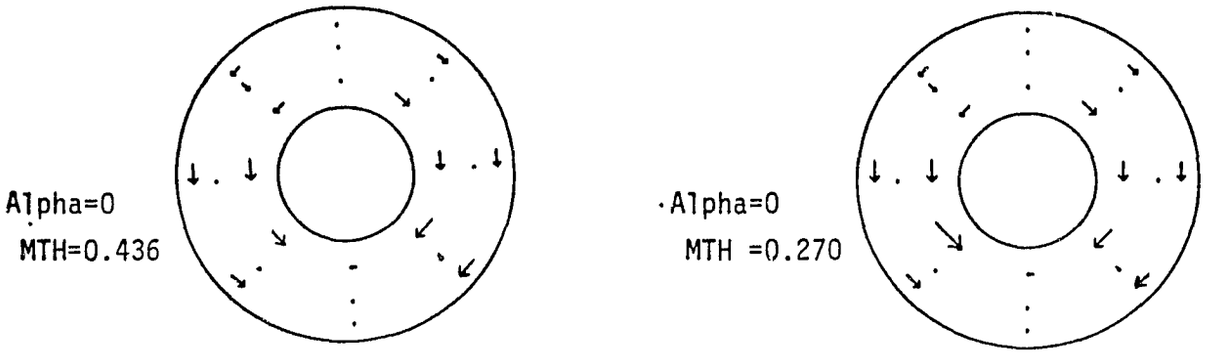

(e) Long Aft Inlet with Vortex Generators, Shaft Simulator, Vo=240 knots

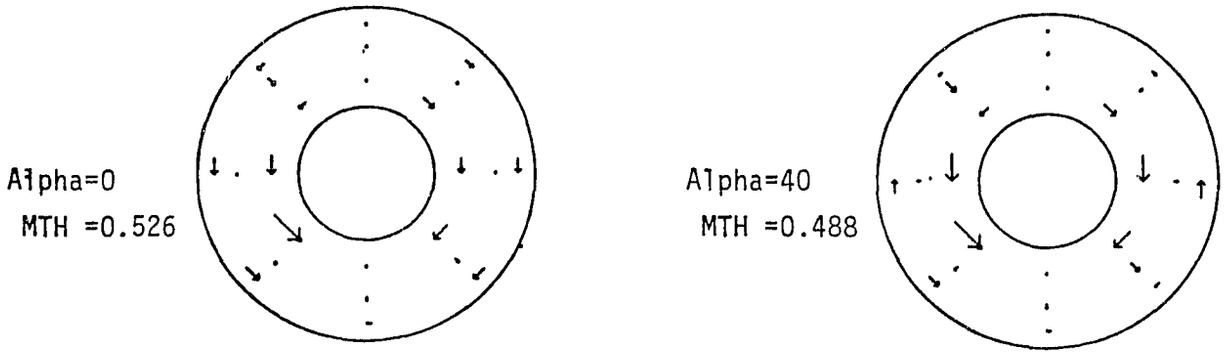

(f) Short Aft Inlet at Vo=85 knots

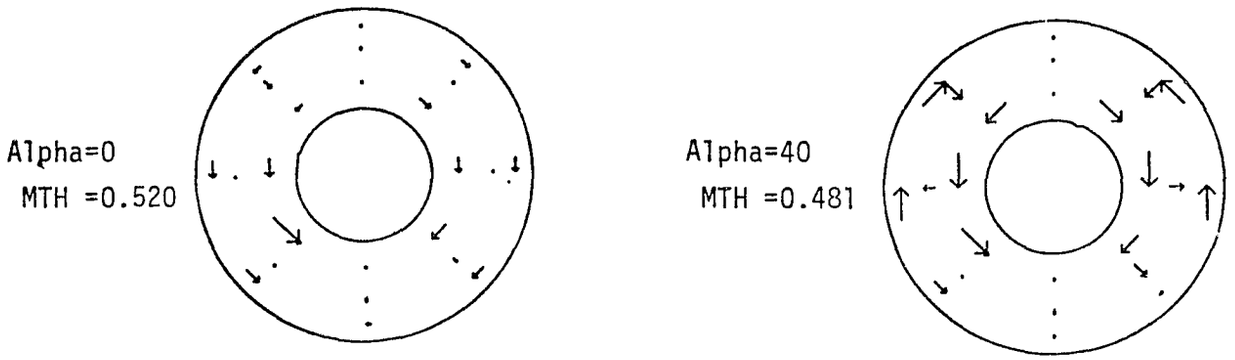

(g) Short Aft Inlet at Vo=135 knots

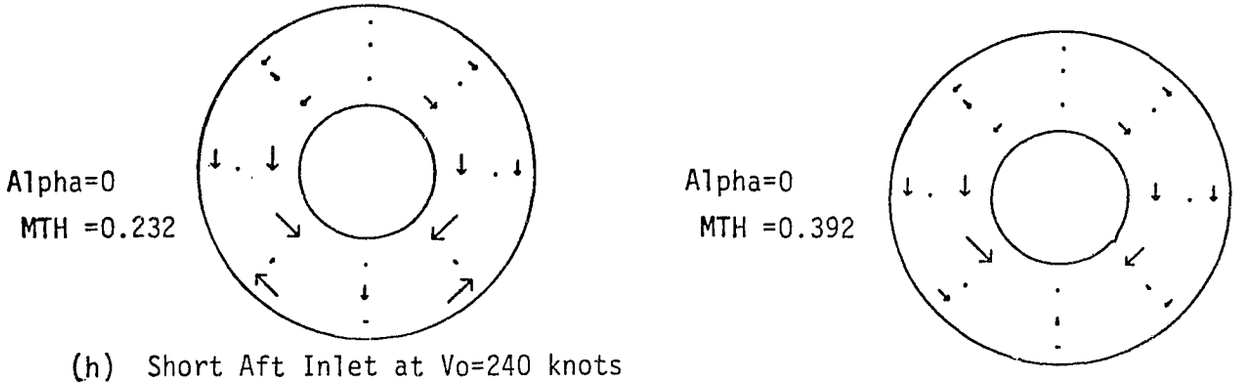

(h) Short Aft Inlet at Vo=240 knots

FIGURE 50 Continued

7.0 CONCLUSIONS AND RECOMMENDATIONS

An approximately .25 scale model of a Tandem Fan nacelle designed for a Type A (Subsonic Cruise) V/STOL aircraft configuration was tested in the NASA Lewis Research Center 10-by-10 foot (3.048-by-3.048 meter) wind tunnel. A 12-inch (30.48 cm), tip driven, turbofan simulator was used to provide the suction source for the aft fan inlet. The front fan inlet was faired over for this test entry. Model variables consisted of a long aft inlet cowl, a short aft inlet cowl, a shaft simulator, blow-in door passages and diffuser vortex generators. Inlet pressure recovery, distortion and inlet angle of attack separation limits were evaluated at tunnel velocities from 0 to 240 knots (0 to 123.5 m/s), angles of attack from -10 to 40 degrees and inlet flow rates representative of throat Mach numbers of 0.1 to 0.6.

High inlet performance and stable operation was verified at all design forward speed and angle of attack conditions. The pressure recovery levels at the fan face achieved by the long aft inlet were consistently around 99%, with distortion levels limited to 8% for the tunnel conditions tested. The blow-in door passages produced a loss (1%) in pressure recovery and an increase (1%) in pressure distortion. Application of vortex generators to the diffuser lower surface improved the overall pressure recovery slightly at the higher speeds. The shaft simulator had no appreciable effect on either the pressure recovery or the distortion of the long aft inlet configuration. The short aft inlet pressure recovery levels are consistenly greater than 99% except at high angles of attack (30^{o} and 40^{o}) and high forward speeds (85 and 135 knots). Corresponding dirtortion levels are less than 5% at all conditions evaluated except at the high angles of attack (30^{o} and 40^{o}) and the higher forward speeds (85 and 135 knots) where the distortion climbs to 10%.

Based on the results of this test, it is recommended that the blow-in door passages be resized or recontoured in the aft inlet cowl to reduce the local pressure disturbances induced by the flow into the diffuser from these auxiliary passages. It is also recommended that the aft inlet configurations be evaluated with combinations of angle of attack and yaw to simulate cross wind flight conditions.

REFERENCES

1. NASA Contract NAS3-21468, "Inlet Development for a Tandem Fan Propulsion System," 27 June 1978.

2. "Effect of Entry-Lip Design on Aerodynamic and Acoustics of High-Throat-Mach number inlets for the Quiet, Clean, Short Haul Experimental Engine." NASA TMX-3222, B. A. Miller, May 1975 .

3. "The Engine Inlet on the 747," ASME 69-GT-41, W. S. Viall, March 1969.

4. "Inlet Development for the L-500," J. P. Hancock, B. L. Hinson, AIAA 69-448.

5. "Experimental Optimization of Subsonic Inlet Design Parameters," A. H. Kraig, D. L. Motycka, B. J. Stewart, AIAA 66-690.

6. "A Combined Potential and Viscous Flow Solution for V/STOL Engine Inlets," A. H. Ybarra, W. W. Rhoades, N. O. Stockman, AIAA paper 78-142, January 1978.

7. "Design Report Model 1109-A 12-inch tip-turbine fan TR77-101, Revision A", G. Linsker, Tech Development Incorporated TD-1109M, 4 February 1977.

8. "Fortram Program to Generate Engine Inlet Flow Contour Maps and Distortion Parameters", NASA TMX 2967, J. H. Dicus, February 1974.

9. "Flow-Direction Measurement with Fixed-Position Probes" NASA TMX-1904, T. J. Dudzinski and L. N. Krause, 1969.